UNIVERSITY OF CALIFORNIA
RIVERSIDE

The Nexus Between Endothelial Cell Homeostasis and Cholesterol Regulation

A Dissertation submitted in partial satisfaction
of the requirements for the degree of

Doctor of Philosophy

in

Biochemistry and Molecular Biology

by

Marcella Martin

December 2017

Dissertation Committee:
Dr. John Y-J. Shyy, Co-Chairperson
Dr. Declan F. McCole, Co-Chairperson
Dr. Emma H. Wilson

The Dissertation of Marcella Martin is approved:

_____

_____

Committee Co-Chairperson

_____

Committee Co-Chairperson

University of California, Riverside

ACKNOWLEDGEMENTS

I would like to give my utmost gratitude to my graduate research advisor, Dr. John Y-J. Shyy, for his invaluable guidance and support. His demand for high quality work and giving me intellectual freedom has formed the scientist I am today. I would also like to thank Drs. Declan F. McCole and Emma H. Wilson for their willingness and helpfulness as my defense committee. None of this work could have been possible without the help from my lab mates and international collaborators including Drs. Jian Kang, Zhen Chen, Yifei Miao, Ming He, Jiao Zhang, Hsi-Yuan Huang, Wei-Ting Wang, Hsiao-Chin Hong, Tzu-Pin Shentu, Yue Han, Traci Marin, Brendan Gongol, Zhao Li, Jin Zhang, Liang Bai, Jie Li, Mano R. Maurya, Shakti Gupta, Guangjin Zhou, Panjamaporn Sangwung, Yong-Jiang Xu, Ting Lei, Hsien-Da Huang, Mohit Jain, Mukesh K. Jain, Shankar Subramaniam, Simon Wong, and James Hagood. I would like to acknowledge the funding sources that made this body of work possible including the NIH training grant (5T32HL007444) and the NHBLI. Finally, I would like to thank my family and friends who have provided constant love and support throughout my graduate career.

The text of this dissertation, in part, is a reprint of the material as it appears in *Circulation*, Oct 3, 2017. The co-first authors, Dr. Zhao Li and I, listed in that publication directed and supervised the research which forms the basis of part of this dissertation.

ABSTRACT OF THE DISSERTATION

The Nexus Between Endothelial Homeostasis and Cholesterol Regulation

by

Marcella Martin

Doctor of Philosophy, Graduate Program in Biochemistry and Molecular Biology
University of California, Riverside, December 2017
Dr. John Y-J. Shyy, Co-Chairperson
Dr. Declan McCole, Co-Chairperson

Maintaining vascular endothelial cell (EC) homeostasis is integral to preventing cardiovascular disease. Here, we demonstrate that EC function is tightly regulated with cholesterol homeostasis. The reciprocal cholesterol efflux and cholesterol biosynthesis pathways also contribute to EC function or dysfunction, respectively. This study focuses on a two-pronged approach: 1) How a key regulator of EC function, namely Krüppel-like factor 4 (KLF4), relates to cholesterol efflux and oxidation to promote an anti-inflammatory and anti-oxidative effect in ECs to prevent cardiovascular disease; and 2) How key mediators of cholesterol biosynthesis, i.e., sterol regulatory element-binding protein 2 (SREBP2), relate to the regulation of EC dysfunction contributing to cardiovascular disease. To investigate both pathways, I began with a systems biology approach by using RNA-sequencing of ECs in which KLF4 or SREBP2 is overexpressed. From this global view, novel pathways regulated by KLF4 or SREBP2 that exert opposing functional outcome in ECs were identified. Furthermore, KLF4 was demonstrated to

promote endothelial homeostasis in part through the activation of cholesterol oxidation and efflux via the induction of cholesterol-25-hydroxylase (Ch25h) and liver X receptor (LXR). Additionally, KLF4-regulated suppression of the pro-inflammatory SREBP2 and NLRP3 inflammasome pathway contributed to an athero-protective phenotype in mice, further defining that KLF4 regulates a counterbalance between LXR and SREBP2. In contrast, SREBP2 was determined to be both necessary and sufficient to induce EC dysfunction through the upregulation of endothelial-to-mesenchymal transition (EndoMT). This is further implicated in the pro-fibrotic cardiovascular disease, idiopathic pulmonary fibrosis. This two-sided and reciprocal approach provided evidence that cholesterol homeostasis must be tightly regulated by KLF4 in order to maintain EC function. Moreover, when cholesterol regulation is shifted towards SREBP2, ECs become dysfunctional leading to exacerbated cardiovascular disease. The opposing functions of these two key transcription factors provide insight into the complex regulatory network between EC function and cholesterol balance.

TABLE OF CONTENTS

List of Figures

List of Abbreviations

25-HC: 25-hydroxycholesterol

AA: aortic arch

ABCA1: ATP-binding cassette transporters family A1

ABCG1: ATP-binding cassette transporters family G1

ApoE: apolipoprotein E

Arg1: arginase-1

aSMA: alpha smooth muscle actin

BLM: bleomycin

BMDMs: bone marrow-derived macrophages

CCL5: chemokine C-C motif ligand 5

Ch25h: cholesterol-25-hydroxylase

chil3: chitinase-like 3

ChIP: chromatin immunoprecipitation

Col1A1: collagen 1 type alpha 1

COX2: cyclooxygenase-2

CTGF: connective tissue growth factor

DNMT1: DNA methyltransferase 1

ECM: extracellular matrix

ECs: endothelial cells

EMT: epithelial-to-mesenchymal transition

EndoMT: endothelial-to-mesenchymal transition

eNOS: endothelial nitric oxide synthase

FN: fibronectin

H&E: haematoxylin and eosin

HMG-CoAR: 3-hydroxy-3-methylglutaryl-coenzyme A reductase

HUVECs: human umbilical vein endothelial cells

IL-1β: interleukin-1 beta

iNOS: inducible nitric oxide synthase

i.p.: intraperitoneal

IPF: idiopathic pulmonary fibrosis

KD: Kawasaki disease

KLF4: kruppel-like factor 4

KLF2: kruppel-like factor 2

KO: knockout

LDL: low-density lipoprotein

LDLR: low-density lipoprotein receptor

LXR: liver X receptor

MCP-1: monocyte chemoattractant protein 1

Mrc1: mannose receptor, C type 1

MSP: methylation specific PCR

N-Cad: neural cadherin

NLRP3: NOD-like receptor family, pyrin domain containing protein 3

NO: nitric oxide

OS: oscillatory shear stress

Ox-LDL: oxidized low-density lipoprotein

PDGF: platelet-derived growth factor

PMs: peritoneal macrophages

PPARα: peroxisome proliferator activated receptor alpha

PS: pulsatile shear stress

RCT: reverse cholesterol transport

retnla: resistin like alpha

ROS: reactive oxygen species

S1P/S2P: site-1 and site-2 protease

SCAP: SREBP cleavage activating protein

SREBP2: sterol regulatory element-binding protein 2

TA: thoracic aorta

Tg: transgenic

TGFβ: transforming growth factor beta

TLR: toll-like receptor

TNFα: tumor necrosis factor alpha

WHO: World Health Organization

WT: wildtype

VE-Cad: vascular endothelial cadherin

VSMCs: vascular smooth muscle cells

vWF: von Willebrand factor

CHAPTER 1

Introduction

1.1 Vascular dysfunction related to cardiovascular disease

Cardiovascular diseases, which include dysfunction of the heart and/or blood vessels, remains to be the leading cause of death worldwide and claimed more than 15 million lives in 2015 according to the World Health Organization (WHO) (http://www.who.int/mediacentre/factsheets/fs310/en/). Thus, it is imperative to understand the physiology and pathophysiology of vasculature with respect to cardiovascular diseases. The majority of deaths are related to ischemic heart conditions or stroke, both of which are caused from lack of blood flow to the heart or brain, respectively. A prominent driver of these ischemic diseases is atherosclerosis, classically characterized by the hardening or narrowing of conduit or mid-size arteries. Risk factors for atherosclerosis include hypertension, high levels of circulating cholesterol, Western high fat diet, physical inactivity, and increased aged[1-3].

The progression of atherosclerosis is multifaceted and includes dysfunction of the three major layers of the blood vessel: the intima, media, and adventitia. Vascular endothelial cells (ECs) comprise the luminal side of the inner most layer of the intima. As the first responders to physiological and pathophysiological stimuli in the circulation, ECs are pivotal mediators of vascular wall in health and disease. Functional ECs protect the blood vessel from infiltrating leukocytes, promote vascular dilation, and have an anti-inflammatory, anti-oxidative phenotype[4, 5]. Conversely, dysfunctional ECs recruit leukocytes to the vessel wall and promote inflammation and oxidative stress[6, 7]. In a pro-

inflammatory environment, ECs express adhesion molecules such as vascular cell adhesion molecule-1 (VCAM1), intracellular adhesion molecule-1 (ICAM1), and E-selectin to recruit circulating monocytes[8, 9]. Monocytes can then infiltrate the sub-endothelial space where they differentiate into macrophages and begin to uptake cholesterol[10, 11]. In pathophysiological conditions, there is excessive uptake of cholesterol, an upregulation of cholesterol esterification, and suppressed reverse cholesterol transport (RCT)[12]. The unregulated accumulation of lipids leads to an induction of oxidized-low density lipoprotein (ox-LDL), which is pro-inflammatory and promotes foam cell formation[13]. Foam cells have limited ability to migrate and amass into foci that comprise the necrotic core of atherosclerotic lesions[14]. Infiltrating macrophages can also be polarized into either a pro-inflammatory M1 phenotype (containing markers for cyclooxygenase-2 [COX2], Gro1, tumor necrosis factor alpha [TNFα], chemokine C-C motif ligand 5 [CCL5], inducible nitric oxide synthase [iNOS], and interleukin [IL]-6), or an anti-inflammatory M2 phenotype (expressing markers such as peroxisome proliferator activated receptor gamma [PPARγ], mannose receptor, C type 1 [Mrc1], chitinase-like 3 [Chil3], arginase-1 [Arg1], resistin-like alpha [Retnla], and IL-10)[15, 16]. This pro-inflammatory microenvironment signals to the media layer of the vessel, comprised of vascular smooth muscle cells (VSMCs), causing VSMC proliferation and migration leading to intimal thickening[17]. VSMCs also secrete extracellular matrix (ECM) proteins to form a thick, fibrous cap that covers the necrotic core[18, 19]. The fibrotic cap is prone to thrombose and rupture, making VSMCs a key mediator of plaque instability. The outermost layer of the vessel, the adventitia, is composed of fibroblasts. There is convincing evidence revealing

that upon injury, the fibroblast population becomes activated and differentiate into myofibroblasts, which are highly proliferative and migratory[20]. Although most notably recognized for their regulation of wound healing and fibrotic disorders[21], myofibroblasts also play a role in intimal thickening and vessel stiffening in atherosclerosis[22-24].

Although atherosclerosis may contribute to a large number of common causes of death, there are also a multitude of cardiovascular diseases that also rely on EC function, including by not limited to, aneurysm formation and dissection, deep venous thrombosis, pulmonary embolism, and fibrotic disorders. There are also a number of emerging diseases that are not canonically known to be vascular dependent. However, increasing studies have found that diseases such as pulmonary fibrosis are highly regulated by EC function[25, 26]. Chronic obstructive pulmonary disease, including pulmonary fibrosis, is in the top 5 leading causes of death worldwide and claimed 3.2 million lives in 2015 according to the WHO (http://www.who.int/mediacentre/factsheets/fs310/en/). Idiopathic pulmonary fibrosis (IPF) is a progressive interstitial lung disease with a median survival rate of 3-5 years[27]. The clinical presentation of IPF relies on the formation of fibroblastic foci, areas of active myofibroblasts depositing ECM[27, 28]. IPF does not respond to anti-inflammatories or steroids and the only effective treatment is lung transplantation[29]. It was hypothesized that an unknown initial injury causes an acute inflammatory response followed by dysregulated wound repair leading to fibrosis[30]. More recent studies indicate that inflammation plays little role in the progression of this disease[31, 32]. Being a progressive fibrotic disease, IPF patients have an accumulation of activated myofibroblasts in the interstitial space between the alveoli and the capillaries. The prototypical proliferative

signals, transforming growth factor beta (TGFβ) and platelet-derived growth factor (PDGF) pathways, are stimulated resulting in the myofibroblasts to secrete excessive amounts of collagen and fibronectin (FN)[33, 34]. However, therapeutics targeting these growth factors have not benefited IPF patient prognosis[35]. Despite the lung being comprised of more than 30% ECs[36], the role of EC dysfunction in the progression of IPF remains elusive. It is therefore crucial to investigate the role of ECs in pulmonary fibrosis disease progression.

1.2 Endothelial homeostasis and vascular tone

A functional endothelium promotes vasorelaxation through the production of endothelial nitric oxide synthase (eNOS)-derived nitric oxide (NO)[37]. eNOS catalyzes the conversion of L-arginine to L-citrulline and NO[38]. NO is the most potent soluble vasodilator and freely diffuses from ECs to the sub-endothelial space to be up taken by VSMCs[39, 40]. Once inside the VSMCs, NO actives guanylate cyclase and stimulates the production of cyclic guanosine monophosphate (cGMP), thereby reducing VSMC contractibility and relaxing the vessel[41]. Therefore, the regulation of eNOS is critical in maintaining vascular tone. ECs are constantly exposed to shear stress, hemodynamic forces produced by the local blood flow patterns. Experimental and computational evidence from the past has indicated that unidirectional, pulsatile shear stress (PS), occurring in the straight regions of the vessel, has anti-inflammatory properties, promotes EC homeostasis, and is resistant to atherosclerosis[42-44]. In contrast, local blood flow patterns in areas of the vessel that contain bifurcations or curvatures are disturbed and produce an oscillatory shear stress (OS)[45-47]. In these regions, ECs are pro-inflammatory and the vessel is predisposed

to atherosclerosis. The integrity of EC homeostasis is vital in maintaining vascular tone as evidenced by the focal distribution of atherosclerotic lesions.

Krüppel-like factor 4 (KLF4) is a well-documented transcription factor that is induced by atheroprotective flow or PS[48-50]. Among its anti-inflammatory effects, namely suppressing the expression of adhesion molecules such as VCAM1 to reduce monocyte adhesion, KLF4 is also a key mediator of eNOS transcriptional upregulation[48]. Conversely, when KLF4 is genetically ablated specifically in ECs in mice *in vivo*, atherosclerosis is accelerated regardless topographic locations in the arterial tree[49]. Clinically, cardiovascular protective agents, such as 3-hydroxy-3-methylglutaryl-coenzyme A reductase (HMG-CoAR) inhibitors, also known as statins, are known to induce eNOS activity[51]. Statins are lipid lowering and are the most commonly prescribed drug for cardiovascular disease. Although initially found to inhibit HMG-CoAR, statins have been shown to have pleiotropic effects in vascular function. One important function of statins is the induction of KLF4 to promote eNOS-derived NO bioavailability[52, 53]. Given the common induction in endothelium by athero-protective flow and statins *in vitro* and *in vivo*, KLF4 is a master regulator of EC homeostasis (see brief summary of KLF4 regulation in Table 1.1).

Table 1.1 Summary of KLF4 Regulation in ECs

Authors	***Signaling***	***Function/observation***
Hamik A et al[48]	KLF4⊣VCAM1	Anti-inflammatory, anti-thrombotic, and anti-adhesion *in vitro*
Zhou G et al[49]	KLF4⊣VCAM1 and PAI-1	Anti-adhesive, anti-thrombotic, and anti-atherosclerotic *in vivo*
Ohnesorge N et al[52]	Erk5→KLF4	Vasoprotective phenotype
Maejima T et al[53]	Pitavastatin→KLF4	EC homeostasis
Egorova AD et al[54]	Primary cilia→KLF4	Inhibits disturbed flow-induced endothelial-to-mesenchymal transition
Clark PR et al[55]	MEK5→KLF4	Athero-protective flow-induced
Villarreal G et al[56]	MEF2→KLF4	Athero-protective flow-, simvastatin-, and resveratrol-induced
Cowan CE et al[57]	KLF4→VE-Cadherin	Increases endothelial barrier function
Shatat MA et al[58]	KLF4⊣ ET-1	Protects from pulmonary hypertension *in vivo*
Hale AT et al[50]	KLF4⊣Notch	Prevents tumor angiogenesis *in vivo*

Abbreviations: Kruppel-like factor 4 (KLF4), vascular cell adhesion molecule-1 (VCAM1), plasminogen activator inhibitor-1 (PAI-1), extracellular signal-regulated kinase 5 (Erk5), mitogen-activated protein kinase kinase 5 (MEK5), MADS box transcription enhancer factor 2 (MEF2), vascular endothelial (VE)-Cadherin, and endothelin-1 (ET-1).

1.3 Balance of cholesterol regulation

Similar to endothelial homeostasis, the cholesterol pathway is also tightly regulated. There is constant fluctuation between cholesterol biosynthesis and cholesterol efflux. The key mediator of cholesterol biosynthesis and uptake is the transcription factor sterol regulatory element-binding protein 2 (SREBP2)[59]. When the cell is in cholesterol rich conditions, intracellular sterols can bind to the sterol sensing domain of SREBP cleavage-activating protein (SCAP), which causes a conformational change to allow SCAP to sequester SREBP2 in the endoplasmic reticulum[60]. Conversely, when there are low intracellular cholesterol levels, the SCAP-SREBP2 complex is transported in a vesicle to the Golgi apparatus. Once in the Golgi, the N-terminal portion of SREBP2 is cleaved by site-1 and site-2 proteases (S1P and S2P). The N-terminal, and active portion, of SREBP2 [SREBP2(N)] can then translocate to the nucleus to serve as a transcription factor for genes that increase intracellular cholesterol levels (e.g., HMG-CoAR and LDL receptor)[61]. Antagonistically, cholesterol efflux and oxidation pathways provide means to reduce intracellular cholesterol levels by secreting or utilizing free cholesterol to produce oxysterols, such as 25-hydroxycholesterol (25-HC). The key transcription factor regulating these pathways is liver X receptor (LXR), which directly transactivates genes such as ATP-binding cassette transporters ABCA1 and ABCG1, which are integral to cholesterol efflux[62]. Furthermore, cholesterol-25-hydroxylase (Ch25h) is the enzyme that produces 25-HC from free cholesterol in the cell. Interestingly, 25-HC is not only a ligand for the activation of LXR, but is also an antagonist to SREBP2 N-terminal cleavage[60]. Additional fine-tuning of this cholesterol regulatory network is an intronic microRNA located in intron

16 of the human *SREBF2* gene, microRNA-33 (miR-33). miR-33 targets the 3'-UTR of ABCA1 and ABCG1 to suppress their expression, thereby repressing cholesterol efflux[63]. This delicate balance of cholesterol homeostasis (illustrated in Figure 1.1) within the cell is also integral to the regulation of endothelial dysfunction.

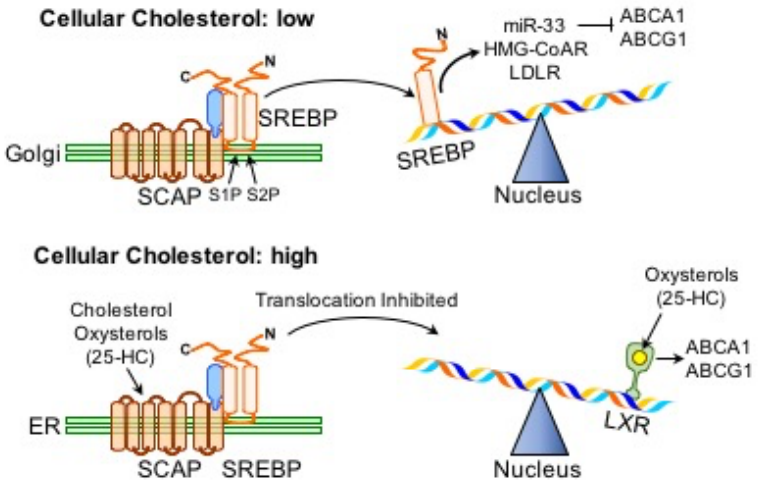

Figure 1.1 The balance of intracellular cholesterol regulation
Figure adapted from Spann N, et al. *Nature Immunol* 2013.

1.4 Endothelial dysfunction, inflammasome activation, and endothelial-to-mesenchymal transition (EndoMT)

Pro-inflammatory and pro-oxidative stresses (e.g., disturbed blood flow patterns and ox-LDL) result in EC dysfunction, characterized by reduced eNOS-derived NO bioavailability and vasoconstriction, increased monocyte adhesion, and increased secretion of pro-inflammatory cytokines. Interestingly, we had previously found that SREBP2 was upregulated by both disturbed flow and ox-LDL[64, 65]. Although SREBP2 was found to be shear stress-sensitive in ECs, functional outcome due to SREBP2 induction remains unknown. Unlike macrophages or hepatocytes, ECs are not canonically known to uptake

or produce large quantities of cholesterol[66]. We therefore postulated that SREBP2 may impose other functions in ECs by regulating genes other than cholesterol biosynthesis and uptake. Our lab then identified that SREBP2 contributes to the pro-inflammatory phenotype in ECs through the induction of the NOD-like receptor family, pyrin domain containing protein 3 (NLRP3) inflammasome[64]. The NLRP3 inflammasome is part of the innate immune response and is activated in a two-step process (i.e., Signal 1 and Signal 2). Signal 1 promotes the transcriptional induction of the inflammasome components, including pro-caspase-1 and pro-interleukin (IL)-1β[67]. Signal 2 is the oligomerization of the inflammasome components (i.e., NLRP3, ASC, and pro-caspase-1), which results in the auto-cleavage of pro-caspase-1 into active caspase-1[67]. Active caspase-1 can then cleave pro-IL-1β to the biologically active form of IL-1β. The cleaved IL-1β can then diffuse through the cell to provide paracrine inflammatory signals and induce innate immune response distally[67]. Furthermore, SREBP2, as a transcription factor, was demonstrated to transactivate pro-caspase-1 and pro-IL-1β, Signal 1 of NLRP3 inflammasome activation[64]. We also found that the induction of the NLRP3 inflammasome seemed to be cholesterol independent in ECs[64]. This highlights that the role of SREBP2 in ECs may be involved in distinct regulatory pathways than from other cholesterol regulating cell types.

Chronic stimulation with pro-inflammatory cytokines such as IL-1β can also lead to EC dysfunction not only through the induction of the innate immune response, but also through the activation of endothelial-to-mesenchymal transition (EndoMT)[68, 69]. Initially, EndoMT was identified to be crucial in the formation of the mesenchymal cushion that is

needed for the development of the cardiac valves in embryos[70]. In the process of EndoMT, ECs lose their EC-specific markers such as CD31, vascular endothelial (VE)-cadherin, and KLF4, while gaining mesenchymal-specific markers including α-smooth muscle actin (αSMA), neural (N)-cadherin, and vimentin[71]. In addition to the genotypic changes, there is also a phenotypic switch from a quiescent EC to a cell resembling a myofibroblast-like cell, which is highly proliferative, migratory, and has marked increased ECM deposition[71]. Consistently, EndoMT has recently been implicated in many proliferative disorders such as cardiac and kidney fibrosis[72, 73]. However, the percentage of pro-fibrotic cells in these diseases that originate from ECs remains a question. Although the role of EndoMT in disease is relatively controversial, a number of recent studies suggest that the drivers of this transition are pro-inflammatory and pro-oxidative stress inducers[71, 74].

1.5 Purpose of study

This study focuses on a two-pronged approach: 1) How a key regulator of EC function, namely KLF4, relate to cholesterol efflux and oxidation to promote an anti-inflammatory and anti-oxidative effect in ECs to prevent cardiovascular disease; and 2) How key mediators of cholesterol biosynthesis, i.e., SREBP2, relate to the regulation of EC dysfunction contributing to cardiovascular disease. To investigate both pathways, I begin with a systems biology approach by using RNA-sequencing of ECs in which KLF4 or SREBP2 is overexpressed. From this global view, I identified novel pathways regulated by KLF4 (Chapter 2) or SREBP2 (Chapter 3) that exert opposing functional outcome in ECs. Chapter 2 demonstrates that KLF4 promotes endothelial homeostasis in part through the activation of cholesterol oxidation and efflux via the induction of Ch25h and LXR.

Additionally, KLF4-regulated suppression of the pro-inflammatory SREBP2 and NLRP3 inflammasome pathway contributes to an athero-protective phenotype in mice. In Chapter 3, SREBP2 is identified as both necessary and sufficient to induce EC dysfunction through the upregulation of EndoMT. This is further implicated in the pro-fibrotic disease, IPF. These two-sided and reciprocal approaches provide evidence that cholesterol homeostasis must be tightly regulated by KLF4 in order to maintain EC function. Furthermore, when cholesterol regulation is shifted towards SREBP2, then ECs become dysfunctional and exacerbate cardiovascular disease (Figure 1.2).

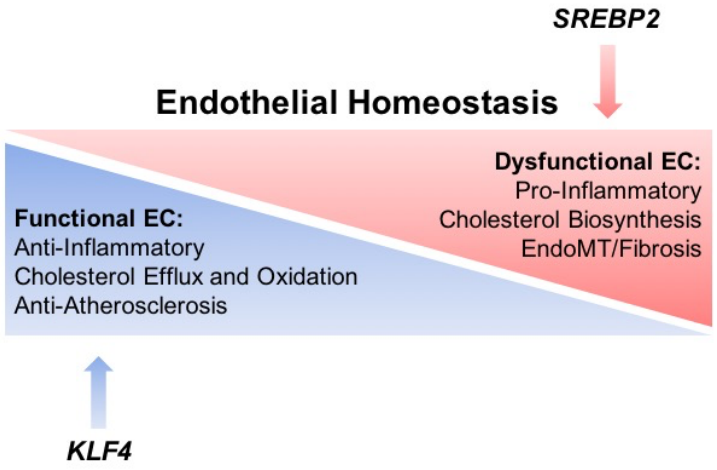

Figure 1.2 Simplified diagram illustrating the two-sided approach of this dissertation. KLF4 promotes EC function through its known anti-inflammatory effects. I further demonstrate that KLF4 mediates cholesterol efflux and oxidation contributing to an anti-atherosclerotic phenotype. In contrast, SREBP2, a canonical mediator of cholesterol biosynthesis, promotes EC dysfunction via unresolved innate immune response. I identify another process of EC dysfunction, EndoMT that leads to increased tissue fibrosis.

References

1. Rafieian-Kopaei M, Setorki M, Doudi M, Baradaran A and Nasri H. Atherosclerosis: Process, Indicators, Risk Factors and New Hopes. *International Journal of Preventive Medicine*. 2014;5:927-46.

2. Gofman JW, Young W and Tandy R. Ischemic heart disease, atherosclerosis, and longevity. *Circulation*. 1966;34:679-97.

3. Mozaffarian D, Benjamin EJ, Go AS, Arnett DK, Blaha MJ, Cushman M, de Ferranti S, Despres JP, Fullerton HJ, Howard VJ, Huffman MD, Judd SE, Kissela BM, Lackland DT, Lichtman JH, Lisabeth LD, Liu S, Mackey RH, Matchar DB, McGuire DK, Mohler ER, 3rd, Moy CS, Muntner P, Mussolino ME, Nasir K, Neumar RW, Nichol G, Palaniappan L, Pandey DK, Reeves MJ, Rodriguez CJ, Sorlie PD, Stein J, Towfighi A, Turan TN, Virani SS, Willey JZ, Woo D, Yeh RW and Turner MB. Heart disease and stroke statistics--2015 update: a report from the American Heart Association. *Circulation*. 2015;131:e29-322.

4. Deanfield JE, Halcox JP and Rabelink TJ. Endothelial function and dysfunction: testing and clinical relevance. *Circulation*. 2007;115:1285-95.

5. Verma S and Anderson TJ. Fundamentals of endothelial function for the clinical cardiologist. *Circulation*. 2002;105:546-9.

6. Biegelsen ES and Loscalzo J. Endothelial function and atherosclerosis. *Coronary artery disease*. 1999;10:241-56.

7. Quyyumi AA. Endothelial function in health and disease: new insights into the genesis of cardiovascular disease. *The American journal of medicine*. 1998;105:32s-39s.

8. Kim I, Moon SO, Kim SH, Kim HJ, Koh YS and Koh GY. Vascular endothelial growth factor expression of intercellular adhesion molecule 1 (ICAM-1), vascular cell adhesion molecule 1 (VCAM-1), and E-selectin through nuclear factor-kappa B activation in endothelial cells. *The Journal of biological chemistry*. 2001;276:7614-20.

9. Wagener FA, Feldman E, de Witte T and Abraham NG. Heme induces the expression of adhesion molecules ICAM-1, VCAM-1, and E selectin in vascular endothelial cells. *Proceedings of the Society for Experimental Biology and Medicine Society for Experimental Biology and Medicine (New York, NY)*. 1997;216:456-63.

10. Yang J, Zhang L, Yu C, Yang XF and Wang H. Monocyte and macrophage differentiation: circulation inflammatory monocyte as biomarker for inflammatory diseases. *Biomarker Research*. 2014;2:1.

11. Jaipersad AS, Lip GY, Silverman S and Shantsila E. The role of monocytes in angiogenesis and atherosclerosis. *Journal of the American College of Cardiology*. 2014;63:1-11.

12. Chistiakov DA, Bobryshev YV and Orekhov AN. Macrophage-mediated cholesterol handling in atherosclerosis. *Journal of cellular and molecular medicine*. 2016;20:17-28.

13. Jones NL, Reagan JW and Willingham MC. The pathogenesis of foam cell formation: modified LDL stimulates uptake of co-incubated LDL via macropinocytosis. *Arteriosclerosis, thrombosis, and vascular biology*. 2000;20:773-81.

14. Moore KJ and Tabas I. Macrophages in the pathogenesis of atherosclerosis. *Cell*. 2011;145:341-55.

15. Martinez FO and Gordon S. The M1 and M2 paradigm of macrophage activation: time for reassessment. *F1000Prime Reports*. 2014;6.

16. Italiani P and Boraschi D. From Monocytes to M1/M2 Macrophages: Phenotypical vs. Functional Differentiation. *Frontiers in Immunology*. 2014;5.

17. Louis SF and Zahradka P. Vascular smooth muscle cell motility: From migration to invasion. *Experimental & Clinical Cardiology*. 2010;15:e75-85.

18. Newby AC and Zaltsman AB. Fibrous cap formation or destruction — the critical importance of vascular smooth muscle cell proliferation, migration and matrix formation. *Cardiovascular Research*. 1999;41:345-360.

19. Bennett MR, Sinha S and Owens GK. Vascular smooth muscle cells in atherosclerosis. *Circulation research*. 2016;118:692-702.

20. Hinz B, Phan SH, Thannickal VJ, Galli A, Bochaton-Piallat ML and Gabbiani G. The Myofibroblast: One Function, Multiple Origins. *The American Journal of Pathology*. 2007;170:1807-16.

21. Kendall RT and Feghali-Bostwick CA. Fibroblasts in fibrosis: novel roles and mediators. *Frontiers in Pharmacology*. 2014;5.

22. Bayes-Genis A, Campbell JH, Carlson PJ, Holmes DR, Jr. and Schwartz RS. Macrophages, myofibroblasts and neointimal hyperplasia after coronary artery injury and repair. *Atherosclerosis*. 2002;163:89-98.

23. Zalewski A and Shi Y. Vascular Myofibroblasts. *Lessons From Coronary Repair and Remodeling*. 1997;17:417-422.

24. Forte A, Della Corte A, De Feo M, Cerasuolo F and Cipollaro M. Role of myofibroblasts in vascular remodelling: focus on restenosis and aneurysm. *Cardiovasc Res*. 2010;88:395-405.

25. Magro CM, Waldman WJ, Knight DA, Allen JN, Nadasdy T, Frambach GE, Ross P and Marsh CB. Idiopathic pulmonary fibrosis related to endothelial injury and antiendothelial cell antibodies. *Human immunology*. 2006;67:284-97.

26. Leach HG, Chrobak I, Han R and Trojanowska M. Endothelial cells recruit macrophages and contribute to a fibrotic milieu in bleomycin lung injury. *American journal of respiratory cell and molecular biology*. 2013;49:1093-101.

27. Wolters PJ, Collard HR and Jones KD. Pathogenesis of idiopathic pulmonary fibrosis. *Annual review of pathology*. 2014;9:157-79.

28. Blackwell TS, Tager AM, Borok Z, Moore BB, Schwartz DA, Anstrom KJ, Bar-Joseph Z, Bitterman P, Blackburn MR, Bradford W, Brown KK, Chapman HA, Collard HR, Cosgrove GP, Deterding R, Doyle R, Flaherty KR, Garcia CK, Hagood JS, Henke CA, Herzog E, Hogaboam CM, Horowitz JC, King TE, Jr., Loyd JE, Lawson WE, Marsh CB, Noble PW, Noth I, Sheppard D, Olsson J, Ortiz LA, O'Riordan TG, Oury TD, Raghu G, Roman J, Sime PJ, Sisson TH, Tschumperlin D, Violette SM, Weaver TE, Wells RG, White ES, Kaminski N, Martinez FJ, Wynn TA, Thannickal VJ and Eu JP. Future directions in idiopathic pulmonary fibrosis research. An NHLBI workshop report. *American journal of respiratory and critical care medicine*. 2014;189:214-22.

29. Juarez MM, Chan AL, Norris AG, Morrissey BM and Albertson TE. Acute exacerbation of idiopathic pulmonary fibrosis-a review of current and novel pharmacotherapies. *Journal of thoracic disease*. 2015;7:499-519.

30. Bringardner BD, Baran CP, Eubank TD and Marsh CB. The role of inflammation in the pathogenesis of idiopathic pulmonary fibrosis. *Antioxidants & redox signaling*. 2008;10:287-301.

31. Meltzer EB and Noble PW. Idiopathic pulmonary fibrosis. *Orphanet journal of rare diseases*. 2008;3:8.

32. Kottmann RM, Hogan CM, Phipps RP and Sime PJ. Determinants of initiation and progression of idiopathic pulmonary fibrosis. *Respirology (Carlton, Vic)*. 2009;14:917-33.

33. Fernandez IE and Eickelberg O. The impact of TGF-beta on lung fibrosis: from targeting to biomarkers. *Proceedings of the American Thoracic Society*. 2012;9:111-6.

34. Antoniades HN, Bravo MA, Avila RE, Galanopoulos T, Neville-Golden J, Maxwell M and Selman M. Platelet-derived growth factor in idiopathic pulmonary fibrosis. *The Journal of clinical investigation*. 1990;86:1055-64.

35. Puglisi S, Torrisi SE, Vindigni V, Giuliano R, Palmucci S, Mule M and Vancheri C. New perspectives on management of idiopathic pulmonary fibrosis. *Therapeutic advances in chronic disease*. 2016;7:108-20.

36. Crapo JD, Barry BE, Gehr P, Bachofen M and Weibel ER. Cell number and cell characteristics of the normal human lung. *The American review of respiratory disease*. 1982;126:332-7.

37. Förstermann U and Sessa WC. Nitric oxide synthases: regulation and function. *European Heart Journal*. 2012;33:829-37.

38. Babu BR, Frey C and Griffith OW. L-arginine binding to nitric-oxide synthase. The role of H-bonds to the nonreactive guanidinium nitrogens. *The Journal of biological chemistry*. 1999;274:25218-26.

39. Zhao Y, Vanhoutte PM and Leung SWS. Vascular nitric oxide: Beyond eNOS. *Journal of Pharmacological Sciences*. 2015;129:83-94.

40. Förstermann U and Li H. Therapeutic effect of enhancing endothelial nitric oxide synthase (eNOS) expression and preventing eNOS uncoupling. *Br J Pharmacol*. 2011;164:213-23.

41. Hussain MB, Hobbs AJ and MacAllister RJ. Autoregulation of nitric oxide-soluble guanylate cyclase-cyclic GMP signalling in mouse thoracic aorta. *British Journal of Pharmacology*. 1999;128:1082-1088.

42. Dimmeler S, Fleming I, Fisslthaler B, Hermann C, Busse R and Zeiher AM. Activation of nitric oxide synthase in endothelial cells by Akt-dependent phosphorylation. *Nature*. 1999;399:601-5.

43. Boo YC, Sorescu G, Boyd N, Shiojima I, Walsh K, Du J and Jo H. Shear stress stimulates phosphorylation of endothelial nitric-oxide synthase at Ser1179 by Akt-independent mechanisms: role of protein kinase A. *The Journal of biological chemistry*. 2002;277:3388-96.

44. Guo X and Kassab GS. Role of shear stress on nitrite and NOS protein content in different size conduit arteries of swine. *Acta physiologica (Oxford, England)*. 2009;197:99-106.

45. Davies PF. Hemodynamic shear stress and the endothelium in cardiovascular pathophysiology. *Nature clinical practice Cardiovascular medicine*. 2009;6:16-26.

46. Chiu JJ and Chien S. Effects of Disturbed Flow on Vascular Endothelium: Pathophysiological Basis and Clinical Perspectives. *Physiological reviews*. 2011;91.

47. Cunningham KS and Gotlieb AI. The role of shear stress in the pathogenesis of atherosclerosis. *Laboratory investigation; a journal of technical methods and pathology*. 2005;85:9-23.

48. Hamik A, Lin Z, Kumar A, Balcells M, Sinha S, Katz J, Feinberg MW, Gerzsten RE, Edelman ER and Jain MK. Kruppel-like factor 4 regulates endothelial inflammation. *The Journal of biological chemistry*. 2007;282:13769-79.

49. Zhou G, Hamik A, Nayak L, Tian H, Shi H, Lu Y, Sharma N, Liao X, Hale A, Boerboom L, Feaver RE, Gao H, Desai A, Schmaier A, Gerson SL, Wang Y, Atkins GB, Blackman BR, Simon DI and Jain MK. Endothelial Kruppel-like factor 4 protects against atherothrombosis in mice. *The Journal of clinical investigation*. 2012;122:4727-31.

50. Hale AT, Tian H, Anih E, Recio FO, 3rd, Shatat MA, Johnson T, Liao X, Ramirez-Bergeron DL, Proweller A, Ishikawa M and Hamik A. Endothelial Kruppel-like factor 4 regulates angiogenesis and the Notch signaling pathway. *The Journal of biological chemistry*. 2014;289:12016-28.

51. Rikitake Y and Liao JK. Rho GTPases, Statins, and Nitric Oxide. *Circulation research*. 2005;97:1232-5.

52. Ohnesorge N, Viemann D, Schmidt N, Czymai T, Spiering D, Schmolke M, Ludwig S, Roth J, Goebeler M and Schmidt M. Erk5 activation elicits a vasoprotective endothelial phenotype via induction of Kruppel-like factor 4 (KLF4). *The Journal of biological chemistry*. 2010;285:26199-210.

53. Maejima T, Inoue T, Kanki Y, Kohro T, Li G, Ohta Y, Kimura H, Kobayashi M, Taguchi A, Tsutsumi S, Iwanari H, Yamamoto S, Aruga H, Dong S, Stevens JF, Poh HM, Yamamoto K, Kawamura T, Mimura I, Suehiro J, Sugiyama A, Kaneki K, Shibata H, Yoshinaka Y, Doi T, Asanuma A, Tanabe S, Tanaka T, Minami T, Hamakubo T, Sakai J, Nozaki N, Aburatani H, Nangaku M, Ruan X, Tanabe H, Ruan Y, Ihara S, Endo A, Kodama T and Wada Y. Direct evidence for pitavastatin induced chromatin structure change in the KLF4 gene in endothelial cells. *PloS one*. 2014;9:e96005.

54. Egorova AD, Khedoe PP, Goumans MJ, Yoder BK, Nauli SM, ten Dijke P, Poelmann RE and Hierck BP. Lack of primary cilia primes shear-induced endothelial-to-mesenchymal transition. *Circulation research*. 2011;108:1093-101.

55. Clark PR, Jensen TJ, Kluger MS, Morelock M, Hanidu A, Qi Z, Tatake RJ and Pober JS. MEK5 is activated by shear stress, activates ERK5 and induces KLF4 to modulate TNF responses in human dermal microvascular endothelial cells. *Microcirculation (New York, NY : 1994)*. 2011;18:102-17.

56. Villarreal G, Jr., Zhang Y, Larman HB, Gracia-Sancho J, Koo A and Garcia-Cardena G. Defining the regulation of KLF4 expression and its downstream transcriptional targets in vascular endothelial cells. *Biochemical and biophysical research communications*. 2010;391:984-9.

57. Cowan CE, Kohler EE, Dugan TA, Mirza MK, Malik AB and Wary KK. Kruppel-like factor-4 transcriptionally regulates VE-cadherin expression and endothelial barrier function. *Circulation research*. 2010;107:959-66.

58. Shatat MA, Tian H, Zhang R, Tandon G, Hale A, Fritz JS, Zhou G, Martinez-Gonzalez J, Rodriguez C, Champion HC, Jain MK and Hamik A. Endothelial Kruppel-like factor 4 modulates pulmonary arterial hypertension. *American journal of respiratory cell and molecular biology*. 2014;50:647-53.

59. Wong J, Quinn Carmel M and Brown Andrew J. SREBP-2 positively regulates transcription of the cholesterol efflux gene, ABCA1, by generating oxysterol ligands for LXR. *Biochemical Journal*. 2006;400:485-491.

60. Spann NJ and Glass CK. Sterols and oxysterols in immune cell function. *Nature immunology*. 2013;14:893-900.

61. Horton JD, Goldstein JL and Brown MS. SREBPs: activators of the complete program of cholesterol and fatty acid synthesis in the liver. *The Journal of clinical investigation*. 2002;109:1125-31.

62. Beyea MM, Heslop CL, Sawyez CG, Edwards JY, Markle JG, Hegele RA and Huff MW. Selective up-regulation of LXR-regulated genes ABCA1, ABCG1, and APOE in macrophages through increased endogenous synthesis of 24(S),25-epoxycholesterol. *The Journal of biological chemistry*. 2007;282:5207-16.

63. Gerin I, Clerbaux L-A, Haumont O, Lanthier N, Das AK, Burant CF, Leclercq IA, MacDougald OA and Bommer GT. Expression of miR-33 from an SREBP2 Intron Inhibits Cholesterol Export and Fatty Acid Oxidation. *The Journal of biological chemistry*. 2010;285:33652-33661.

64. Xiao H, Lu M, Lin TY, Chen Z, Chen G, Wang WC, Marin T, Shentu TP, Wen L, Gongol B, Sun W, Liang X, Chen J, Huang HD, Pedra JH, Johnson DA and Shyy JY. Sterol regulatory element binding protein 2 activation of NLRP3 inflammasome in endothelium mediates hemodynamic-induced atherosclerosis susceptibility. *Circulation*. 2013;128:632-42.

65. Chen Z, Wen L, Martin M, Hsu CY, Fang L, Lin FM, Lin TY, Geary MJ, Geary GG, Zhao Y, Johnson DA, Chen JW, Lin SJ, Chien S, Huang HD, Miller YI, Huang PH and Shyy JY. Oxidative stress activates endothelial innate immunity via sterol regulatory element binding protein 2 (SREBP2) transactivation of microRNA-92a. *Circulation*. 2015;131:805-14.

66. Hassan HH, Denis M, Krimbou L, Marcil M and Genest J. Cellular cholesterol homeostasis in vascular endothelial cells. *The Canadian Journal of Cardiology*. 2006;22:35b-40b.

67. Jo E-K, Kim JK, Shin D-M and Sasakawa C. Molecular mechanisms regulating NLRP3 inflammasome activation. *Cellular and Molecular Immunology*. 2016;13:148-159.

68. Rieder F, Kessler SP, West GA, Bhilocha S, de la Motte C, Sadler TM, Gopalan B, Stylianou E and Fiocchi C. Inflammation-Induced Endothelial-to-Mesenchymal Transition: A Novel Mechanism of Intestinal Fibrosis. *The American Journal of Pathology*. 2011;179:2660-73.

69. Maleszewska M, Moonen JR, Huijkman N, van de Sluis B, Krenning G and Harmsen MC. IL-1beta and TGFbeta2 synergistically induce endothelial to mesenchymal transition in an NFkappaB-dependent manner. *Immunobiology*. 2013;218:443-54.

70. Kovacic JC, Mercader N, Torres M, Boehm M and Fuster V. Epithelial- and Endothelial- to Mesenchymal Transition: from Cardiovascular Development to Disease. *Circulation*. 2012;125:1795-808.

71. Piera-Velazquez S, Mendoza FA and Jimenez SA. Endothelial to Mesenchymal Transition (EndoMT) in the Pathogenesis of Human Fibrotic Diseases. *Journal of clinical medicine*. 2016;5.

72. Zeisberg EM, Tarnavski O, Zeisberg M, Dorfman AL, McMullen JR, Gustafsson E, Chandraker A, Yuan X, Pu WT, Roberts AB, Neilson EG, Sayegh MH, Izumo S and Kalluri R. Endothelial-to-mesenchymal transition contributes to cardiac fibrosis. *Nature medicine*. 2007;13:952.

73. Zeisberg EM, Potenta SE, Sugimoto H, Zeisberg M and Kalluri R. Fibroblasts in Kidney Fibrosis Emerge via Endothelial-to-Mesenchymal Transition. *Journal of the American Society of Nephrology : JASN*. 2008;19:2282-2287.

74. Chen PY, Qin L, Baeyens N, Li G, Afolabi T, Budatha M, Tellides G, Schwartz MA and Simons M. Endothelial-to-mesenchymal transition drives atherosclerosis progression. *The Journal of clinical investigation*. 2015;125:4514-28.

CHAPTER 2

Abstract

Background: Atherosclerosis is a multifaceted inflammatory disease involving cells in the vascular wall [e.g., endothelial cells (ECs)] as well as circulating and resident immunogenic cells (e.g., monocytes/macrophages). Acting as a ligand for liver X receptor (LXR), but an inhibitor of sterol regulatory element binding protein 2 (SREBP2), 25-hydroxycholesterol (25-HC) and its catalyzing enzyme cholesterol-25-hydroxylase (Ch25h) are important in regulating cellular inflammatory status and cholesterol biosynthesis in both ECs and monocytes/macrophages.

Methods: Bioinformatic analyses were used to investigate RNA-seq data to identify cholesterol oxidation and efflux genes regulated by KLF4. *In vitro* experiments involving cultured ECs and macrophages and *in vivo* methods involving mice with Ch25h ablation were then used to explore the atheroprotective role of KLF4-Ch25h/LXR.

Results: Vasoprotective stimuli increased the expression of Ch25h and LXR via krüppel-like factor 4 (KLF4). The KLF4-Ch25h/LXR homeostatic axis functions through suppressing inflammation, evidenced by the reduction of inflammasome activity in ECs and the promotion of M1 to M2 phenotypic transition in macrophages. The increased atherosclerosis in $ApoE^{-/-}/Ch25h^{-/-}$ mice further demonstrates the beneficial role of the KLF4-Ch25h/LXR axis in vascular function and disease.

Conclusions: KLF4 transactivates Ch25h and LXR thereby promoting the synergistic effects between ECs and macrophages to protect against atherosclerosis susceptibility.

Introduction

Krüppel-like factor 4 (KLF4) is a master transcription factor regulating the anti-inflammatory phenotype of both vascular endothelial cells (ECs) and monocytes/macrophages. Physiological stimuli (e.g., atheroprotective flow) and cardiovascular drugs (e.g., statins) exert their beneficial effects in part through the induction of KLF4 in ECs and monocytes[1, 2]. While a higher level of KLF4 in ECs regulates the expression of genes such as endothelial nitric oxide synthase (eNOS)[3, 4], induction of KLF4 in the macrophage favors the transition from the pro-inflammatory M1 to anti-inflammatory M2 phenotype[5]. At the disease level, the atheroprotective role of KLF4 in ECs and monocytes/macrophages is demonstrated by increased atherosclerosis in ApoE-null mice with either EC-specific or myeloid-specific KLF4 ablation[6, 7].

Cholesterol 25-hydroxylase (Ch25h) modulates cholesterol and lipid metabolism by converting cholesterol to 25-hydroxycholesterol (25-HC)[8]. Recent studies demonstrate that 25-HC, the product of Ch25h, increases the anti-viral effect and innate immunity in the host[9-11]. Liu *et al.* indicated that interferons (i.e., IFNα and IFNγ) enhance Ch25h-25-HC which suppressed viral growth through blocking virus fusion to the host cell membrane[12]. Reboldi *et al.* found that Ch25h-25-HC suppresses NOD-like receptor family, pyrin domain containing protein 3 (NLRP3) inflammasome-dependent interleukin-1β (IL-1β) production in macrophages and inhibits septic shock in mouse models[13]. Sterol regulatory element binding protein 2 (SREBP2) and liver X receptor (LXR) are two transcription factors that regulate cholesterol biosynthesis and metabolism reciprocally[14]. SREBP2 is a key mediator of genes involved in cholesterol biosynthesis [e.g., 3-hydroxy-

3-methylglutaryl-coenzyme A (HMG-CoA) reductase] and uptake [e.g., low density lipoprotein (LDL) receptor] as well as induces NLRP3 inflammasome in ECs[15]. Belonging to the nuclear receptor superfamily, LXR transactivates genes such as ATP-binding cassette (ABC) transporters, ABCA1 and ABCG1, to promote reverse cholesterol transport (RCT)[16]. Ligand-dependent LXR activation in ECs is associated with reduced oxidative stress and increased eNOS activity[17]. Furthermore, administration of a synthetic LXR ligand to $ApoE^{-/-}$ or $LDLR^{-/-}$ mice decreased atherosclerosis[18]. By contrast, bone marrow transplantation from $LXR\alpha/\beta^{-/-}$ mice to $ApoE^{-/-}$ or $LDLR^{-/-}$ recipients resulted in a marked increase of atherosclerotic lesion size[19]. Interestingly, 25-HC inhibits the transcriptional activity of SREBP2[20], while serving as an agonistic ligand for LXR[21].

The initiation, development, and advancement of atherosclerosis involve multiple inflammatory events in the endothelium, circulatory monocytes, and resident macrophages in the arterial wall. The sum of the pro-inflammatory responses counteracting the anti-inflammatory responses in these cell types determines the progression and severity of atherosclerosis. Given the dual role of 25-HC in inhibiting SREBP2 and activating LXR, we postulate that physiological stimuli and cardiovascular therapeutics that induce KLF4 in the endothelium and/or monocytes/macrophages are atheroprotective, in part through the regulation of Ch25h and LXR. Our results demonstrate that KLF4 transactivates Ch25h and LXR in ECs and macrophages *in vitro* and *in vivo*. Furthermore, the KLF4-Ch25h/LXR axis is atheroprotective, indicated by the increased atherosclerosis in $Ch25h^{-/-}/ApoE^{-/-}$ mice.

Methods

Library construction and data processing Total RNA was extracted and purified using mirVana mRNA isolation kit (Thermo Fisher Scientific) according to the manufacturer's instructions. RNA libraries were prepared for sequencing using standard Illumina protocols. Base calling and quality scoring were performed by an updated implementation of Real-Time Analysis (RTA), termed RTA v2, on the NextSeq 500 system. bcl2fastq Conversion Software v1.8.4 was used to demultiplex data and convert BCL files to FASTQ file formats. Sequenced reads were trimmed for adaptor sequence, and masked for low-complexity or low-quality sequence. Reads were then mapped to the hg19 whole genome for KLF4 overexpression data and mm9 for the Ch25h$^{-/-}$ mouse data using tophat v2.0.14[22]. Reads per kilobase of exon per megabase of library size (RPKM) were calculated using cufflinks v2.2.1[23, 24], which assembles transcripts, estimates their abundances, and tests for differential expression and regulation in RNA-seq samples (see flow chart below).

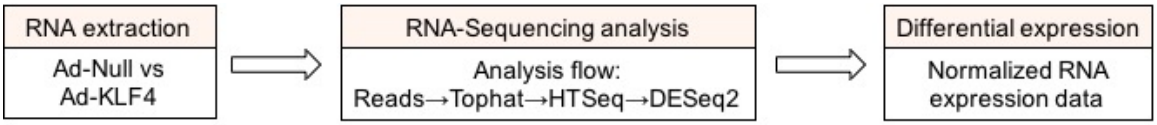

The mapping statistics of adenoviral constructs (Ad-KLF4 versus Ad-null) RNA-seq data are shown in Figure 2.1A. Overall, more than 75% of reads were mapped to the genome. To illustrate the general gene expression pattern of ECs with Ad-KLF4 compared to Ad-null, a genome-wide RNA-seq heat map is shown in Figure 2.1B, the selected genes with at least 3 RPKM were used for hierarchical clustering. Additionally, the volcano plot in Figure 2.1C indicating the thresholds used for analysis.

Gene expression network projection Gene expression data using fold change from two biological repeats of HUVECs infected with Ad-null or Ad-KLF4 were projected to a custom sterol metabolism pathway simplified from Bloch and Kandustch-Russell pathway (http://lipidmaps.org/pathways/vanted.hmtl). Pathway includes key enzymes and metabolites using Mayachemtools (http://myachemtools.org/) to generate a network gml file to be visualized using Vanted[25, 26].

Binding site prediction Potential KLF4 binding sites on selected human and mouse genes were predicted with the use of the weight matrix-based program MATCH[27] to scan the promoter regions of the indicated genes. The promoter regions were defined as -3000 to 500 from the transcriptional start site of the genes. CpG islands were predicted by WashU EPI Genome Browser. Primers were designed according to ENCODE ChIP data.

Intracellular cholesterol and cholesterol efflux measurements Intracellular cholesterol level was measured using a cholesterol fluorometric assay kit from Cayman Chemical. Briefly, macrophages cultured in 6-well plates were lysed with 0.5% Triton X-100 and centrifuged at 13,000 rpm at 4°C for 30 min. Supernatants were then used for the cholesterol measurement. The level of intracellular cholesterol was normalized to the protein concentration of the sample. Cholesterol efflux was measured using Cholesterol Efflux assay kit from Abcam. Briefly, cholesterol was fluorescently labeled and incubated with the isolated peritoneal macrophages (PMs) overnight, HDL was used as the cholesterol acceptor. Fluorescence in the supernatant and cell lysates was measured and

cholesterol efflux was estimated as the percentage ratio of fluorescence intensity in the supernatant to the sum of supernatant and PM lysates.

Peritoneal macrophage isolation Mice were injected with 3% thioglycolate three days prior to sacrifice. PMs were isolated from the mouse peritoneal cavity with PBS. Cells were cultured in DMEM containing 10% fetal bovine serum and 1% penicillin-streptomycin.

Antibodies and reagents Anti-KLF4 and anti-vimentin antibodies were from Cell Signaling; anti-Ch25h, anti-LXRα, anti-β-actin, horseradish peroxide-conjugated anti-mouse and anti-rabbit antibodies were from Santa Cruz; anti-CD31 antibody was from R&D; anti-H3K4me3 and anti-H3K27ac antibodies were from Abcam. 25-HC, and atorvastatin were from Sigma Aldrich.

Cell culture, shear stress, and siRNA knockdown HUVECs were cultured in M199 supplemented with 15% fetal bovine serum, 1 ng/ml recombinant human fibroblast growth factor, 90 μg/ml heparin, 20 mM, HEPES (pH 7.4), and 100 U/ml penicillin-streptomycin. Bovine aortic endothelial cells (BAECs) and PMs were cultured in Dulbecco's modified Eagle's medium (DMEM) supplemented with 10% FBS and 100 U/ml penicillin-streptomycin. A circulating flow system was used to impose shear stress on ECs. The atheroprotective pulsatile shear flow (PS) or atheroprone oscillatory shear flow (OS) generated shear stresses of 12±4 or 1±4 dynes/cm^2, respectively[1]. The flow system was enclosed in a chamber held at 37°C and ventilated with 95% humidified air plus 5% CO_2. For siRNA knockdown, HUVECs were transfected with KLF4 siRNA at 50 nmol/L with

Lipofectamine 2000 (Life Technologies), siRNA sequences can be found below (Table 2.1).

Table 2.1 siRNA sequences used for transfection

Name	Species	Sequence
NC	Homo sapiens Mus musculus	5'-UUCUCCGAACGUGUCACGUTT-3'
KLF4	Homo sapiens	5'-CCAUUACCAAGAGCUCAUGCCACCC-3'
Ch25h	Homo sapiens	5'-CCUUCCACGUGGUCAACAUTT-3'
Ch25h	Mus musculus	5'-GAUGCGCUGUACACUUGAUTT-3'

Reverse-Transcriptase Quantitative PCR (RT-qPCR) Total RNA was isolated from cells or tissue using Trizol (Life Technologies). The extracted RNA was reverse transcribed using Superscript reverse transcriptase (Vazyme), and normalized to GAPDH as the internal control. We normalized qPCR data using $2^{-\Delta CT\ [-(CT\ of\ target\ gene-CT\ of\ reference\ gene)]}$, followed by the $2^{-\Delta CT}$ of each experimental group divided by that of the averaged control groups. Relative mRNA expression was determined using iQ^{TM} SYBR Green PCR supermix (Bio-Rad) in the ABI 7500 Real-time detection system. Primers sequences are shown in below in Table 2.2.

Table 2.2 primers used for RT-qPCR

Name	Species	Sequence
GADPH	Homo sapiens Mus musculus	Forward: ACCACAGTCCATGCCATCAC Reverse: TCCACCACCCTGTTGCTGTA

KLF4	Homo sapiens	Forward: AGAGTTCCCATCTCAAGG Reverse: AATGCCTCTTCATGTGTAAG
KLF4	Mus musculus	Forward: GAACTCACACAGGCGAGAAA Reverse: ATGTGTAAGGCAAGGTGGTC
KLF2	Homo sapiens	Forward: AAGACCTACACCAAGAGTT Reverse: CTACATGTGCCGTTTCAT
Ch25h	Homo sapiens	Forward: ACATGGAGTTCTTCGTGTGG Reverse: CCCAGACGCTCATATACTGC
Ch25h	Mus musculus	Forward: GTAGACATTCAGCGTGGTGT Reverse: ATGTGAGGTTAGAGCCCAGT
LXRα	Homo sapiens	Forward: TCTGGAGACATCTCGGAGGTA Reverse: GGCCCTGGAGAACTCGAAG
LXRβ	Homo sapiens	Forward: CCACGAGACAGAGTGTAT Reverse: GATGTTGATGGCGATGAG
ABCA1	Homo sapiens	Forward: AACTCTACATCTCCCTTCCCG Reverse: CTCCTGTCGCATGTCACTCC
ABCG1	Homo sapiens	Forward: ACTGCAGCATCGTGTACTGGA Reverse: CGTCTCGTCGATGTCACAGTG
SREBP2	Homo sapiens	Forward: CCCTGGGAGACATCGACGA Reverse: CGTTGCACTGAAGGGTCCA
miR-33-5p-RT	Homo sapiens	5'-CTCAACTGGTGTCGTGGAGTCG GCAATTCAGTTGAGTGCAATGC-3'
miR-33-5p	Homo sapiens	Forward:CACTCCAGCTGGGAGTGCATTGTAGTTGC Reverse: CTGGTGTCGTGGAGTCGG
NLRP3	Homo sapiens	Forward: TGCCGGGGCCTCTTTTCAGT Reverse: CCACAGCGCCCCAACCACAA
NLRP3	Mus musculus	Forward: TGTGAGAAGCAGGTTCTACTCT Reverse: GACTGTTGAGGTCCACACTCT
IL-1β	Mus musculus	Forward: ATGAGAGCATCCAGCTTCAA Reverse: TGAAGGAAAAGAAGGTGCTC
COX2	Mus musculus	Forward: CTGACCCCCAAGGCTCAAAT Reverse: TCCATCCTTGAAAAGGCGCA
Gro1	Mus musculus	Forward: GACCATGGCTGGGATTCACC Reverse: CGCGACCATTCTTGAGTGTG
TNFα	Mus musculus	Forward: TGAGCACAGAAAGCATGATCC Reverse: GCCATTTGGGAACTTCTCATC
CCL5	Mus musculus	Forward: GTGCCCACGTCAAGGAGTAT Reverse: CTCTGGGTTGGCACACACTT
iNOS	Mus musculus	Forward: GCTTGCCCCTGGAAGTTTCT Reverse: CCTCACATACTGTGGACGGG
IL-6	Mus musculus	Forward: CGGCCTTCCCTACTTCACAA Reverse: TTCTGCAAGTGCATCATCGT

PPARγ	Mus musculus	Forward:CCACAGTTGATTTCTCCAGCATTTC Reverse: CAGGTTCTACTTTGATCGCACTTTG
Mrc	Mus musculus	Forward: GTGGAGTGATGGAACCCCAG Reverse: CTGTCCGCCCAGTATCCATC
Chil3	Mus musculus	Forward: CCAGCAGAAGCTCTCCAGAAG Reverse: TCAGCTGGTAGGAAGATCCCA
Arg	Mus musculus	Forward: CTTGCGAGACGTAGACCCTG Reverse: CTTCCTTCCCAGCAGGTAGC
Retnla	Mus musculus	Forward: CTGGGATGACTGCTACTGGG Reverse: CAGTGGTCCAGTCAACGAGTA
IL-10	Mus musculus	Forward: TAACTGCACCCACTTCCCAG Reverse: AAGGCTTGGCAACCCAAGTA
SREBP1	Mus musculus	Forward: GCAGCCACCATCTAGCCTG Reverse: CAGCAGTGAGTCTGCCTTGAT
ACC1	Mus musculus	Forward: AGCAGGGACTATGTCCTGAA Reverse: GACTCTCTTCTCCAGAGACA
FASN	Mus musculus	Forward: ACTTGGGTGCTGACTACAAC Reverse: CAGGGAGCTATGGATGATGT

Western blotting Total proteins were isolated using RIPA kit (Pierce Biotechnology, Rockford, IL). and resolved by SDS-PAGE and transferred onto polyvinylidene fluoride (PVDF) membranes. The membranes were immunoblotted with primary and secondary antibodies and visualized using enhanced chemiluminescence (ECL) from Millipore.

Promoter constructs and luciferase reporter assays The 5'-upstream regions of human *Ch25h, LXRα,* and *LXRβ* genes were PCR-amplified using a high fidelity DNA polymerase (Vazyme) with human genomic DNA as the template, primers are shown in Table 2.3. The DNA fragment spanning from (-2205 to -795 bp for Ch25h, -2111 to 1111 bp for LXRα, and -2972 to 992 bp for LXRβ) were subcloned into the pGL3-basic plasmid containing the firefly luciferase reporter gene (Promega), and verified by sequencing. For the Ch25h Site 1 deletion mutant, the region between -913 and 902 bp was omitted. The reporter

plasmids were co-transfected with pRSV-β-gal into BAECs, bovine cells were used in place of human as HUVECs are notorious for limited plasmid transfection efficiency, using lipofectamine 2000 (Life Technologies). Luciferase activities were measured and normalized to β-galactosidase activity at 24 hr post transfection.

Table 2.3 primers used for luciferase construct cloning

Ch25h-FL-luc	Homo sapiens	Forward: CGAggtaccATCTAGAAATCAAAGCAGCA Reverse: ATTacgcgtTCCCAGTGTGTAAAGTACGG
Ch25h-ΔSite 1-luc	Homo sapiens	Forward: GTATCTCAATCACTTAATTCAGCAAACCACCTG Reverse: GAATTAAGTGATTGAGATACAACGGGCTTTTTA
LXRα	Homo sapiens	Forward: TAAggtaccAAATCCAGCTCCTTGCCTGA Reverse: AATgctagcCAGACAGACCAGAGAGCCTT
LXRβ	Homo sapiens	Forward: ACTggtaccGACTCCTTGGTTCAAGAGAT Reverse: TAAgctagcAAAGCTCAGTCTCGGACCGG

Chromatin immunoprecipitation (ChIP) assays ChIP assays were performed according to established protocol using anti-KLF4 (Cell Signaling), anti-H3K4me3 and anti-H3K27ac (Abcam), and anti-rabbit IgG (Santa Cruz). Briefly, ECs were cross-linked with 0.75% formaldehyde at room temp for 10 min and quenched with 125 mM glycine. Cells were lysed in RIPA buffer and sonicated to fragment the DNA to a size of 500-1000 bp. Cell lysates were then incubated with Dynabeads (Invitrogen) conjugated to the indicated antibodies. Immunoprecipitated DNA fragments were reverse cross-linked and DNA binding was quantified as percentage of input using qPCR (see list of primers below (Table 2.4).

Table 2.4 primers used for ChIP assays

Name	Species	Sequence
Ch25h-Site 1	Homo sapiens	Forward: ATCACCTGGTCCTTCAATA Reverse: GCCCGTTGTATCTCAATT
Ch25h-Site 2-4	Homo sapiens	Forward: TGATGAACGTCACACTGCTC Reverse: AAGTGAGAGTGATGCAGGTC
LXRα-Site 1	Homo sapiens	Forward: GGGTCCTGAGGAGTAGAGTG Reverse: CGATACACAGCAAACGCAC
LXRα-Site 2-3	Homo sapiens	Forward: TTAAGTGGCCAGTCATGCAC Reverse: ATGAGCTGCAGAATGAGCGA
LXRα-Site 4-5	Homo sapiens	Forward: TGGTTAACTGACCAAACCC Reverse: CTTTTGCAGCCAGTAGGCTT
LXRβ Site 1	Homo sapiens	Forward: CCGTCCTCATGGCTCATTATA Reverse: CTTGGGCTGTTCACTGTGAT
LXRβ Site 2	Homo sapiens	Forward: TCAAATCTGGCCAGGCACA Reverse: TAGCTGGGATTACAGGTGC
LXRβ Site 3-4	Homo sapiens	Forward: GGGCATGATGGGAGGTGATG Reverse: TTCCAGGTTCAGCCCCTAAA
Ch25h-H3K4me3	Homo sapiens	Forward: TTATTCAAGCTTCGCATCGC Reverse: GAAGAAGGGCGACTGTAGG
Ch25h-H3K4me3	Mus musculus	Forward: TTCTTTAGCAGGGAAAGGGA Reverse: AGCCCACGTAAGTGATGATA
Ch25h-H3K27ac	Homo sapiens	Forward: AATCCTACTTCTTGGCAGGG Reverse: TGTCCAGCCCTTTACTCCTT
Ch25h-H3K27ac	Mus musculus	Forward: AAATGGGAAGAGCCTGAATC Reverse: GTATTTCACAGGTAACCACT

Methylation specific qPCR (MSP) assays Genomic DNA was isolated using QIAamp DNA Mini Kit (Qiagen) from indicated cells or tissues. Bisulfite conversion was processed using EpiTect Bisulfite kit (Qiagen). Following bisulfite conversion, DNA methylation status was quantified by qPCR with primers (listed below in Table 2.5) that specifically recognize the methylated cytosines.

Table 2.5 primers used for MSP assays

UBB	Homo sapiens	Forward: ATAGTGGGTTTTGTTGATTTGA Reverse: CCTTTCTCACACTAAAATTCCA
UBB	Mus musculus	Forward: GATTTAGTAGGTTTTTAAATTTTTATT Reverse: ATACCCTCTTTATCCTAAATCTTAA
Ch25h	Homo sapiens	Forward: ATTTGGTTTTTTAATAGTTTTTCGG Reverse: ACTAAATTTAACTCCCAATCTACGC
Ch25h	Mus musculus	Forward: GGATATTATAAGGATAAGGGAGGC Reverse: CAAAAACTACTTTACGAAAAACGAA

LC-MS/MS The extract of intracellular 25-HC was based on the Bligh-Dyer method with the modification of a secondary aqueous phase extraction to enrich compounds as previously described[2]. Briefly, THP1 cells were treated with Ad-KLF4 or Ad-Null for 72 hr. Cells were washed 3 times and suspended in DPBS. Oxysterols were extracted by adding $CHCl_3$/MeOH (2:1, v/v) containing isotopically labeled 25-HC and BHT (50 μg/mL). Following sonication and centrifugation, the supernatant was collected and dried using a Thermo Savant vacuum concentrator (Thermo Scientific) with the resulting pellet re-suspended in 50 μl MeOH for LC-MS analysis.

The LC-MS analysis was performed on Agilent 1290 Infinity II UPLC system (Agilent Technologies) coupled to an Agilent 6495 triple quadrupole mass spectrometer equipped with an electrospray ionization (ESI) source. The separation was performed on an Agilent Eclipse plus C18 RRHD column (2.1×50 mm, 1.8 μm) at a column temperature

of 35°C. The flow rate was set at 0.3 ml/min and the injection volume was set at 20 μL for each individual analysis.

The mass spectrometer was operated in positive ion mode with an ion spray voltage of 4000 V, nebulizing gas pressure of 35 psi and a heated capillary temperature 350°C. The amount of 25-HC was analyzed using Multiple Reaction Monitoring mode using a precursor ion of 420.3 $[M+NH_4]^+$, product ion of 385.3, collision energy of 25eV and dwell time 200 ms. The acquired data was analyzed by Agilent MassHunter workstation software (version B.07.01) and the concentration of 25-HC was determined using calibration curves of isotopically labeled standard spiked into cell extract at 1, 2.5, 5, 10, 25 and 50 nM.

ApoE$^{-/-}$/Ch25h$^{-/-}$ mouse line and atherosclerosis study Animal protocols were approved by Institutional Animal Care and Use Committee of Xi'an Jiaotong University (No. XJTULAC2014-208). ApoE$^{-/-}$ and Ch25h$^{-/-}$ animals were crossbred to obtain ApoE$^{-/-}$/Ch25h$^{-/-}$ and their ApoE$^{-/-}$/Ch25h$^{+/+}$ littermates. To create atherosclerosis, 6-week-old male ApoE$^{-/-}$/Ch25h$^{-/-}$ and the ApoE$^{-/-}$/Ch25h$^{+/+}$ mice were fed a high-fat, high-cholesterol diet (HFD) containing 21% fat, and 1.5% cholesterol (D12079B from Research Diet). Twelve weeks after the HFD, the aorta was isolated to assess the extent and distribution of atherosclerotic lesions by Oil Red-O staining. Lesion area was measured with ImageJ and expressed as a percentage of the total area of aorta. Plasma levels of total cholesterol, high-density lipoprotein cholesterol, low-density lipoprotein cholesterol, and triglycerides were determined using a kit from Nanjing Jiancheng Bioengineering Institution.

Statistical analysis All data are expressed as mean±SEM. Student's t test was used for comparisons between two groups, or ANOVA for comparisons between multiple groups. If $p<0.05$ after ANOVA analysis, we then used Bonferroni post-hoc to assess the differences between the two indicated groups, with adjusted $p<0.05$ considered to be statistically significant.

Accession numbers Transcriptome data of KLF4 overexpression in HUVECs (GSE90982); Transcriptome data of PMs isolated from $ApoE^{-/-}/Ch25h^{-/-}$ mice (GSE90983).

Results

KLF4 regulates cholesterol metabolic pathways in ECs

Because endothelial homeostasis is manifested by an optimal level of KLF4 in ECs, we performed RNA-sequencing (RNA-seq) to investigate the transcriptional profile of ECs with adenovirus-mediated overexpression of KLF4 (Ad-KLF4) compared to empty vector (Ad-null). Using gene ontology pathway enrichment tools, i.e., Metascape[28], we analyzed the top 300 upregulated genes to infer the modulated biological processes. KLF4 overexpression increased nitric oxide biosynthesis (GO: 0006809), as well as those involved in vascular development and function [e.g., blood vessel morphogenesis (GO: 0048514), circulatory system process (GO: 0003013), and leukocyte migration (GO: 0050900)]. Unexpectedly, KLF4 overexpression also affected response to lipid (GO: 0033993) (Figure 2.2A). Following this initial analysis, we further assessed the KLF4-mediated genes that are associated with lipid regulation. Exhibited in the heat map in Figure 2.2B, cholesterol efflux and oxidation genes were upregulated, whereas the cholesterol biosynthesis genes were downregulated. More specifically, LXRα and LXRβ and their targets [e.g., ABCA1, ABCG1, ApoE, and myosin regulatory light chain interacting protein (MYLIP)] were upregulated, while SREBP2 and its targets (e.g., HMG-CoA reductase and squalene epoxidase) were downregulated. In line with the beneficial effects of KLF4, the expression level of genes involved in EC homeostasis [e.g., peroxisome proliferator activated receptor (PPARα), eNOS, and interleukin (IL)-10] increased and that of pro-inflammatory genes [e.g., NLRP3, monocyte chemoattractant protein (MCP)-1] decreased.

25-HC is not only an agonistic ligand of LXR but also suppresses SREBP2 activation. Thus, the coordinated induction of LXR and suppression of SREBP2 in the RNA-sequencing data suggests that KLF4 might increase the level of 25-HC[20, 21]. Indeed, Ch25h, the enzyme that converts cholesterol to 25-HC, involved in the sterol oxidation KEGG pathway (hsa00120) was upregulated by KLF4 (Figures 2.2B and 2.2C). Figure 2.2C further highlights the Ch25h-mediated switch from cholesterol biosynthesis suppression to activation of cholesterol efflux genes in a cholesterol regulation network. Thus, we concentrated on the role of Ch25h in KLF4-dependent EC homeostasis.

KLF4 transactivates Ch25h in ECs

Given the dual role of 25-HC, we postulated that Ch25h is regulated by KLF4 in ECs, which was validated by the increased expression of Ch25h at both the transcriptional and translational levels in ECs overexpressing KLF4 (Figures 2.3A and 2.3B). By using lung ECs isolated from mice with endothelial-specific KLF4 overexpression or KLF4 knockout (i.e., EC-KLF4-Tg or EC-KLF4-KO, respectively), we inferred whether KLF4 induces Ch25h in endothelium *in vivo*. As expected, the Ch25h mRNA level was significantly lower in ECs from EC-KLF4-KO mice when compared to ECs from EC-KLF4-Tg mice (Figure 2.3C).

Next, we used the bioinformatics tool MATCH to identify 4 putative KLF4 binding sites in the *Ch25h* promoter region and gene body (i.e., -913/902, +607/618, +656/667, and +712/723 bp from the TSS) based on the KLF4 consensus sequence outlined in Figure 2.3D. To implement the *in silico* prediction, we performed chromatin immunoprecipitation (ChIP) assay to examine whether KLF4 can bind to the *Ch25h* gene. As shown in Figure

2.3E, KLF4 overexpression in human umbilical vein endothelial cells (HUVECs) had increased enrichment of KLF4 binding to the *Ch25h* promoter at the Site 1 upstream from the TSS whereas the 3 putative sites within the gene body, between +607/618, +656/667, and +712/723 bp, had no significant KLF4 binding. We then created a plasmid construct (Ch25h-Luc) containing the upstream region of the *Ch25h* promoter fused to the luciferase reporter. KLF4 overexpression increased luciferase activity in ECs transfected with Ch25h-Luc when compared with cells infected with Ad-null (Figure 2.3F). Furthermore, deletion of the region between -913 to -902 bp containing the predicted KLF4 binding Site 1 did not induce luciferase activity (Figure 2.3F), indicating that this region is needed for KLF4 binding and transactivation of *Ch25h*. Because atheroprotective flow is known to increase the expression of KLF4[1, 2], we next investigated whether pulsatile shear stress (PS), which mimics atheroprotective flow *in vitro*, induces Ch25h in ECs, and if so, whether such induction is KLF4-dependent. As shown in Figures 2.3G and 2.3H, the level of KLF4 and Ch25h mRNA and the encoded proteins were all increased by PS, compared to atheroprone flow mimicked by oscillatory shear stress (OS). Conversely, KLF4 knockdown using siRNA decreased PS-induced Ch25h (Figures 2.3I and 2.3J). In sum, these results suggest that PS-induced Ch25h is dependent on KLF4 transactivation in ECs.

PS transcriptionally induces Ch25h through epigenetic regulation

KLF4 has been suggested to facilitate the recruitment of transcriptional machinery even to genes within compact chromatin[29]. With KLF4 transactivation of Ch25h in the context of atheroprotective flow, we next examined the epigenetic modulations involved in such activation of the *Ch25h* gene. Utilizing WashU EpiGenome Browser

(epigenomegateway.wustl.edu/browser), we identified a CpG island located in the *Ch25h* upstream region between -490 and -989 bp (Figure 2.4A). This online available data suggests that the *Ch25h* promoter/enhancer region resembles a euchromatic state in HUVECs, which is revealed by the enrichment of the histone modifications including H3K27ac, H3K4me1, and H3K4me3, as well as increased binding of RNA polymerase II (Pol II) (Figure 2.4A). To investigate whether PS modulates the euchromatic status of this regulatory region, we used methylation-specific qPCR (MSP) to detect DNA methylation and histone-ChIP qPCR to identify the levels of histone markers associated with active transcription (i.e., H3K4me3 and H3K27ac) in the upstream region of the *Ch25h* gene. Compared with OS, PS significantly decreased DNA methylation, but enriched H3K4me3 and H3K27ac in the upstream region (Figures 2.4B-D), indicating that PS rendered an open and active upstream region for the facilitation of the *Ch25h* gene induction. Similar epigenetic modulations were also observed in ECs overexpressing KLF4 (Figure 2.4E-G).

For *in vivo* validation of flow-induced Ch25h, we isolated intima, which contains the endothelium[30, 31], from the aortic arch (AA) and thoracic aorta (TA) of C57BL/6 mice. The flow pattern in AA and TA are atheroprone and atheroprotective, respectively[32]. As shown in Figure 2.4H, the expression of Ch25h mRNA was increased in the TA than that of the AA. Consistently, DNA methylation was reduced while H3K4me3 and H3K27ac were enriched in the *Ch25h* promoter in the TA when compared with the AA (Figures 2.4I-K). Taken together, these data suggest that epigenetic modulations are highly involved in the atheroprotective flow-induced Ch25h via KLF4.

In parallel to atheroprotective flow, vasoprotective drugs (e.g., statins) also induce KLF4[31, 33]. Thus, we postulated that statins may also achieve its pleotropic effects in ECs in part through the increase of Ch25h. Indeed, treating ECs with atorvastatin induced Ch25h transcriptionally and translationally in a KLF4-dependent manner. Such induction was attenuated when KLF4 was knocked down (Figures 2.5A and 2.5B). To study the effects of statins *in vivo*, C57BL/6 mice were intraperitoneally (i.p.) injected with 50 mg/kg atorvastatin for 24 hr. The expression of Ch25h in aorta was significantly increased (Figure 2.5C). The statin-induced Ch25h, like that of PS, also involved the epigenetic changes in the promoter region of the *Ch25h* gene, namely, a decrease in DNA methylation together with an enrichment of active histone marks, H3K4me3 and H3K27ac (Figures 2.5D-F).

KLF4 transactivates LXR

We next investigated whether the KLF4-Ch25h axis activates LXR. As seen in Figures 2.6A and 2.6B, KLF4 overexpression increased the transcription and translation of LXRα. Furthermore, LXRα and its downstream targets, ABCA1 and ABCG1, were found to be reduced in ECs from EC-KLF4-KO when compared to ECs from EC-KLF4-Tg mice (Figures 2.6C and 2.6D). Consistently, KLF4 overexpression upregulated LXRα target genes (i.e., ABCA1 and ABCG1) while Ch25h knockdown attenuated the KLF4 induction of ABCA1 and ABCG1 (Figure 2.6E). With respect to EC inflammatory status, KLF4 overexpression suppressed SREBP2 and NLRP3 expression, while Ch25h knockdown de-repressed these pro-inflammatory mediators (Figure 2.6F).

To identify whether direct activation of LXR using an agonist could rescue the loss of KLF4, we treated lung ECs isolated from EC-KLF4-KO with T0901317. As shown in

Figure 2.7A, T0901317 induced the expression of ABCA1 and ABCG1 to the same level in wild-type and EC-KLF4-KO lung ECs. However, such treatment with LXR agonist reduced the suppression of pro-inflammatory SREBP2 and NLRP3 in EC-KLF4-KO lung ECs (Figure 2.7A). These data further suggest that KLF4 is upstream of LXRα, thus the LXR agonist can restore the anti-inflammatory phenotype seen when KLF4 is knocked out. To investigate the role of endogenous KLF4 in maintaining EC homeostasis in response to lipids, we treated lung ECs from wild-type and EC-KLF4-KO mice with water soluble cholesterol (i.e., cholesterol-methyl-beta-cyclodextrin). In wild-type lung ECs, cholesterol treatment induced the expression of Ch25h, LXRα, ABCA1, ABCG1 (Figure 7B). Cholesterol, as the substrate for Ch25h, could then be converted to 25-HC promoting LXRα expression and cholesterol efflux to maintain EC homeostasis. Conversely, KLF4-KO ECs had reduced induction of Ch25h, LXRα, and LXR downstream targets with or without cholesterol rich conditions (Figure 2.7B). Furthermore, when KLF4-KO ECs were treated with cholesterol, NLRP3 was elevated, suggesting that EC homeostasis could not be maintained and the balance was pushed towards a pro-inflammatory phenotype (Figure 2.7B). As a rescue experiment, we found that NLRP3 inflammasome activity, revealed by IL-18 cleavage, was also suppressed when ECs were treated with 25-HC or T0901317 (Figure 2.7C). However, using KLF4 overexpression to attempt to rescue LXR in ECs isolated from $Ch25h^{-/-}$ mice resulted in induction of LXR, ABCA1, and ABCG1, while SREBP2 and NLRP3 remained unchanged (Figure 2.7D). These results are consistent with the siRNA knockdown experiments in Figures 2.6E and 2.6F, which suggest the causality among KLF4 and Ch25h. To further evaluate whether the beneficial role of KLF4 is

dependent on LXR, we overexpressed KLF4 in ECs and then treated with GSK 2033 (an LXR antagonist). GSK 2033 caused the blockade of ABCA1, ABCG1, eNOS, while elevating NLRP3 (Figure 2.7E). In sum, these data suggest that KLF4-mediated EC homeostasis is dependent on both Ch25h and LXR.

Using MATCH, we predicted the presence of several putative KLF4 binding sites located in the promoter region of the *LXRα* gene (Figure 2.8A), suggesting that KLF4 may directly transactivate *LXRα*. Using ChIP assays, we demonstrated that KLF4 overexpression resulted in KLF4 enrichment in the *LXRα* promoter (Figure 2.8B). Further validation using luciferase reporters determined that KLF4 overexpression increased luciferase activity, which indicated KLF4 transactivation of LXRα (Figure 2.8C). Given that PS transcriptionally upregulates LXRα[34], we next demonstrated that KLF4 knockdown with siRNA attenuated PS-induced LXRα (Figure 2.8D). For *in vivo* relevance, we found that LXRα, ABCA1, and ABCG1 expression was augmented in TA when compared to AA (Figure 2.8E). ECs express both LXRα and LXRβ[35]. Noticeably, KLF4 regulated LXRβ in a similar manner as that of LXRα (Figure 2.9). Collectively, data in Figures 2.6-2.9 suggest that PS-induced KLF4 upregulates ABCA1 and ABCG1 in ECs, which is dependent on Ch25h and LXR.

KLF4-Ch25h/LXR promotes macrophage polarization

The atheroprotective role of KLF4 is not only due to its effects in ECs, but also in circulating monocytes and resident macrophages in the vessel wall[6, 7]. To examine whether KLF4 regulation of Ch25h and LXR is common in macrophages, we overexpressed KLF4

in a mouse macrophage cell line (i.e., RAW264.7 cells). The expression of Ch25h, LXRα, LXRβ, ABCA1, and ABCG1 were all increased (Figure 2.10A). Furthermore, LC-MS/MS data suggested that intracellular concentration of 25-HC was increased in cultured THP-1 monocytes overexpressing KLF4 (Figure 2.10B). Treating bone marrow-derived macrophages (BMDMs) with 25-HC resulted in a temporal suppression of SREBP2 and its downstream targets in cholesterol biosynthesis as well as increased Ch25h and LXR targets[36]. Further analysis of these mined data demonstrates that 25-HC also decreased the expression of those involved in NLRP3 inflammasome (i.e., NLRP3, ASC, IL-1β and IL-18) and pro-inflammatory M1 pathways [i.e., IL-6, TNFα, Gro1, and cyclooxygenase-2 (COX2)], while increased those anti-inflammatory M2 markers [i.e., mannose receptor, C type 1 (Mrc1), arginase-1 (Arg1)] (Figure 2.10C). In light of these analyses and because KLF4 overexpression in macrophages leads to the M1-to-M2 transition[5], we investigated the causative effect of Ch25h-25-HC in the KLF4-mediated macrophage polarization. When RAW264.7 cells were treated with 25-HC, we validated that the mRNA expression of pro-inflammatory genes (e.g., NLRP3, IL-1β) and M1 marker genes [i.e., COX2, TNFα, chemokine (C-C motif) ligand 5 (CCL5), inducible nitric oxide synthase (iNOS), and IL-6] were suppressed while those of the M2 marker genes [i.e., peroxisome proliferator-activated receptor γ (PPARγ), Mrc1, chitinase-like 3 (chil3), Arg1, resistin like alpha (retnla), and IL-10] were increased (Figure 2.10D). In contrast, Ch25h knockdown in RAW264.7 cells increased the expression of the aforementioned pro-inflammatory and M1 marker genes while decreased the mRNA levels of the M2 marker genes when compared with the control siRNA (Figure 2.10E). To further examine the role of Ch25h in

macrophage polarization *in vivo*, we isolated peritoneal macrophages (PMs) from Ch25h$^{-/-}$ mice and their Ch25h$^{+/+}$ littermates. As seen in Figures 2.10F-2.10H, reduced expression of LXR and LXR targets, increased expression of SREBP and SREBP downstream, a higher total cholesterol content, and decreased cholesterol efflux were found in Ch25h$^{-/-}$ macrophages, when compared with those in Ch25h$^{+/+}$ littermates. In addition, Ch25h$^{-/-}$ macrophages showed increased levels of inflammatory and M1 markers while suppressing M2 markers (Figure 2.10I). As a rescue experiment, Ch25h$^{-/-}$ macrophages co-incubated with 25-HC exhibited decreased expression of inflammatory and M1 markers while increasing the expression of M2 markers (Figure 2.10J).

Similar to ECs, LXR agonist was able to induce the expression of ABCA1 and ABCG1 in peritoneal macrophages (PMs) isolated from myeloid-specific KLF4-KO (mye-KLF4-KO) mice (Figure 2.11A). We also examined the role of endogenous KLF4 in macrophages under cholesterol rich conditions by treating PMs isolated from mye-KLF4-KO or wild-type mice with cholesterol. Results shown in Figure 2.11B demonstrated that KLF4 ablation led to reduced cholesterol efflux and enhanced pro-inflammatory status in PMs. These data suggest that KLF4 may have analogous atheroprotective functions in both ECs and macrophages. Correspondingly, KLF4-mediated M2 markers were inhibited while M1 markers were de-suppressed when macrophages were treated with an LXR antagonist (Figure 2.11C). Furthermore, KLF4 overexpression in Ch25h$^{-/-}$ macrophages resulted in incremental induction of LXR and LXR downstream targets (Figure 2.11D), similar to the rescue experiment performed in Ch25h$^{-/-}$ ECs (Figure 2.7D). Collectively, Figures 2.10-2.11 demonstrated that KLF4 substantially induced Ch25h and LXR in

macrophages, similar to that in ECs. Functionally, such induction promoted M2 polarization and regulated cholesterol content in part through augmented RCT.

Ch25h ablation increases atherosclerosis susceptibility

Because of the involvement of Ch25h-25-HC in functional endothelium and anti-inflammatory phenotype in macrophages, we utilized $Ch25h^{-/-}$ mice to investigate the comprehensive role of Ch25h in atherosclerosis. We introduced $ApoE^{-/-}$ background into $Ch25h^{-/-}$ mice to promote atherosclerotic lesion development. RNA-seq was performed to confirm the pro-inflammatory status and M2 to M1 phenotype in PMs isolated from the $ApoE^{-/-}/Ch25h^{-/-}$ mice. As shown in Figure 2.12A, while Ch25h and LXRα were decreased, the pro-inflammatory CCL5, iNOS, IL-1β, were increased in these PMs. Feeding 12 weeks of an atherogenic diet, the mean lesion area in the aortic root, where the blood flow pattern is most disturbed[30], was ~1.9-fold larger for $ApoE^{-/-}/Ch25h^{-/-}$ mice than $ApoE^{-/-}/Ch25h^{+/+}$ littermates ($89.7 \pm 36.1\ \mu m^2x10^3$ vs. $45.0 \pm 32.3\ \mu m^2x10^3$, respectively) (Figure 2.12B). Additionally, H&E staining revealed increased cell density which was largely composed of infiltrating macrophages demonstrated by MAC1 staining as well as decreased CD31 staining (Figure 2.12B). *En face* Oil Red-O staining revealed that the mean lesion area in the thoracic aorta and that of aortic arch was also augmented for $ApoE^{-/-}/Ch25h^{-/-}$ than $ApoE^{-/-}/Ch25h^{+/+}$ mice ($19.5 \pm 8.5\%$ vs. $10.1 \pm 4.1\%$ and $44.1 \pm 9.0\%$ vs. $29.7 \pm 9.6\%$, respectively; n=13/group) (Figure 2.12C). The total lesion area, expressed as the sum of aortic arch, thoracic aorta, and abdominal aorta remained greater for $ApoE^{-/-}/Ch25h^{-/-}$ when compared to the $ApoE^{-/-}/Ch25h^{+/+}$ littermates ($24.5 \pm 7.3\%$ vs. $13.9 \pm 5.0\%$) (Figure 2.12C). Thus, the systemic ablation of Ch25h plays a critical role in accelerated atherosclerosis.

Discussion

The current study encompassing research on both ECs and macrophages provides experimental evidence of the atheroprotective role of KLF4 via the induction of Ch25h and LXR. Initially, RNA-seq data revealed that KLF4, through transactivating Ch25h and LXR, is a novel mediator of cholesterol homeostasis in ECs in addition to its canonical role in nitric oxide biosynthesis, blood vessel, and circulatory system processes[37,38]. Microarray data from 25-HC-treated BMDMs (Figure 2.10C) and from PMs isolated from the $ApoE^{-/-}$ /$Ch25h^{-/-}$ mice (Figure 2.12A) indicated that 25-HC, the catalytic product of Ch25h, was essential to preserve the M2 macrophage polarization. Because Ch25h and LXR are critically involved in the cross-talk between the immune system and cholesterol metabolism[39], KLF4 plays an important role in maintaining vascular homeostasis through its regulation of Ch25h and LXR. The implication of this finding at the disease level is that increased atherosclerosis susceptibility is a common phenotype between $ApoE^{-/-}$/$Ch25h^{-/-}$ (Figure 2.12) and $ApoE^{-/-}$ mice with KLF4 or LXR ablation in the endothelium or macrophages[16,19,40]. Given atherosclerosis is a multifaceted vascular impairment composed of several cell types including ECs and macrophages[41], the atheroprone phenotype among these mouse lines suggests that the KLF4-Ch25h/LXR axis in ECs and macrophages acts synergistically, which is atheroprotective *in vivo*.

Serving as a ligand to LXR while inhibiting SREBP2 activation, 25-HC maintains a balance between cholesterol efflux and cholesterol biosynthesis[11]. Cholesterol efflux, regulated by LXR downstream targets such as ABCA1 and ABCG1, is known to be influenced by the innate immune response in macrophages[42]. Furthermore, upregulated

SREBP is associated with unresolved innate immunity, leading to inflammasome activation in both ECs and macrophages[15,43]. Here, we further defined that KLF4 regulates a counterbalance between LXR and SREBP via the regulation of Ch25h-25-HC. Although, endogenous KLF4 may be supplemental in mitigating LXR responses as target gene expression remains intact even with the loss of KLF4 (Figures 2.7A and 2.11A). In addition to the beneficial role in regulating LXR and SREBP, 25-HC exerts anti-viral effects through inhibiting viral particle uptake[11] and activates integrated stress response (ISR) genes to reprogram transcription and translation[35]. However, the anti-inflammatory role of 25-HC remains somewhat controversial as others have indicated that the oxysterol promotes macrophage foam cell formation and is increased in atherosclerotic lesions[44]. Such contradiction may be due, in part, to the differences in experimental conditions and requires further investigation.

Endothelial and macrophage homeostasis relies on an optimal level of KLF4, which can be induced by both physiological and pharmacological stimuli such as shear stress and statins[44]. At the tissue level, KLF4 overexpression in the endothelium is atheroprotective[6]. If statin can activate KLF4 in the endothelium *in vivo*, the consequent induction of Ch25h and LXR would be one of the pleotropic effects of statin therapy. KLF4 also mediates macrophage polarization as KLF4 is drastically induced in M2 macrophages but significantly reduced in M1 macrophages[5]. Phenotypically, mice with myeloid KLF4 deficiency are characterized by increased bactericidal activity and delayed wound healing, signifying M1 polarization[5]. Collectively, our data support that Ch25h-25-HC play a major

role in the vascular beneficial effects caused by physiological and pharmacological stimuli (e.g., PS and statins) that activate KLF4.

Regarding stimuli which downregulate KLF4 in the vasculature, we and others have previously shown that oxidative and inflammatory burdens, exemplified by oxLDL, angiotensin II, and hydrogen peroxide, activate the SREBP2-miR-92a axis, which in turn suppresses KLF4 in ECs[47]. Thus, under atherogenic conditions, the KLF4 level is likely to be reduced in both the endothelium and macrophages via SREBP2-miR-92a. Noticeably, KLF4 overexpression not only increased the level of Ch25h and LXR, but also reduced SREBP2 (Figure 2.6F). Given that SREBP2 has an intronic microRNA, miR-33, that targets ABCA1 and ABCG1[48], aberrant KLF4 expression may feed forward to further downregulate RCT. Furthermore, single and double ablation of mouse *abca1* and *abcg1* specifically in the endothelium are pro-atherogenic, not only through the reduction in RCT but also through the perturbation of eNOS[49]. In conjunction with the current study, the suggested mechanisms constitute a regulatory network linking endothelial dysfunction and macrophage polarization, which aggravates atherosclerosis (see Figure 2.13).

In a collaborating project led by Dr. Ming He, KLF4 has also been demonstrated to mitigate other vascular diseases such as Kawasaki disease (KD)[50]. KD is a systemic vasculitis that results in coronary artery abnormalities and the most common cause of acquired heart disease in pediatric patients[51], however the cause of this disease remains a mystery. Sera isolated from KD patients indicates increased levels of the circulating pro-fibrotic marker connective tissue growth factor (CTGF) (Figure 2.14A). Furthermore, by using cultured ECs treated with sera from KD patients, we found that KLF4 expression

was suppressed while CTGF was induced (Figures 2.14B and 2.14C). CTGF lies downstream of the TGFβ pathway and is a known marker of endothelial-to-mesenchymal transition (EndoMT)[52]. Because of the inverse relationship between KLF4 and CTGF, we hypothesized that microRNA (miR) may be involved in the regulation. miR-483 is intronic to the parent gene IGF2, which was found to be transcriptionally regulated by KLF4, and was predicted to target the 3'-UTR of CTGF[50]. Indeed, overexpression of miR-483 suppressed KD-induced CTGF and markers of EndoMT (Figures 2.14D and 2.14E). Atorvastatin, a clinical lipid lowering medication, is known to have pleotropic effects to benefit vascular tone and can induce KLF4 in ECs[53]. KD patients enrolled in a Phase I/IIa clinical trial (Unique Identifier: NCT01431105) were administered atorvastatin in addition to the currently approved treatment. Serum levels of CTGF reduced following atorvastatin treatment when compared to standard treatment (Figure 2.14F). In contrast, circulating miR-483 levels were increased in atorvastatin treated patients (Figure 2.14F). Collectively, KLF4-mediated miR-483 was found to be suppressed in KD thereby promoting the expression of CTGF and EndoMT. However, if KLF4 expression could be rescued, via atorvastatin, we could reverse the induction of CTGF and protect the endothelium.

In summary, these studies identify that KLF4 is a mediator of miR-483 as well as Ch25h and LXR in both ECs and macrophages. As atherogenesis includes dysfunctional endothelium as well as M1 polarized macrophages with attendant decrease of KLF4, we suggest that the congruent KLF4-Ch25h/LXR axis in both cell types is anti-atherogenic. KD-induced vasculitis, specifically relating to EC dysfunction, KLF4 was also found to promote the suppression EndoMT via miR-483 targeting of CTGF.

References

1. Ohnesorge N, Viemann D, Schmidt N, Czymai T, Spiering D, Schmolke M, Ludwig S, Roth J, Goebeler M and Schmidt M. Erk5 activation elicits a vasoprotective endothelial phenotype via induction of Kruppel-like factor 4 (KLF4). J Biol Chem. 2010;285:26199-210.

2. Clark PR, Jensen TJ, Kluger MS, Morelock M, Hanidu A, Qi Z, Tatake RJ and Pober JS. MEK5 is activated by shear stress, activates ERK5 and induces KLF4 to modulate TNF responses in human dermal microvascular endothelial cells. Microcirculation. 2011;18:102-17.

3. Shen B, Smith RS, Jr., Hsu YT, Chao L and Chao J. Kruppel-like factor 4 is a novel mediator of Kallistatin in inhibiting endothelial inflammation via increased endothelial nitric-oxide synthase expression. J Biol Chem. 2009;284:35471-8.

4. Chiplunkar AR, Curtis BC, Eades GL, Kane MS, Fox SJ, Haar JL and Lloyd JA. The Kruppel-like factor 2 and Kruppel-like factor 4 genes interact to maintain endothelial integrity in mouse embryonic vasculogenesis. BMC developmental biology. 2013;13:40.

5. Liao X, Sharma N, Kapadia F, Zhou G, Lu Y, Hong H, Paruchuri K, Mahabeleshwar GH, Dalmas E, Venteclef N, Flask CA, Kim J, Doreian BW, Lu KQ, Kaestner KH, Hamik A, Clement K and Jain MK. Kruppel-like factor 4 regulates macrophage polarization. J Clin Invest. 2011;121:2736-49.

6. Zhou G, Hamik A, Nayak L, Tian H, Shi H, Lu Y, Sharma N, Liao X, Hale A, Boerboom L, Feaver RE, Gao H, Desai A, Schmaier A, Gerson SL, Wang Y, Atkins GB, Blackman BR, Simon DI and Jain MK. Endothelial Kruppel-like factor 4 protects against atherothrombosis in mice. J Clin Invest. 2012;122:4727-31.

7. Sharma N, Lu Y, Zhou G, Liao X, Kapil P, Anand P, Mahabeleshwar GH, Stamler JS and Jain MK. Myeloid KLF4 deficiency augments atherogenesis in ApoE-/- mice. Arteriosclerosis, thrombosis, and vascular biology. 2012;32:2836-2838.

8. Tuong ZK, Lau P, Du X, Condon ND, Goode JM, Oh TG, Yeo JC, Muscat GE and Stow JL. RORalpha and 25-Hydroxycholesterol Crosstalk Regulates Lipid Droplet Homeostasis in Macrophages. PLoS One. 2016;11:e0147179.

9. Bauman DR, Bitmansour AD, McDonald JG, Thompson BM, Liang G and Russell DW. 25-Hydroxycholesterol secreted by macrophages in response to Toll-like receptor activation suppresses immunoglobulin A production. Proc Natl Acad Sci U S A. 2009;106:16764-9.

10. Blanc M, Hsieh WY, Robertson KA, Kropp KA, Forster T, Shui G, Lacaze P, Watterson S, Griffiths SJ, Spann NJ, Meljon A, Talbot S, Krishnan K, Covey DF, Wenk MR, Craigon M, Ruzsics Z, Haas J, Angulo A, Griffiths WJ, Glass CK, Wang Y and Ghazal P. The transcription factor STAT-1 couples macrophage synthesis of 25-hydroxycholesterol to the interferon antiviral response. Immunity. 2013;38:106-18.

11. Cyster JG, Dang EV, Reboldi A and Yi T. 25-Hydroxycholesterols in innate and adaptive immunity. Nat Rev Immunol. 2014;14:731-43.

12. Liu SY, Aliyari R, Chikere K, Li G, Marsden MD, Smith JK, Pernet O, Guo H, Nusbaum R, Zack JA, Freiberg AN, Su L, Lee B and Cheng G. Interferon-inducible cholesterol-25-hydroxylase broadly inhibits viral entry by production of 25-hydroxycholesterol. Immunity. 2013;38:92-105.

13. Reboldi A, Dang EV, McDonald JG, Liang G, Russell DW and Cyster JG. Inflammation. 25-Hydroxycholesterol suppresses interleukin-1-driven inflammation downstream of type I interferon. Science. 2014;345:679-84.

14. Dushkin MI. Macrophage/foam cell is an attribute of inflammation: mechanisms of formation and functional role. Biochemistry Biokhimiia. 2012;77:327-38.

15. Xiao H, Lu M, Lin TY, Chen Z, Chen G, Wang WC, Marin T, Shentu TP, Wen L, Gongol B, Sun W, Liang X, Chen J, Huang HD, Pedra JH, Johnson DA and Shyy JY. Sterol regulatory element binding protein 2 activation of NLRP3 inflammasome in endothelium mediates hemodynamic-induced atherosclerosis susceptibility. Circulation. 2013;128:632-42.

16. Schuster GU. Accumulation of Foam Cells in Liver X Receptor-Deficient Mice. Circulation. 2002;106:1147-1153.

17. Hayashi T, Kotani H, Yamaguchi T, Taguchi K, Iida M, Ina K, Maeda M, Kuzuya M, Hattori Y and Ignarro LJ. Endothelial cellular senescence is inhibited by liver X receptor activation with an additional mechanism for its atheroprotection in diabetes. Proc Natl Acad Sci U S A. 2014;111:1168-73.

18. Joseph SB, McKilligin E, Pei L, Watson MA, Collins AR, Laffitte BA, Chen M, Noh G, Goodman J, Hagger GN, Tran J, Tippin TK, Wang X, Lusis AJ, Hsueh WA, Law RE, Collins JL, Willson TM and Tontonoz P. Synthetic LXR ligand inhibits the development of atherosclerosis in mice. Proc Natl Acad Sci U S A. 2002;99:7604-9.

19. Tangirala RK, Bischoff ED, Joseph SB, Wagner BL, Walczak R, Laffitte BA, Daige CL, Thomas D, Heyman RA, Mangelsdorf DJ, Wang X, Lusis AJ, Tontonoz P and Schulman IG. Identification of macrophage liver X receptors as inhibitors of atherosclerosis. Proc Natl Acad Sci U S A. 2002;99:11896-901.

20. Adams CM, Reitz J, De Brabander JK, Feramisco JD, Li L, Brown MS and Goldstein JL. Cholesterol and 25-hydroxycholesterol inhibit activation of SREBPs by different mechanisms, both involving SCAP and Insigs. J Biol Chem. 2004;279:52772-80.

21. Lehmann JM, Kliewer SA, Moore LB, Smith-Oliver TA, Oliver BB, Su JL, Sundseth SS, Winegar DA, Blanchard DE, Spencer TA and Willson TM. Activation of the nuclear receptor LXR by oxysterols defines a new hormone response pathway. J Biol Chem. 1997;272:3137-40.

22. Kim D, Pertea G, Trapnell C, Pimentel H, Kelley R and Salzberg SL. TopHat2: accurate alignment of transcriptomes in the presence of insertions, deletions and gene fusions. Genome biology. 2013;14:R36.

23. Roberts A, Trapnell C, Donaghey J, Rinn JL and Pachter L. Improving RNA-Seq expression estimates by correcting for fragment bias. Genome biology. 2011;12:R22.

24. Trapnell C, Williams BA, Pertea G, Mortazavi A, Kwan G, van Baren MJ, Salzberg SL, Wold BJ and Pachter L. Transcript assembly and quantification by RNA-Seq reveals unannotated transcripts and isoform switching during cell differentiation. Nature biotechnology. 2010;28:511-5.

25. Rohn H, Junker A, Hartmann A, Grafahrend-Belau E, Treutler H, Klapperstuck M, Czauderna T, Klukas C and Schreiber F. VANTED v2: a framework for systems biology applications. BMC systems biology. 2012;6:139.

26. Maurya MR, Gupta S, Li X, Fahy E, Dinasarapu AR, Sud M, Brown HA, Glass CK, Murphy RC, Russell DW, Dennis EA and Subramaniam S. Analysis of inflammatory and lipid metabolic networks across RAW264.7 and thioglycolate-elicited macrophages. Journal of lipid research. 2013;54:2525-42.

27. Kel AE, Gossling E, Reuter I, Cheremushkin E, Kel-Margoulis OV and Wingender E. MATCH: A tool for searching transcription factor binding sites in DNA sequences. Nucleic acids research. 2003;31:3576-9.

28. Tripathi S, Pohl MO, Zhou Y, Rodriguez-Frandsen A, Wang G, Stein DA, Moulton HM, DeJesus P, Che J, Mulder LC, Yanguez E, Andenmatten D, Pache L, Manicassamy B, Albrecht RA, Gonzalez MG, Nguyen Q, Brass A, Elledge S, White M, Shapira S, Hacohen N, Karlas A, Meyer TF, Shales M, Gatorano A, Johnson JR, Jang G, Johnson T, Verschueren E, Sanders D, Krogan N, Shaw M, Konig R, Stertz S, Garcia-Sastre A and Chanda SK. Meta- and Orthogonal Integration of Influenza "OMICs" Data Defines a Role for UBR4 in Virus Budding. Cell host & microbe. 2015;18:723-35.

29. Soufi A, Garcia MF, Jaroszewicz A, Osman N, Pellegrini M and Zaret KS. Pioneer transcription factors target partial DNA motifs on nucleosomes to initiate reprogramming. Cell. 2015;161:555-68.

30. Assemat P, Armitage JA, Siu KK, Contreras KG, Dart AM, Chin-Dusting JP and Hourigan K. Three-dimensional numerical simulation of blood flow in mouse aortic arch around atherosclerotic plaques. Applied Mathematical Modelling. 2014;38:4175-4185.

31. Yoshida T, Yamashita M, Iwai M and Hayashi M. Endothelial Kruppel-Like Factor 4 Mediates the Protective Effect of Statins against Ischemic AKI. Journal of the American Society of Nephrology : JASN. 2016;27:1379-88.

32. Chiu JJ and Chien S. Effects of Disturbed Flow on Vascular Endothelium: Pathophysiological Basis and Clinical Perspectives. Physiological reviews. 2011;91(1):327-87.

33. Maejima T, Inoue T, Kanki Y, Kohro T, Li G, Ohta Y, Kimura H, Kobayashi M, Taguchi A, Tsutsumi S, Iwanari H, Yamamoto S, Aruga H, Dong S, Stevens JF, Poh HM, Yamamoto K, Kawamura T, Mimura I, Suehiro J, Sugiyama A, Kaneki K, Shibata H, Yoshinaka Y, Doi T, Asanuma A, Tanabe S, Tanaka T, Minami T, Hamakubo T, Sakai J, Nozaki N, Aburatani H, Nangaku M, Ruan X, Tanabe H, Ruan Y, Ihara S, Endo A, Kodama T and Wada Y. Direct evidence for pitavastatin induced chromatin structure change in the KLF4 gene in endothelial cells. PLoS One. 2014;9:e96005.

34. Zhu M, Fu Y, Hou Y, Wang N, Guan Y, Tang C, Shyy JY and Zhu Y. Laminar shear stress regulates liver X receptor in vascular endothelial cells. Arterioscler Thromb Vasc Biol. 2008;28:527-33.

35. Calkin AC and Tontonoz P. Liver x receptor signaling pathways and atherosclerosis. Arterioscler Thromb Vasc Biol. 2010;30:1513-8.

36. Shibata N, Carlin AF, Spann NJ, Saijo K, Morello CS, McDonald JG, Romanoski CE, Maurya MR, Kaikkonen MU, Lam MT, Crotti A, Reichart D, Fox JN, Quehenberger O, Raetz CRH, Sullards MC, Murphy RC, Merrill AH, Brown HA, Dennis EA, Fahy E, Subramaniam S, Cavener DR, Spector DH, Russell DW and Glass CK. 25-Hydroxycholesterol Activates the Integrated Stress Response to Reprogram Transcription and Translation in Macrophages. The Journal of Biological Chemistry. 2013;288:35812-35823.

37. Kunes P, Holubcova Z and Krejsek J. Occurrence and significance of the nuclear transcription factor Kruppel-like factor 4 (KLF4) in the vessel wall. Acta medica (Hradec Kralove). 2009;52:135-9.

38. Yoshida T and Hayashi M. Role of Kruppel-like factor 4 and its binding proteins in vascular disease. Journal of atherosclerosis and thrombosis. 2014;21:402-13.

39. Simon A. Cholesterol metabolism and immunity. The New England journal of medicine. 2014;371:1933-5.

40. Bradley MN, Hong C, Chen M, Joseph SB, Wilpitz DC, Wang X, Lusis AJ, Collins A, Hseuh WA, Collins JL, Tangirala RK and Tontonoz P. Ligand activation of LXR beta reverses atherosclerosis and cellular cholesterol overload in mice lacking LXR alpha and apoE. J Clin Invest. 2007;117:2337-46.

41. Glass CK and Witztum JL. Atherosclerosis. the road ahead. Cell. 2001;104:503-16.

42. Tall AR and Yvan-Charvet L. Cholesterol, inflammation and innate immunity. Nat Rev Immunol. 2015;15:104-16.

43. Im SS, Yousef L, Blaschitz C, Liu JZ, Edwards RA, Young SG, Raffatellu M and Osborne TF. Linking lipid metabolism to the innate immune response in macrophages through sterol regulatory element binding protein-1a. Cell Metab. 2011;13:540-9.

44. Gold ES, Ramsey SA, Sartain MJ, Selinummi J, Podolsky I, Rodriguez DJ, Moritz RL and Aderem A. ATF3 protects against atherosclerosis by suppressing 25-hydroxycholesterol-induced lipid body formation. J Exp Med. 2012;209:807-17.

45. Villarreal G, Jr., Zhang Y, Larman HB, Gracia-Sancho J, Koo A and Garcia-Cardena G. Defining the regulation of KLF4 expression and its downstream transcriptional targets in vascular endothelial cells. Biochemical and biophysical research communications. 2010;391:984-9.

46. Basu P, Sargent TG, Redmond LC, Aisenberg JC, Kransdorf EP, Wang SZ, Ginder GD and Lloyd JA. Evolutionary conservation of KLF transcription factors and functional conservation of human gamma-globin gene regulation in chicken. Genomics. 2004;84:311-9.

47. Chen Z, Wen L, Martin M, Hsu CY, Fang L, Lin FM, Lin TY, Geary MJ, Geary GG, Zhao Y, Johnson DA, Chen JW, Lin SJ, Chien S, Huang HD, Miller YI, Huang PH and Shyy JY. Oxidative stress activates endothelial innate immunity via sterol regulatory element binding protein 2 (SREBP2) transactivation of microRNA-92a. Circulation. 2015;131:805-14.

48. Rayner KJ, Suarez Y, Davalos A, Parathath S, Fitzgerald ML, Tamehiro N, Fisher EA, Moore KJ and Fernandez-Hernando C. MiR-33 contributes to the regulation of cholesterol homeostasis. Science. 2010;328:1570-3.

49. Westerterp M, Tsuchiya K, Tattersall IW, Fotakis P, Bochem AE, Molusky MM, Ntonga V, Abramowicz S, Parks JS, Welch CL, Kitajewski J, Accili D, Tall AR. Deficiency of ATP-binding cassette transporters A1 and G1 in endothelial cells accelerates atherosclerosis in mice. ATVB. 2016;36(7):1328-37.

50. He M, Chen Z, Martin M, Zhang J, Sangwung P, Woo B, Tremoulet A, Shimizu C, Jain MK, Burns JC and Shyy J. miR-483 Targeting of CTGF Suppresses Endothelial-to-Mesenchymal Transition: Therapeutic Implications in Kawasaki Disease. *Circulation research*. 2016.

51. Uehara R and Belay ED. Epidemiology of Kawasaki disease in Asia, Europe, and the United States. *Journal of epidemiology*. 2012;22:79-85.

52. Piera-Velazquez S, Mendoza FA and Jimenez SA. Endothelial to Mesenchymal Transition (EndoMT) in the Pathogenesis of Human Fibrotic Diseases. *Journal of clinical medicine*. 2016;5.

53. Liao JK and Laufs U. PLEIOTROPIC EFFECTS OF STATINS. Annual review of pharmacology and toxicology. 2005;45:89-118.

Figures

A

Samples	# Reads	# Retained reads	# Reads mapped to genome	Percentage of reads mapped to genome
Ad-null-1	13,329,096	12,425,264	10,670,216	80.05%
Ad-KLF4-1	13,406,131	12,488,392	10,603,629	79.10%
Ad-null-2	20,038,657	18,850,053	15,752,381	78.61%
Ad-KLF4-2	17,303,238	16,284,745	14,008,566	80.96%

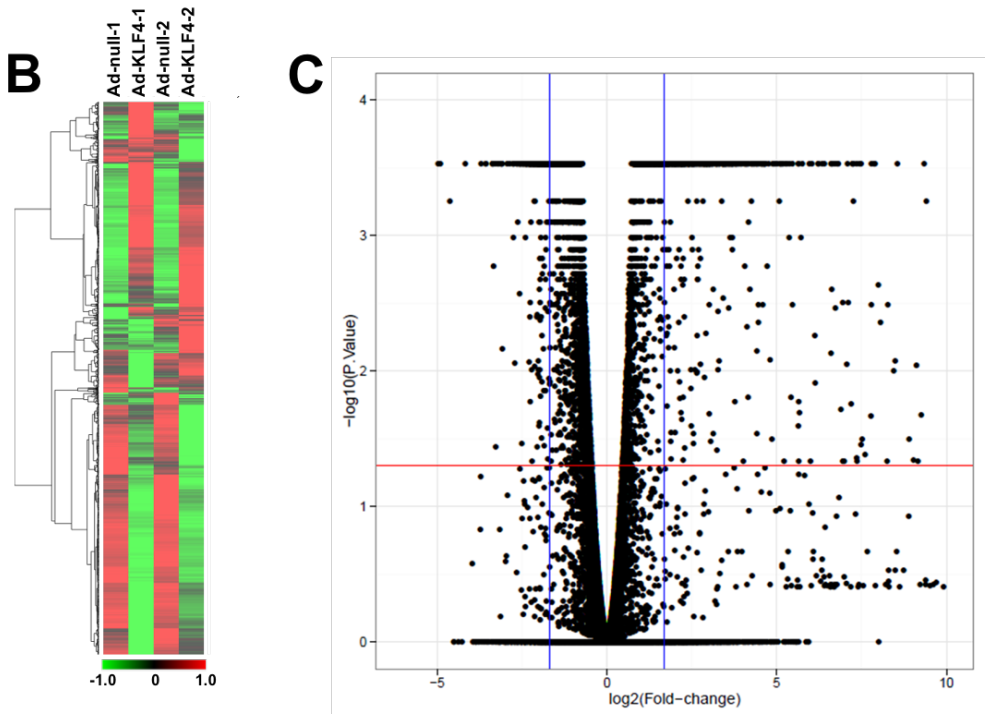

Figure 2.1. Overall RNA-seq statistics and mapping for KLF4 overexpression. (**A**) Mapping statistics of Ad-KLF4 vs Ad-null RNA-seq data demonstrating that more than 75% of reads were mapped to the genome. **(B)** A genome-wide RNA-seq heat map illustrating the selected genes with at least 3 RPKM were used for hierarchical clustering using Z-score. **(C)** Volcano plot indicating the thresholds shown as solid lines (red=q-value of <0.05 and blue=absolute log2 fold change ≥1.75).

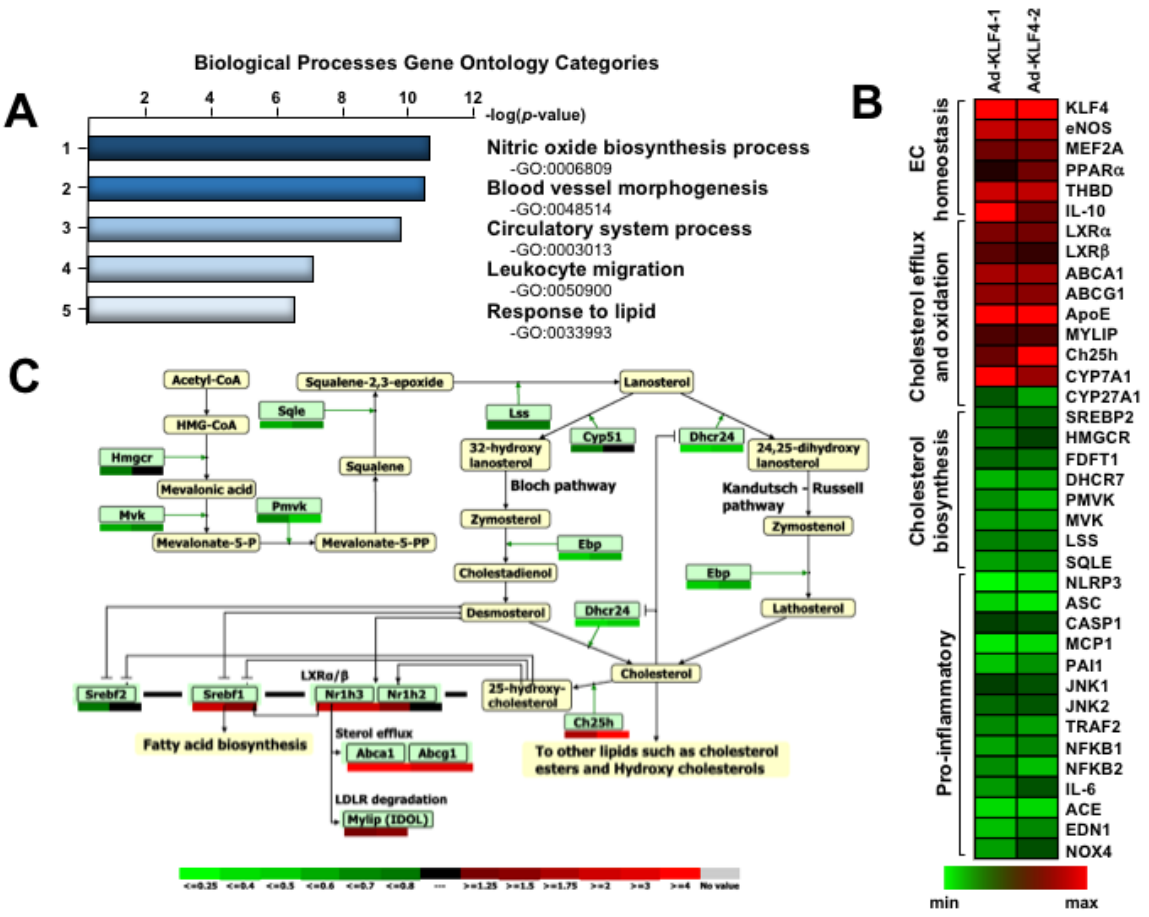

Figure 2.2. KLF4 regulates cholesterol metabolism in ECs. (A-C) HUVECs were infected with Ad-KLF4 or Ad-null for 48 hr prior to RNA isolation followed by RNA-seq analysis. Data presented are results from two biological repeats (Ad-KLF4 divided by Ad-null). (A) Gene ontology (GO) enrichment using Metascape of the top 300 upregulated genes plotted as -log(p-value). (B) Heat map comparison of Ad-null versus Ad-KLF4 using log2 fold changes of the indicated genes. (C) Network projection of customized sterol metabolism pathway.

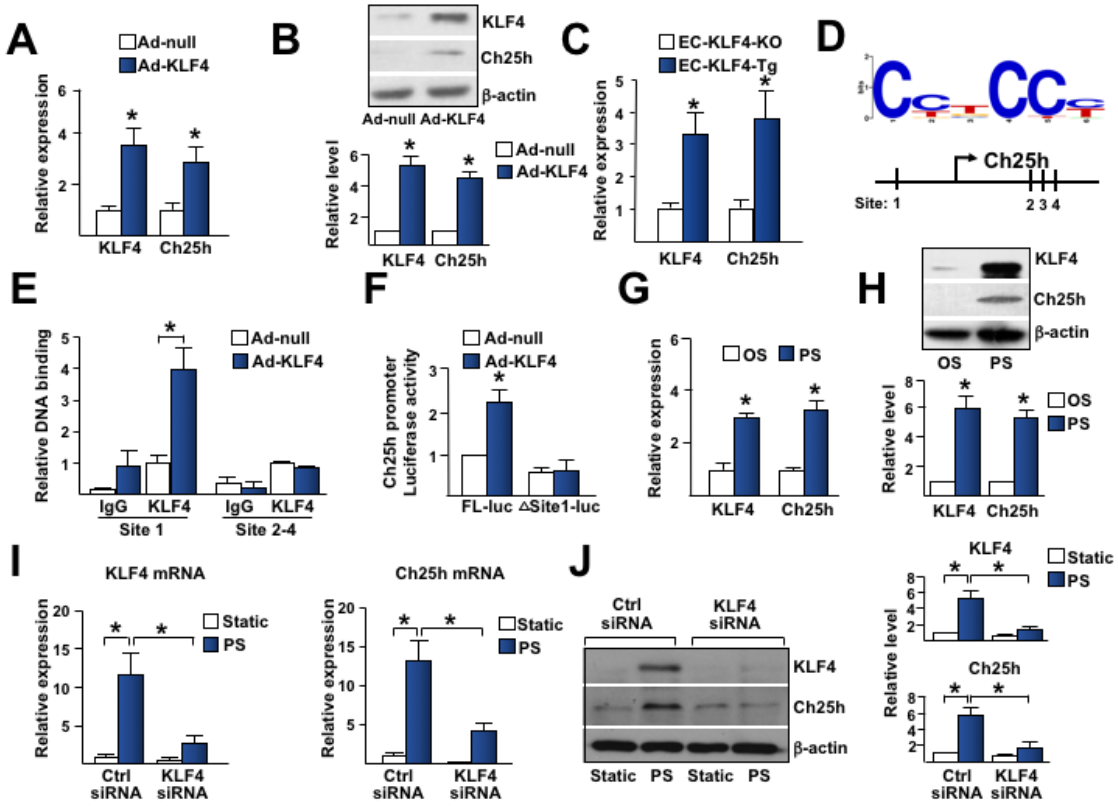

Figure 2.3. KLF4 transactivates Ch25h in ECs. **(A, B)** HUVECs were infected with Ad-KLF4 or Ad-null for 24 hr. Expression levels of KLF4 and Ch25h mRNA and protein were measured by qPCR and Western blot, respectively. **(C)** Lung ECs were isolated from EC-specific KLF4 knockout (EC-KLF4-KO) or EC-specific overexpression of KLF4 (EC-KLF4-Tg) mice (n=3 per group). Levels of KLF4 and Ch25h mRNA were measured by qPCR. **(D)** Depiction of the predicted KLF4 binding sites at -913 to -902 bp (Site 1), 607 to 618 bp (Site 2), 656 to 667 bp (Site 3) and 712 to 723 bp (Site 4) in the human *Ch25h* gene. (**E)** HUVECs infected with Ad-KLF4 or Ad-null were analyzed by ChIP assay with the use of anti-KLF4. KLF4 promoter enrichment was quantified by qPCR. IgG was used as an isotype control. **(F)** Bovine aortic endothelial cells (BAECs) were transfected a luciferase reporter fused with the *Ch25h* promoter region (Ch25h-Luc) or with a Site 1 deletion (Ch25hΔS1-Luc) together with pRSV-β-gal reporter for 6 hr, followed by infection with Ad-KLF4 for an additional 24 hr. Luciferase activity was measured and normalized to that of β-gal. **(G, H)** HUVECs were subjected to OS (1±4 dyn/cm^2) or PS (12±4 dyn/cm^2) for 24 hr. **(I, J)** HUVECs were transfected with control siRNA or KLF4 siRNA prior to PS stimulation or kept as a static control for 24 hr. KLF4 and Ch25h mRNA and protein expression were measured by qPCR (G, I) and Western blot (H, J), respectively. Error bars represent mean±SEM from three independent experiments. *p<0.05 between the indicated groups.

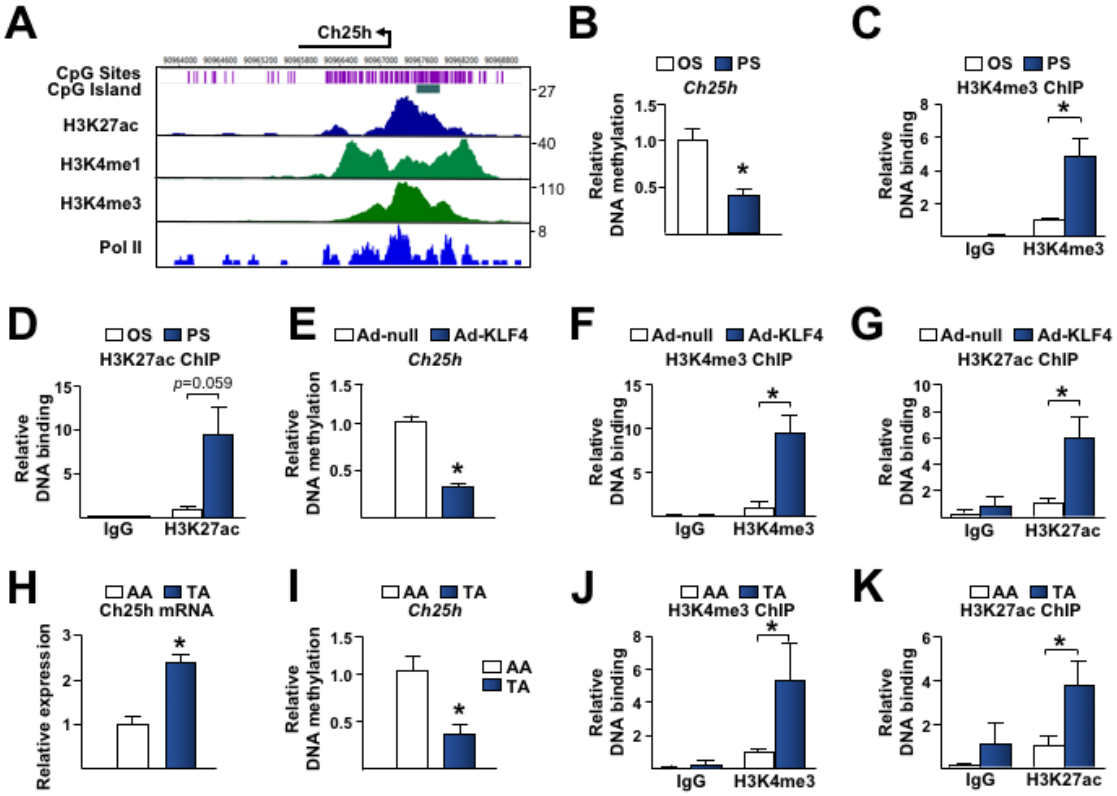

Figure 2.4. PS transcriptionally induces Ch25h. (A) WashU EpiGenome Browser depiction of the CpG islands and the binding landscape of H3K27ac, H3K4me1, H3K4me3, and Pol II at the promoter of the human *Ch25h* gene. The epigenetic landscapes shown were from HUVECs without stimulation. **(B-D)** HUVECs were subjected to PS or OS for 12 hr. **(E-G)** HUVECs were infected with Ad-KLF4 or Ad-null for 24 hr. In (B, E), DNA methylation status of the *Ch25h* promoter was measured by methylation-specific (MSP) qPCR. In (C, D, F, G), the binding of H3K4me3 and H3K27ac at the *Ch25h* promoter was detected using histone-ChIP qPCR. IgG was used as an isotype control. **(H-K)** Intima was collected from the AA or TA regions of C57BL/6 mice (n=9). In (H), total mRNA was quantified by qPCR. DNA methylation status is shown in (I). The modifications of H3K4me3 and H3K27ac are revealed in (J, K). Data presented are mean±SEM from three independent experiments. *p<0.05 between the indicated groups.

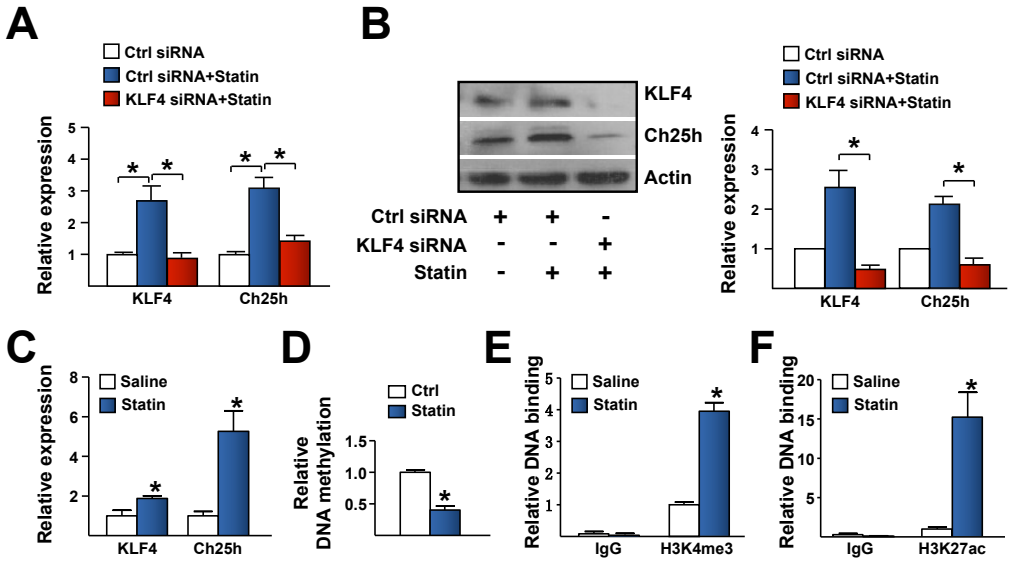

Figure 2.5. Statin-induced KLF4 mediates Ch25h expression. (A, B) HUVECs were transfected with control or KLF4 siRNA (50 nM) for 18 hr prior to treating with or without atorvastatin (1 μM) for 24 hr. The mRNA expression of KLF4 and Ch25h was measured by qPCR **(A)** and the protein level by Western blot **(B)**. C57BL/6 mice were injected with or without atorvastatin (50 mg/kg) for 24 hr. **(C)** Aortic intima was collected from C57BL/6 mice (experiments were performed from three different batches of three pooled mice), total mRNA was quantified by qPCR. **(D-F)** HUVECs were treated with atorvastatin (1 μM) for 24 hr, followed by measuring the modifications of (D) DNA methylation by MSP-qPCR, (E, F) H3K4me3 and H3K27ac by ChIP assays on the *Ch25h* promoter. Data presented are mean±SEM from three independent experiments. *p<0.05 between the indicated groups.

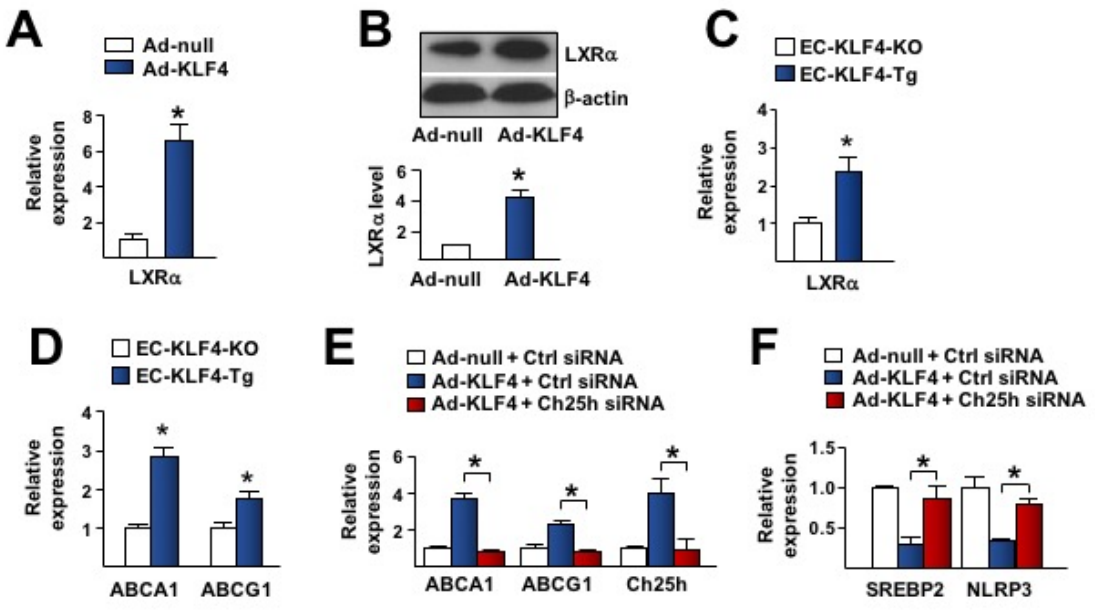

Figure 2.6. KLF4 induces LXRα. (A, B) HUVECs were infected with Ad-null or Ad-KLF4. Expression levels of LXRα mRNA (A) and protein (B) were measured by qPCR and Western blot, respectively. **(C, D)** The mRNA level of LXRα, ABCA1, and ABCG1 in lung ECs isolated from EC-KLF4-KO or EC-KLF4-Tg mice (n=3 per group) was detected by qPCR. **(E, F)** HUVECs infected with Ad-null or Ad-KLF4 were transfected with control siRNA or Ch25h siRNA. The level of ABCA1, ABCG1, Ch25h, SREBP2, and NLRP3 mRNA was assessed by qPCR.

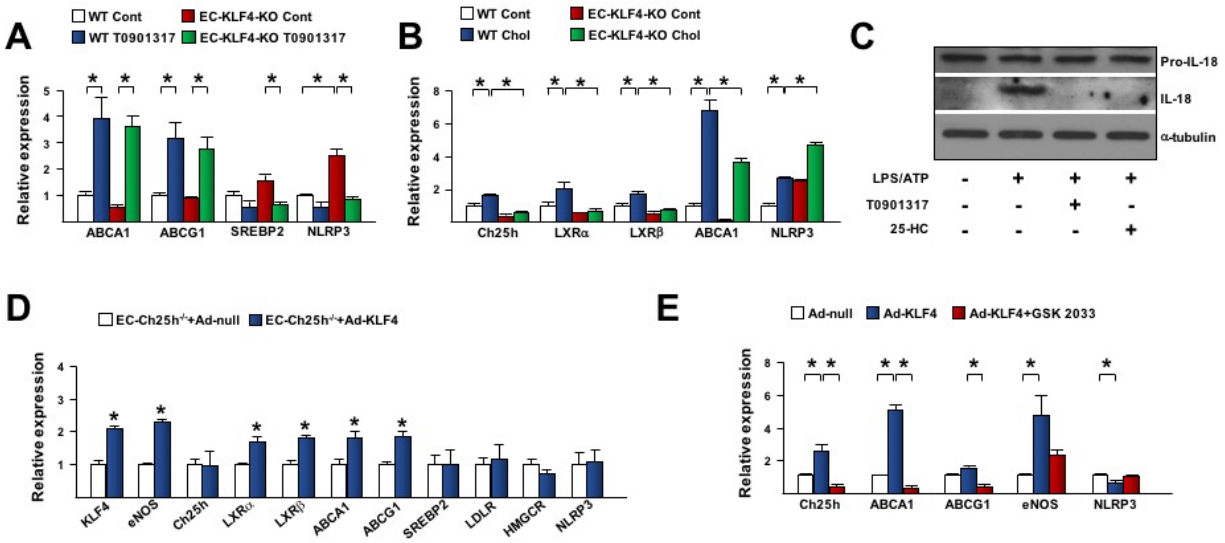

Figure 2.7. KLF4-LXR axis in ECs. (**A-B**) Lung ECs were isolated from WT or EC-KLF4-KO mice (n=3 per group). (A) Lung ECs were treated with the LXR agonist T0901317 (5 μM) for 16 hr. The mRNA expression of the indicated LXR downstream and inflammatory genes was quantified using qPCR. (B) Lung ECs were stimulated with cholesterol-methyl-beta-cyclodextrin at 2 mg/mL for 16 hr. The mRNA expression of the indicated genes was quantified using qPCR. (**C**) HUVECs were pre-treated with either T0901317 (5 μM) or 25-HC (1 μM) for 2 hr prior to treatment with LPS (100 ng/mL) for 16 hr with the addition of ATP (5 mM) for the last 30 min. Pro-IL-18 and the biologically active cleaved form of IL-18 was quantified using Western blot. (**D**) Lung ECs were isolated from $Ch25h^{-/-}$ mice and infected with Ad-null or Ad-KLF4 for 48 hr. The mRNA expression was quantified using qPCR. (**E**) HUVECs were infected with Ad-null or Ad-KLF4 24 hr prior to treatment with the LXR antagonist GSK 2033 (1 μM) for an additional 24 hr. The mRNA expression of the indicated genes was quantified using qPCR. Error bars represent mean±SEM from two to three independent experiments. *p<0.05 between the indicated groups.

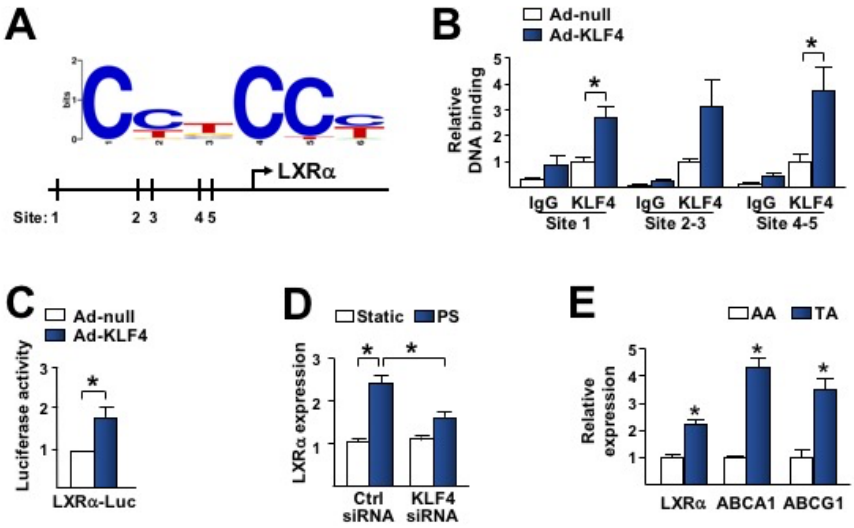

Figure 2.8. **KLF4 transcriptionally activates LXRα.** (**A**) Depiction of the predicted KLF4 binding sites at -3643 to 3632 bp (Site 1), -419 to -408 bp (Site 2), -313 to -302 bp (Site3), -219 to -208 bp (Site 4) and -133 to -122 bp (Site 5) in the human *LXRα* promoter region. **(B)** HUVECs were infected with Ad-null or Ad-KLF4 followed by ChIP assays using anti-KLF4. IgG was used as an isotype control. (**C**) BAECs were transfected with LXRα-Luc together with pRSV-β-gal reporter plasmids followed by infection with Ad-KLF4. Luciferase activity was normalized to that of β-gal. (**D**) HUVECs were transfected with control siRNA or KLF4 siRNA followed by stimulation with PS or kept under static conditions for an additional 24 hr. (**E**) Lung ECs were isolated EC-KLF4-KO and EC-KLF4-Tg mice (n=3 per group). The mRNA expression of LXRα, ABCA1, and ABCG1 were measured by qPCR. LXRα mRNA was quantified using qPCR. Error bars represent mean±SEM from three independent experiments. *p<0.05 between the indicated groups.

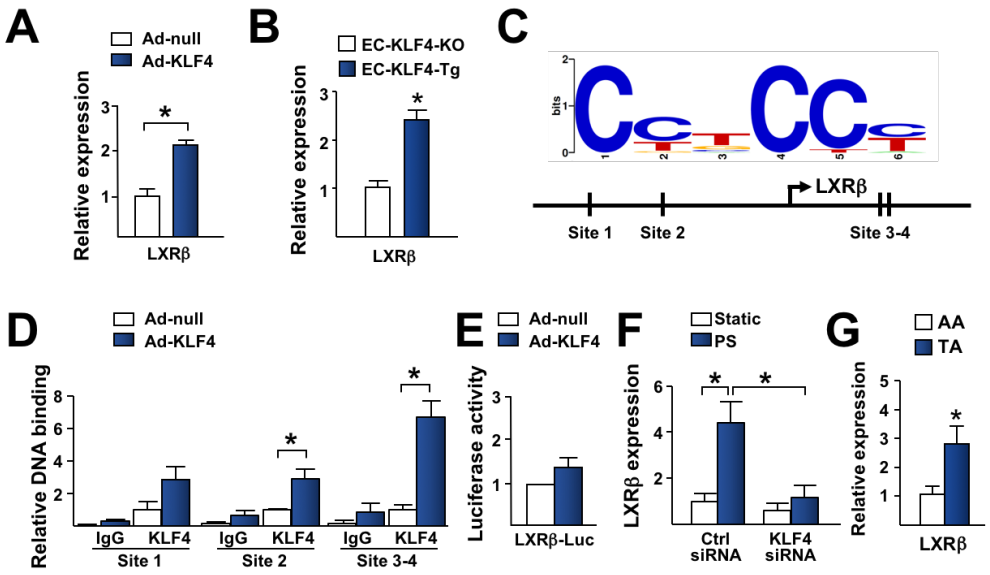

Figure 2.9. KLF4 transactivates LXRβ. (A) HUVECs were infected with Ad-null or Ad-KLF4 for 24 hr. The mRNA expression was detected by qPCR. **(B)** Lung ECs were isolated from EC-specific KLF4 knockout (EC-KLF4-KO) or EC-specific overexpression of KLF4 (EC-KLF4-Tg) mice (n=3 per group). mRNA was measured by qPCR. (**C**) Depiction of the predicted KLF4 binding sites, at -2425/-2424 bp (Site 1), -894/-883 bp (Site 2), 550/511 bp (Site 3), and 574/581 bp (Site 4) in the human *LXRβ* promoter region. IgG was used as an isotype control. **(D)** HUVECs were infected with Ad-null or Ad-KLF4 followed by ChIP assays using anti-KLF4. (**E**) BAECs were transfected with LXRβ-Luc together with pRSV-β-gal reporter plasmids followed by infection with Ad-KLF4. Luciferase activity was normalized to that of β-gal. (**F**) HUVECs were transfected with control or KLF4 siRNA (50 nM) for 18 hr followed by exposure to PS or kept under static conditions for an additional 24 hr. LXRβ mRNA was quantified using qPCR. Error bars represent mean±SEM from three independent experiments. *p<0.05 between the indicated groups.

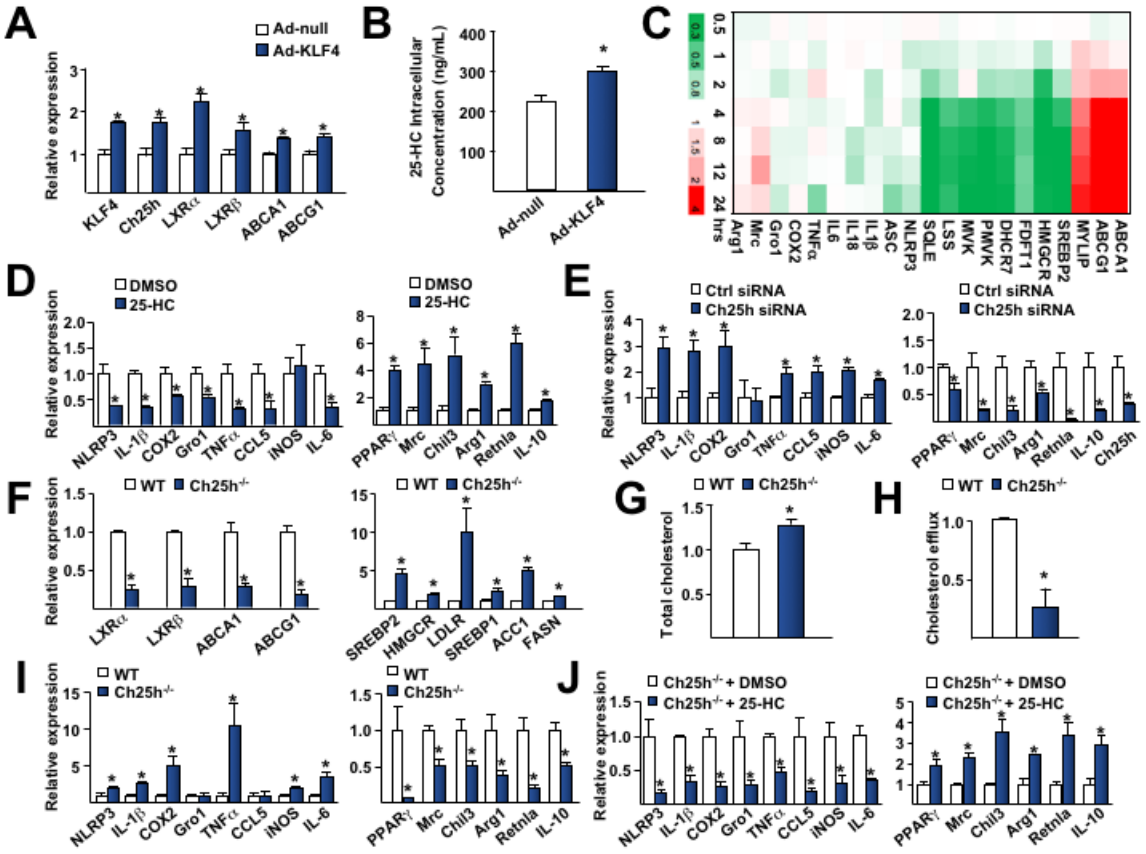

Figure 2.10. KLF4 regulation of Ch25h/LXR in macrophages promotes M2 polarization. (A) RAW264.7 cells were infected with Ad-KLF4 or Ad-null prior to qPCR assessment of the indicated mRNA. **(B)** LC-MS/MS measurement of intracellular 25-HC level of THP1 cells infected with Ad-KLF4 or Ad-null. **(C)** BMDMs from C57BL/6 mice were treated with 25-HC (5 nM) for the indicated time points. The mRNA expression profiles were analyzed by microarray as described in Shibata et al., 2013. The heat map shown indicate values plotted as relative fold change, compared with those from untreated controls. **(D, E)** RAW264.7 cells were treated with 25-HC (1 μM) or DMSO for 24 hr (D) or transfected with Ch25h siRNA or control siRNA (E). The mRNA levels of pro-inflammatory genes (NLRP3, IL-1β), M1 marker genes (COX2, Gro1, TNFα, CCL5, iNOS, and IL-6), and M2 marker genes (PPARγ, MRC, Chil3, Arg1, Retnla, and IL-10) were measured by qPCR. **(F-I)** PMs were isolated from 8-week old $Ch25h^{-/-}$ mice and their $Ch25h^{+/+}$ littermates (n=12 per group). The mRNA levels of the indicated genes were quantified by qPCR (F, I). In (G, H), the total cholesterol content and cholesterol efflux were measured. **(J)** PMs isolated from 8-week old $Ch25h^{-/-}$ mice (n=12) were treated with or without 25-HC (1 μM) for 24 hr. The mRNA levels of indicated genes were measured by qPCR. Error bars represent mean±SEM from three independent experiments. *p<0.05 between indicated groups.

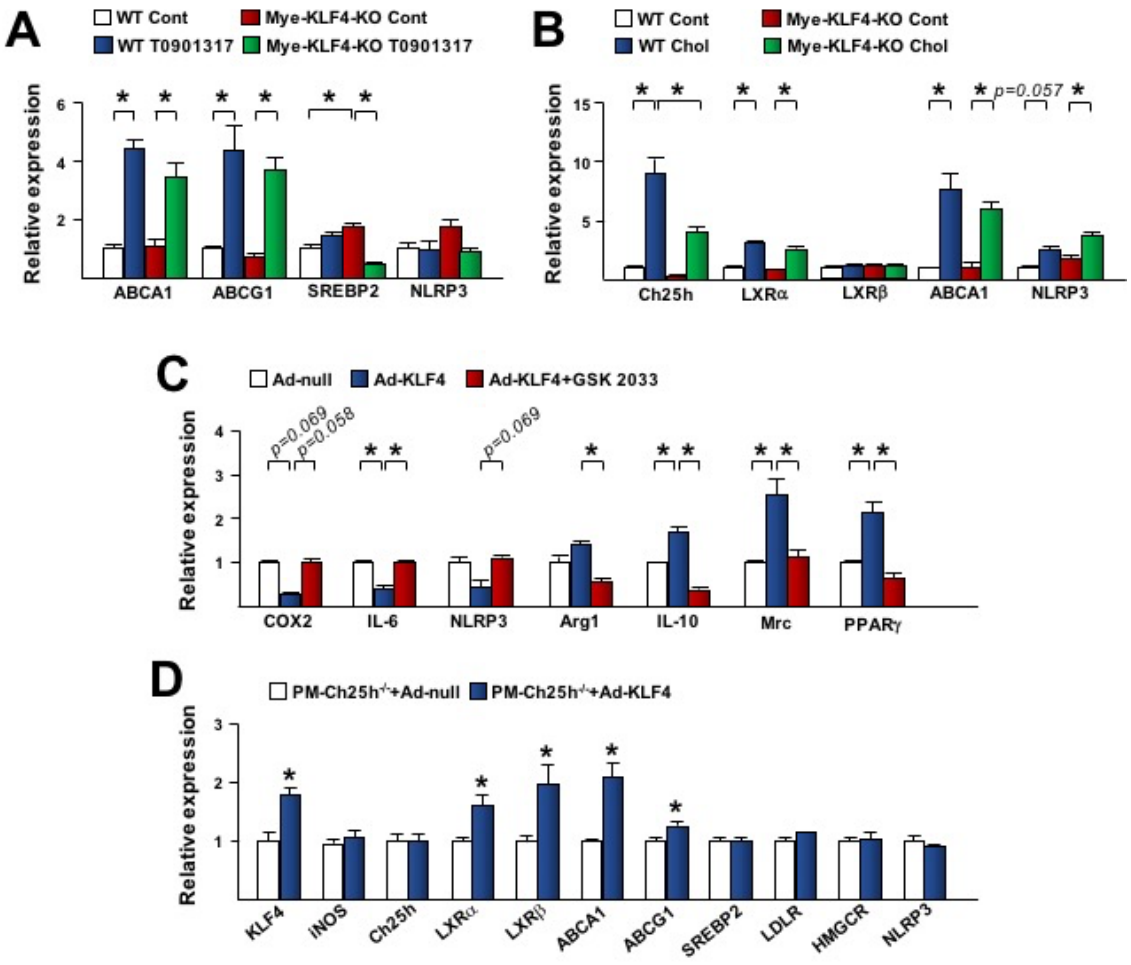

Figure 2.11. KLF4-LXR axis in macrophages. (**A-B**) Peritoneal macrophages (PMs) were isolated from WT or Mye-KLF4-KO mice (n=3 per group). (A) PMs were treated with the LXR agonist T0901317 (5 μM) for 16 hr. The mRNA expression of the indicated LXR downstream and inflammatory genes was quantified using qPCR. (B) PMs were supplemented with water soluble cholesterol (cholesterol-methyl-beta-cyclodextrin) at 2 mg/mL for 16 hr. The mRNA expression of the indicated genes was quantified using qPCR. (**C**) PMs were isolated from Ch25h$^{-/-}$ mice and infected with Ad-null or Ad-KLF4 for 48 hr. The mRNA expression of the indicated genes was quantified using qPCR. (**D**) HUVECs were infected with Ad-Null or Ad-KLF4 24 hr prior to treatment with the LXR antagonist GSK 2033 (1 μM) for an additional 24 hr. The mRNA expression of the indicated M1 or M2 genes were quantified using qPCR. Error bars represent mean±SEM from two to three independent experiments. *p<0.05 between the indicated groups.

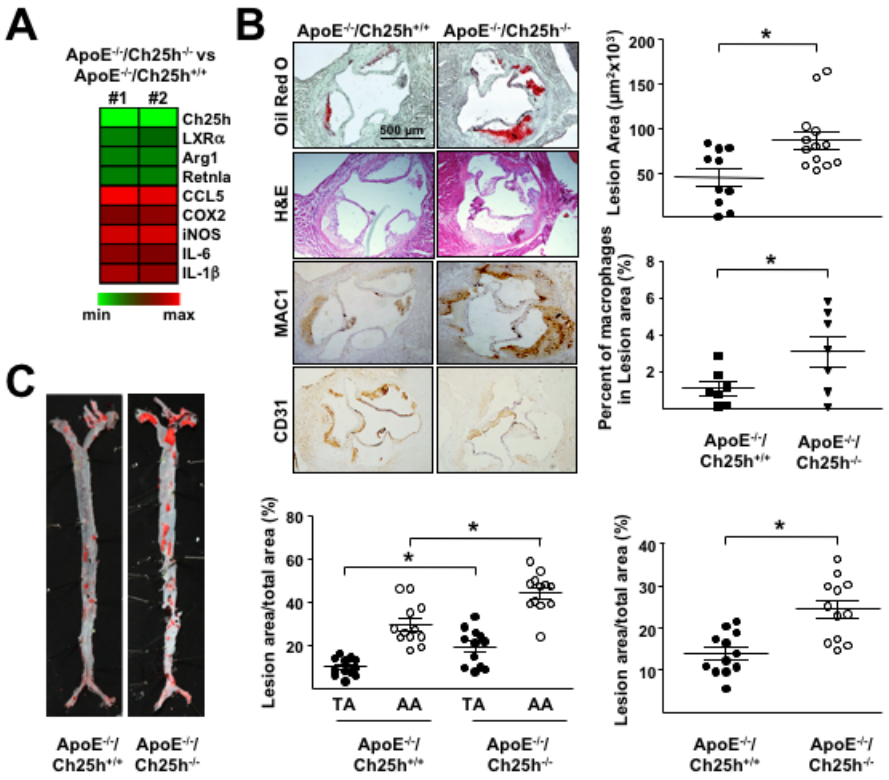

Figure 2.12. Ch25h ablation increases atherosclerosis susceptibility. (A) Two biological replicates of RNA-seq performed on PMs isolated from ApoE$^{-/-}$/Ch25h$^{-/-}$ compared to ApoE$^{-/-}$/Ch25h$^{+/+}$ mice (n=12 per group). Heat map is plotted as log2 fold change. **(B)** Six-week old ApoE$^{-/-}$/Ch25h$^{+/+}$ (n=13) and ApoE$^{-/-}$/Ch25h$^{-/-}$ (n=13) mice fed a high-fat diet for 12 weeks. Histological sections of aortic roots were stained with Oil Red O, H&E, MAC1, and CD31. Graphs on the right represent quantification of the Oil Red O-positive areas and percentage of macrophages in the lesions. **(C)** Representative *en face* Oil Red O staining of the whole aorta from ApoE$^{-/-}$/Ch25h$^{-/-}$ mice and ApoE$^{-/-}$/Ch25h$^{+/+}$ littermates (n=10 per group). Graphs below represent quantification of the lesion area in thoracic aorta (TA) versus aortic arch (AA) as well as total lesion area, summed from that of AA (i.e., aortic root, ascending aorta, and descending thoracic aorta to the 4th thoracic vertebra), TA (i.e., descending aorta from the 4th thoracic vertebra to the renal arteries), and abdominal aorta (i.e., below the renal arteries). Error bars represent mean±SEM from three independent experiments. *p<0.05 between the indicated groups.

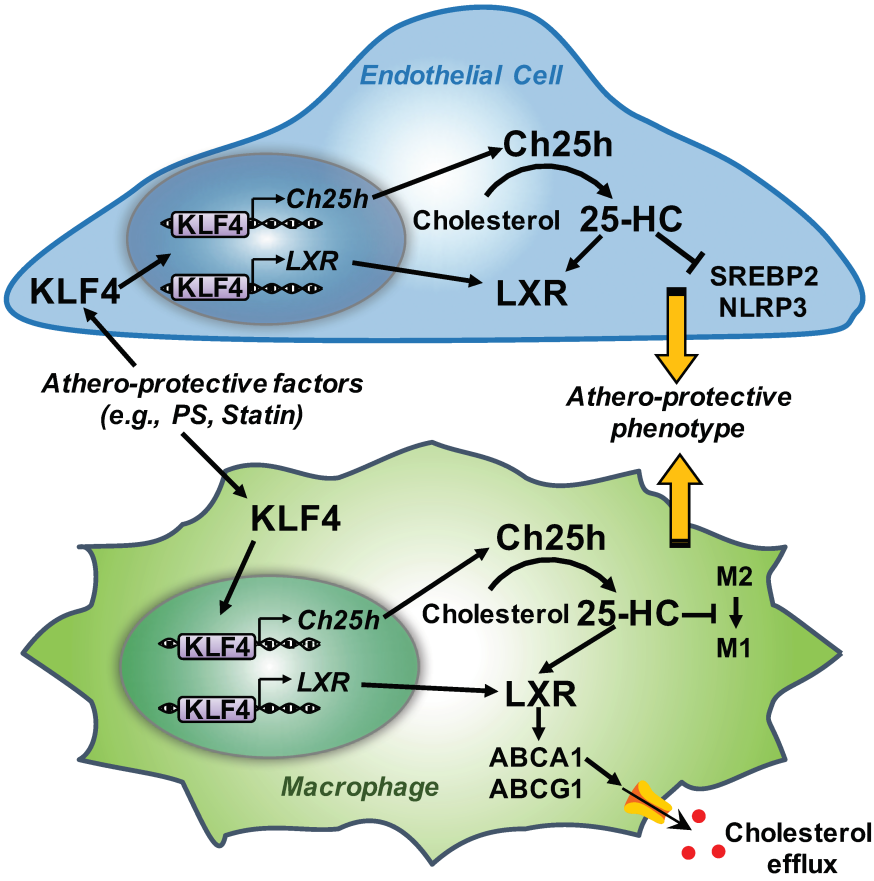

Figure 2.13. KLF4 mediates Ch25h and LXR in ECs and macrophages to promote a atheroprotective phenotype. Atheroprotective factors, such as PS and statins, induce KLF4 in ECs and macrophages. KLF4 then transactivates Ch25h and LXR thereby promoting the suppression of SREBP2 and NLRP3 inflammasome in ECs as well as cholesterol efflux and M1 to M2 transition in macrophages. The synergism between the anti-inflammatory effects in both ECs and macrophages contributes to the atheroprotective phenotype.

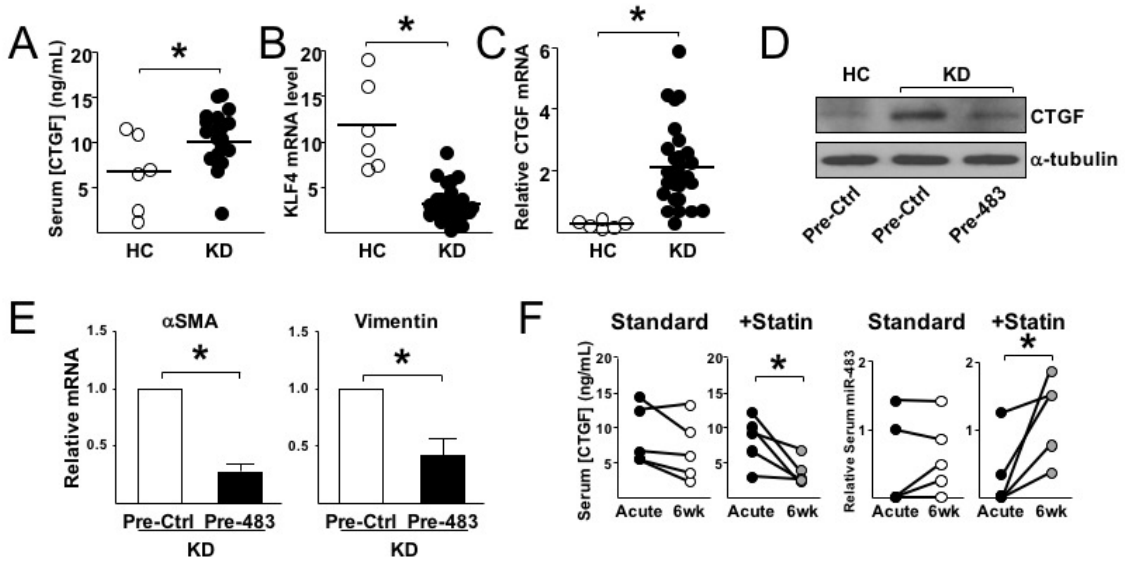

Figure 2.14. KLF4-induced miR-483 targets CTGF to suppress EndoMT in Kawasaki disease (KD). This figure is an adaptation from He M, et al. *Circ Res* 2017. (A) Levels of circulating CTGF was measured in the sera age-matched healthy controls (HC; n=6) or KD subjects (n=20) by ELISA. (B, C) HUVECs were treated with medium containing 15% sera from HC or KD subjects for 96 hr. KLF4 and CTGF mRNA was measured using qPCR. (D, E) HUVECs were treated with pooled sera for 48 hr, then treated with pre-miR-483 or pre-Ctrl for an additional 48 hr. CTGF was measured using Western blot (D) and mesenchymal markers were measured using qPCR (E). (F) Circulating levels of CTGF and miR-483 were compared between KD subjects prior to treatment (acute) or 6 wk post-standard treatment with or without the addition of atorvastatin (0.25 mg/kg/day; n=5 per group). Controls were age and illness day matched. Error bars represent mean±SEM from three independent experiments. *$p<0.05$ between the indicated groups.

CHAPTER 3

Abstract

Background: Idiopathic pulmonary fibrosis (IPF) is a progressive lung disease with limited treatment options. Therapeutics targeting epithelial dysfunction and fibroblast proliferation have made little progress in the clinic. However, the role of endothelial cell (EC) dysfunction in pulmonary fibrosis has been often overlooked. Sterol regulatory element-binding protein 2 (SREBP2) is a known mediator of EC dysfunction.

Methods: RNA-sequencing was performed on ECs with SREBP2 overexpression. Endothelial-to-mesenchymal transition (EndoMT) markers were compared between SREBP2 overexpression and bleomycin (BLM) in cultured ECs. Endothelial-specific SREBP2 overexpression transgenic (EC-SREBP2[N]-Tg) mice were administered BLM to induce pulmonary fibrosis and compared to human IPF samples.

Results: SREBP2 overexpression in ECs lead to the induction of TGF, Wnt, and cytoskeleton remodeling gene ontology pathway. Investigating the genes associated with this pathway indicated increased mesenchymal cell differentiation, hence EndoMT. Both SREBP2 overexpression and BLM treatment led to increased expression of mesenchymal genes such as snai1 family transcriptional repressor 1 (snai1), α-smooth muscle actin (αSMA), vimentin, and neural cadherin (N-cad). Furthermore, SREBP2 was found to directly bind to the promoter regions and transactivate the mesenchymal genes. This was also associated with phenotypic switch in the EC to behave more myofibroblast-like, including increased proliferation, stress fiber formation, and ECM deposition. Mouse

models treated with BLM demonstrated exacerbated lung vascular remodeling and increased EndoMT in the EC-SREBP2(N)-Tg mice when compared to wildtype littermates. Significantly, SREBP2 was also found to be markedly increased in IPF patient lung samples.

Conclusions: SREBP2 promotes EndoMT through directly transactiving mesenchymal genes (i.e., snai1, αSMA, vimentin, and N-Cad). SREBP2 activation in ECs will increase EndoMT leading to an induction of fibrosis. Targeting SREBP2 may be a potential therapeutic in pulmonary fibrosis.

Introduction

Idiopathic pulmonary fibrosis (IPF) is a progressive interstitial lung disease with a median survival rate of 3-5 years[1]. The clinical presentation of IPF relies on the formation of fibroblastic foci, areas of active myofibroblasts depositing extracellular matrix, which leads to the classical "honeycombing" effect seen in CT scans where the alveoli become stiff and dilated[1, 2]. Different from interstitial pneumonia, IPF does not respond to anti-inflammatories or steroids and the only effective treatment is lung transplantation[3]. It was initially hypothesized that there was an unknown initial injury causing an acute inflammatory response followed by dysregulated wound repair leading to fibrosis[4]. However, more recent studies indicate that inflammation plays little role in the progression of this disease[5, 6].

Being a progressive fibrotic disease, IPF patients have an accumulation of activated myofibroblasts in the interstitial space between the alveoli and the capillaries. The prototypical proliferative signals, transforming growth factor beta (TGFβ) and platelet-derived growth factor (PDGF) pathways, are stimulated resulting in the myofibroblasts to secrete exuberant amounts of collagen and fibronectin (FN)[7]. However, therapeutics targeting these growth factors have not benefited IPF patient prognosis[8]. Furthermore, recent studies have identified that the myofibroblasts found in the interstitium are not only activated resident lung fibroblasts. These myofibroblasts can also reside from circulating fibrocytes or from epithelial/endothelial transdifferentiated into mesenchymal cells[9]. More likely the case, it is the combination and cross-talk from all of the aforementioned cell types. Epithelial-to-mesenchymal transition (EMT) and the closely related endothelial-to-

mesenchymal transition (EndoMT) have both been shown to be induced in IPF patients and play a role in the progression of fibrosis[10-12]. However, despite the fact that capillary endothelium comprises about 1/3 of the cells in the lung[13], relatively little is known about the contribution of endothelial cells to IPF. Stress inducers, such as TGFβ and reactive oxygen species (ROS), are known to promote mesenchymal transition, although the mechanism remains poorly understood.

Bleomycin (BLM), a chemotherapy agent with a major side effect of inducing pulmonary fibrosis in approximately 10% of patients[14-16], reacts with oxygen to create superoxide and free radicals to induce DNA double-stranded breaks. As a result, there is increased intracellular ROS. Lung tissue lacks the enzyme needed to break down BLM[17], causing its accumulation that leads to lung toxicity in patients. Consequently, BLM is now widely accepted as a model to induce pulmonary fibrosis in mice. Intratracheal administration of BLM is the most commonly used method to induce pulmonary fibrosis in mice[18]. However, this method does not resemble the onset of IPF in humans as the damage is more inflammatory and bronchiocentric. A more systemic administration method, such as intraperitoneal (i.p.) or tail vein injection, exhibits subplueral collagen deposition, which is more similar to the pathology of IPF patients[18]. Several studies also show that IPF patients who are treated with oxygen, for example, when put under general anesthesia during surgery, have increased fibrotic progression and lung toxicity[19, 20]. This detrimental effect of hyperoxia has been demonstrated to cause increased ROS in the lung. Interestingly, we have previously found that sterol regulatory binding protein 2 (SREBP2) is a highly oxidative stress responsive protein in endothelial cells (ECs)[21].

SREBP2 is a transcription factor that is canonical in regulating cholesterol biosynthesis and uptake. Although its function has been well-characterized in the liver, we have recently identified SREBP2 to be necessary for the NOD-like receptor family, pyrin domain containing protein 3 (NLRP3) inflammasome in ECs[22]. It is important to note that ECs do not readily accumulate cholesterol, as opposed to liver cells or macrophages, and SREBP2-mediated NLRP3 inflammasome activation was found to be cholesterol independent in ECs[22]. There is evidence that SREBP2 is needed in fibrotic disease as well, however these studies indicated the need is more for generating cholesterol for the membrane lipid bilayer in proliferating cells[23, 24]. We postulate that SREBP2 maybe be playing a pivotal role in the oxidative stress-induced fibrotic pathway. As there are a limited number of current therapies for IPF, finding novel therapeutic targets in the disease progression is imperative. Because SREBP2 can link oxidative stress response and fibrosis, targeting of this protein may lead to better prognostic outcomes in patients.

Methods

RNA-sequencing library construction and data processing Total RNA was isolated from human umbilical vein endothelial cells (HUVECs) infected with Ad-SREBP2 or Ad-null (empty vector). mRNA was isolated using mirVana mRNA isolation kit (Thermo Fisher Scientific). Standard Illumina protocols were used to construct the RNA libraries and sequencing. Analysis was performed using base calling and quality scoring by using Real-Time Analysis version 2 (RTA v2) on the NextSeq 500 system. Data were demultiplexed and converted to FASTQ files using Bcl2fastq conversion software v1.8.4. Sequence reads were trimmed of their adaptor sequences, and masked for low complexity or low-quality sequence. Reads were mapped to the h19 genome using tophat v2.0.14[25]. Data was normalized to RPKM using cufflinks v2.2.1 to assemble transcripts and estimate mRNA abundance[26, 27].

EC culture, siRNA transfection, and adenovirus infection HUVECs were cultured at 37°C with 95% humidified air and 5% CO_2 in M199 supplemented with 15% fetal bovine serum, 1 ng/ml recombinant human fibroblast growth factor, 90 μg/ml heparin, 20 mM, HEPES (pH 7.4), and 100 U/ml penicillin-streptomycin. For siRNA knockdown, HUVECs were transfected with SREBP2 or control siRNA (25 nM) using Lipofectamine RNAiMax (Life Technologies) for up to 72 hr. SREBP2 overexpression was performed using adenovirus compared to empty vector (Ad-null) infection for 72 hr.

Western blot and qPCR analyses Total protein was isolated from cells using NP-40 and resolved by SDS-PAGE. Gels were transferred to polyvinylidene fluoride (PVDF)

membranes and immunoblotted with antibodies against SREBP2 (Abcam), snai1 (Cell Signalling), aSMA (Abcam), vimentin (Cell Signaling), and β-actin (Santa Cruz Biotechnology). Immunobloted bands were visualized using enhanced chemiluminescence (Milipore). Total RNA was isolated from cells or tissue using Trizol (Life Technologies). The extracted RNA was reverse transcribed using 5X PrimeScript reverse transcriptase (Takara), and normalized to β-actin as the internal control. Relative mRNA expression was determined using iQ^{TM} SYBR Green PCR supermix (Bio-Rad) in the Bio-Rad Real-time detection system. Data was normalized using $2^{-\Delta CT\ [-(CT\ of\ target\ gene-CT\ of\ reference\ gene)]}$, followed by the $2^{-\Delta CT}$ of each experimental group divided by that of the averaged control groups. Primers are listed in Table 3.1 below.

Table 3.1 primers used for qPCR assays

β-Actin	Homo sapiens	Forward: CACCAACTGGGACGACAT Reverse: ACAGCCTGGATAGCAACG
SREBP2	Homo sapiens	Forward: CCCTGGGAGACATCGACGA Reverse: CGTTGCACTGAAGGGTCCA
Snai1	Homo sapiens	Forward: CCCCAATCGGAAGCCTAA Reverse: CCTTTCCCACTGTCCTCAT
αSMA	Homo sapiens	Forward: CAGGGCTGTTTTCCCATCCAT Reverse: GCCATGTTCTATCGGGTACTTC
N-Cad	Homo sapiens	Forward: AGCCAACCTTAACTGAGGAGT Reverse: GGCAAGTTGATTGGAGGGATG

Vimentin	Homo sapiens	Forward: GCCCTAGACGAACTGGGTC Reverse: GGCTGCAACTGCCTAATGAG
VE-Cad	Homo sapiens	Forward: CACCTTCTGCGAGGATATGG Reverse: AGGAAGATGAGCAGGGTGAT
KDR	Homo sapiens	Forward: TCAGAACCCATCAGGAGTGAATACG Reverse: TGCTTGGAGGTGGCTACAATCG
KLF4	Homo sapiens	Forward: AGAGTTCCCATCTCAAGG Reverse: AATGCCTCTTCATGTGTAAG
Snai1	Mus musculus	Forward: GTCGTCCTTCTCGTCCACC Reverse: GGCCTGGCACTGGTATCTC
αSMA	Mus musculus	Forward: ATCATGCGTCTGGACTTGG Reverse: AATAGCCACGCTCAGTCAGG
N-Cad	Mus musculus	Forward: GTGGAGGCTTCTGGTGAAAT Reverse: CTGCTGGCTCGCTGCTT
Vimentin	Mus musculus	Forward: CGGAAAGTGGAATCCTTGCA Reverse: CACATCGATCTGGACATGCTGT
eNOS	Mus musculus	Forward: TGGACCTGGATACCCGGAC Reverse: TGGTGACTTTGGCTAGCTGGT
VE-Cad	Mus musculus	Forward: CCGGCGCCAAAAGAGAGA Reverse: CTGGTTTTCCTTCAGCTGGAAGTGGT
vWF	Mus musculus	Forward: CCGGAAGCGACCCTCAGA Reverse: CGGTCAATTTTGCCAAAGATCT

Col1A1	Mus musculus	Forward: GAGAGGTGAACAAGGTCCCG Reverse: AAACCTCTCTCGCCTCTTGC
FN	Mus musculus	Forward: GCATCAGCCCGGATGTTAGA Reverse: GTTGGTGATGAAGGGGGTCT

Tissue collection, histological and immunofluorescence analyses The left lung was fixed in 4% paraformaldehyde (PFA), while the right lung was snap frozen in liquid nitrogen. After dehydration and OCT embedding, the blocks were sectioned at 7 μm thickness. Sections were H&E (Sigma) or Masson's trichrome (Thermo Fisher Scientific) stained according to the manufacturer's instructions. Immunofluorescence staining was performed with primary antibodies against anti-CD31 (Santa Cruz Biotechnology), VE-Cad (Cell signaling), αSMA (Abcam), or SREBP2 (Abcam). After overnight incubation, slides were washed and incubated with Alexa Fluor 488-conjugatedgoat anti-mouse IgG (Life Technologies) or Alexa Fluor 568-conjugated rabbit anti-mouse IgG (Life Technologies).

Angiography Immediately following euthanasia, the superior vena cava, anterior vena cava, and aorta are sutured closed. Microfil (Flow Tech), used as the contrasting agent, is directly injected into the right ventricle to flow up the pulmonary artery and allowed to cure overnight at room temperature. Lungs are then harvested and dehydrated in increasing percentages of absolute ethanol. Finally, lungs are immersed in methyl salicylate for 24 hr, followed by standard imaging procedures.

MSP-qPCR Genomic DNA was isolated using QIAamp DNA Mini Kit (Qiagen) from indicated cells, and then bisulfite converted using EpiTect Bisulfite kit (Qiagen). Following bisulfite conversion, DNA methylation status was quantified by qPCR with primers (listed below in Table 3.2) that specifically recognize the methylated cytosine. UBB was used as an internal control.

Table 3.2 primers used for MSP assays

UBB	Homo sapiens	Forward: ATAGTGGGTTTTGTTGATTTGA Reverse: CCTTTCTCACACTAAAATTCCA
VE-Cad	Homo sapiens	Forward: GGTACGTAGATTATGAGGATAGGC Reverse: AAAATAAACAAACAACAACTCAACG
KDR	Homo sapiens	Forward: AGAGTTTTTGAGAGGTTTCGATATC Reverse: CCTTACGCTAACAACCCGAC
KLF4	Homo sapiens	Forward: GTACGTTTGTAATTTTCGTTATTCG Reverse: ATAAAACAAAATCTCGCTATATCGC

Promoter binding site prediction Sterol regulatory elements (SREs) in which SREBP2 directly binds was predicted on snai1, aSMA, N-Cad, and vimentin promoter regions (-1000 to +500 from the transcriptional start sites [TSS]) using the weight matrix-based program MATCH[28]. CpG islands were predicted using WashU EPI Genome Browser.

Chromatin immunoprecipitation (ChIP) ChIP assays were performed according to established protocol using anti-SREBP2 (Abcam), and the isotype control anti-rabbit IgG (Santa Cruz). Briefly, ECs were cross-linked with 0.75% formaldehyde at room temp for

10 min and quenched with 125 mM glycine. Cells were lysed in RIPA buffer and sonicated to fragment the DNA to a size of 500-1000 bp. Cell lysates were then incubated with Dynabeads (Invitrogen) conjugated to the indicated antibodies. Immunoprecipitated DNA fragments were reverse cross-linked and DNA binding was quantified as percentage of input using qPCR (see list of primers below in Table 3.3).

Table 3.3 primers used for ChIP assays

Snai1-ChIP	Homo sapiens	Forward: GCTACGCGTGGATCGAGGATCTTCACGGG Reverse: GCTAAGCTTAGAAGAACCACTCGCTAGGC
αSMA-ChIP	Homo sapiens	Forward: GCTACGCGTTCTTTCGAGCACCTTCCGAG Reverse: GCTAAGCTTCGCCTCGTTCAGCGACT
N-Cad-ChIP	Homo sapiens	Forward: GCTACGCGTCCGGAGAACAGTCTCCAACT Reverse: GCTAAGCTTGCGAGCTGATGACAAATAGCG
Vimentin-ChIP	Homo sapiens	Forward: GCTACGCGTAACTTAGGGGCGCTCTTGTC Reverse: GCTAAGCTTAGAGCGCCTGAGATTGGAAC

Luciferase Assay The 5'-upstream regions of human *snai1, αSMA, N-Cad, and vimentin* genes were PCR-amplified using KOD hot start high-fidelity DNA polymerase (Milipore) with human genomic DNA as the template, primers are shown in Table 3.4. The DNA fragment spanning from (-937 to -505 bp for snai1, 53 to 124 bp for αSMA, 272 to 837 bp for N-Cad, and 82 to 914 bp for vimentin) were subcloned into the pGL3-basic plasmid containing the firefly luciferase reporter gene (Promega), and verified by sanger sequencing. The reporter plasmids were co-transfected with Renilla into ECs, using lipofectamine 2000 (Life Technologies) for 16 hr. ECs were then infected with Ad-

SREBP2 or Ad-null for an additional 48 hr. Luciferase activities were measured and normalized to Renilla activity using the Dual-Glo Luciferase Reporter Assay kit (Promega).

Table 3.4 primers used for Luciferase assays

Snai1-Luc	Homo sapiens	Forward: GCTACGCGTGGATCGAGGATCTTCACGGG Reverse: GCTAAGCTTAGAAGAACCACTCGCTAGGC
αSMA-Luc	Homo sapiens	Forward: GCTACGCGTTCTTTCGAGCACCTTCCGAG Reverse: GCTAAGCTTCGCCTCGTTCAGCGACT
N-Cad-Luc	Homo sapiens	Forward: GCTACGCGTCCGGAGAACAGTCTCCAACT Reverse: GCTAAGCTTGCGAGCTGATGACAAATAGCG
Vimentin-Luc	Homo sapiens	Forward: GCTACGCGTAACTTAGGGGCGCTCTTGTC Reverse: GCTAAGCTTAGAGCGCCTGAGATTGGAAC

DNMT1 Activity assay DNMT1 activity was measured using a DNMT1 Assay kit (Abcam) following the manufacturer's instructions. Briefly, nuclear extracts of BLM treated HUVECs were isolated using a Nuclear Extraction kit (Abcam). Nuclear extracts were then incubated with capture reagents and antibodies specific to active DNMT1 using ELISA. Colorimetric intensity was used to measure DNMT1 activity.

Lung EC isolation Harvested lungs were immediately finely minced and incubated with Type 1 Collagenase (Thermo Fisher Scientific) for 45 min. The solution was then triturated using 12 cm cannulas, filtered at 70 μm, and spun down at 8000 rpm for 8 min at 4°C. Cell pellets were then resuspended in fresh M199 buffer and selected for using DynaBeads

(Invitrogen) conjugated to CD31 (Santa Cruz Biotechnology) and CD144 (BD Biosciences) for 4 hr. Beads with bound lung ECs were then plated on collagen coated tissue culture dishes and grown for at least three days prior to further experimentation.

Mouse lines and BLM administration All mice were approved for use from the University of California, San Diego Institutional Animal Care and Use Committee (IACUC) and kept in temperature and humidity controlled environment with a 12 hr light/dark cycle and fed ad libitum. EC-SREBP2(N)-Tg mice were generated as previously described[22]. To induce pulmonary fibrosis, mice were administered a total of 5 intraperitoneal (i.p.) injections of BLM (McKesson General; 8 U/kg body weight) over the course of two weeks (Days 0, 4, 7, 10, and 14). Mice were then harvested after an additional 14 days.

Statistical analysis All data are expressed as mean±SEM. Student's t test was used for comparisons between two groups, or ANOVA for comparisons between multiple groups. If $p<0.05$ after ANOVA analysis, we then used Bonferroni post-hoc to assess the differences between the two indicated groups, with adjusted $p<0.05$ considered to be statistically significant.

Results

Our previous studies have demonstrated that SREBP2 plays a key role in oxidative stress-induced endothelial dysfunction, manifested by increased innate immune response, disrupted redox balance, and impaired endothelial nitric oxide synthase (eNOS)-derived NO bioavailability[21, 22]. These findings prompted us to profile the SREBP2-regulated transcriptome in ECs. RNA-sequencing data collected from ECs overexpressing the N-terminal, i.e., the active form of SREBP2 [SREBP2(N)], and the subsequent pathway enrichment analyses revealed that the highest ranked pathway was lipid metabolism, which unsurprisingly included canonical SREBP2-regulated genes. Interestingly, the second highest ranked pathway was that of TGF, Wnt, and cytoskeleton remodeling (Figure 3.1A). Several major proteins induced by SREBP2-overexpression in ECs include snail family transcriptional repressor 1 (snai1), SMADs, bone morphogenetic protein (BMPs), and wingless-type MMTV integration site family members (Wnts) (Figure 3.1B). Furthermore, genes upregulated in this pathway are noticeably mediators of embryonic development, mesenchymal cell differentiation, and Hippo signaling (Figure 3.1C). All of which are implemented in the process of endothelial-to-mesenchymal transition (EndoMT). Collectively, high throughput screening and *in silico* analyses revealed that SREBP2(N) overexpression not only induced lipid metabolism, but also may mediate mesenchymal dedifferentiation and pointed towards a pro-fibrotic phenotype.

Clinically, a fibro-proliferative disorder that is still in need of therapeutic targets is pulmonary fibrosis. As EndoMT emerges to be a key event in the context of vascular remodeling in fibrotic diseases[11], we proposed that SREBP2 may be a crucial regulator in

pulmonary fibrosis. Using bleomycin (BLM) as a model for fibrosis and an oxidative stress inducer (Figure 3.2A), we found that the N-terminal cleavage of SREBP2 was time dependently up-regulated (Figure 3.2B). Additionally, SREBP2 nuclear translocation, indicating N-terminal cleavage and activation, increased following stimulation with BLM (Figure 3.2C). Further evaluation of mesenchymal markers demonstrated that ECs treated with BLM for extended periods up to 72 hr was sufficient to induce snai1, α-smooth muscle actin (αSMA), neural cadherin (N-Cad), and vimentin (Figure 3.2D). In sum, BLM can induce SREBP2 activation, possibly through increased intracellular oxidative stress, thereby potentiating mesenchymal marker expression.

To investigate whether SREBP2 was sufficient to induce mesenchymal markers, we overexpressed the N-terminal and active portion of SREBP2 (i.e., SREBP2[N]) using adenovirus. We found that SREBP2(N) overexpression could indeed recapitulate the induction of snai1, αSMA, N-Cad, and vimentin; similar to that of BLM treatment (Figure 3.3A). Because SREBP2 is a transcription factor, we speculated that SREBP2 may directly regulate mesenchymal gene transcription in ECs. Supporting this hypothesis, the promoter regions of the mesenchymal markers, including snai1, αSMA, N-cad, and vimentin, were found to contain multiple highly conserved putative SREBP2 binding sites or sterol responsive elements (SREs) (Figure 3.3B). Chromatin immunoprecipiation (ChIP) analyses were then performed to validate the bioinformatics prediction. ECs overexpressing SREBP2(N) revealed increased SREBP2 enrichment in the promoters of the respective mesenchymal markers (Figure 3.3C). Further confirmation using luciferase assays also indicated increased SREBP2 binding to the promoter regions of snai1, αSMA,

N-Cad, and vimentin which was inhibited when the predicted SREs were deleted (Figure 3.3D). We next investigated whether BLM-induced EndoMT[12], was dependent on SREBP2. By suppressing SREBP2 with siRNA or betulin (a pan-SREBP inhibitor), we found that mesenchymal markers were substantially attenuated at the protein level in ECs treated with BLM (Figures 3.3E and 3.3F). Taken together, BLM-induced SREBP2 is both necessary and sufficient to induce EndoMT through transactivating mesenchymal markers in ECs.

EndoMT is not only characterized by the gain of mesenchymal markers, but also the loss of EC-specific markers. We next identified that SREBP2(N) overexpression lead to the suppression of classical ECs markers (i.e., Kruppel-like factor 4 [KLF4], vascular endothelial cadherin [VE-Cad], von Willebrand factor [vWF], and vascular endothelial growth factor receptor 2 [KDR]), similar to BLM treatment (Figures 3.4A and 3.4B). This highlights the role of SREBP2 in EndoMT, hallmarked by the EC genotypic switch with increased of mesenchymal markers as well as the reduction of EC markers. Importantly, as cell transdifferentiation is influenced by epigenetic modulations[29], we investigated how SREBP2 effects DNA methylation. It is known that DNA methyltransferase 1 (DNMT1) expression is increased in patients with pulmonary fibrosis[30, 31], BLM treatment also increased the DNMT1 activity in ECs (Figure 3.4C). Furthermore, using methylation specific (MSP) qPCR of bisulfite converted DNA, we analyzed the methylation status in the promoter regions of EC markers. BLM treatment caused significant DNA hypermethylation, consistent with suppressed gene transcription, in the EC markers (Figure 3.4D). Such effect of BLM was mimicked by SREBP2(N) overexpression in ECs (Figure

3.4E). In sum, SREBP2 suppressed EC-specific markers in part through increased DNA methylation in the promoter regions. However, the mechanism by which SREBP2 regulates DNA methylation requires further investigation.

Measuring the expression of EndoMT markers genetically only gives a fundamental snapshot of the EC transdifferentiation process. However, these genetic changes do not capture the biological function of the cell. Here, we aimed to investigate the phenotypic switch accompanied with the genotypic changes in ECs undergoing SREBP2-induced EndoMT. First, we measured cell proliferation. When ECs were overexpressing SREBP2(N), proliferation increased nearly 40% using a cell proliferation marker, phospho-histone 3 (p-H3) (Figure 3.5A). EndoMT also plays a critical role in modulating ECM deposition[11, 32]. Correspondingly, SREBP2(N) overexpression in ECs resulted in increased fibronectin (FN) deposition (Figure 3.5B). Furthermore, F-actin staining indicated increased stress fiber formation and microfilament bundles, consistent with a contractile cell. SREBP2(N) overexpression alone was sufficient for actin fiber reorganization (Figure 3.5C). Moreover, BLM-induced stress fiber formation was attenuated when SREBP2 was inhibited with betulin (Figure 3.5D). Thus, SREBP2 mediates not only the transactivation of EC-specific genes, but also the phenotypic switch associated with EndoMT including the proliferation, ECM deposition, and stress fiber formation.

To identify the role of SREBP2-induced EndoMT at the tissue level *in vivo*, we utilized a mouse line that overexpresses SREBP2(N) specifically in ECs [EC-SREBP2(N)-Tg mice]. Isolation of the lung ECs from EC-SREBP2(N)-Tg mice demonstrated increased

mesenchymal markers (i.e., αSMA, snai1, N-Cad, and vimentin), suppressed endothelial specific markers (i.e., eNOS, VE-Cad, and KLF4), and increased ECM genes (i.e., Col1A1 and FN) when compared to age matched wild-type (WT) mice (Figure 3.6A). This indicated that at the basal level, without any stimulus, SREBP2 overexpression is sufficient to promote EndoMT at the tissue level. At the disease level, we next systemically administered BLM to mice via i.p. injection to investigate SREBP2-induced EndoMT contributing to pulmonary fibrosis in a pathophysiological setting. Following BLM treatment, lungs were collected from EC-SREBP2(N)-Tg and WT controls for immunohistological analyses. In order to identify lung vasculature, we immunostained for VE-cad (EC marker) and αSMA (mesenchymal marker). WT mice treated with saline exhibited the highest expression of VE-cad (green) and lowest αSMA (red), evidenced by the merged image having a majority of green staining in the pulmonary vessels (Figure 3.6B). Interestingly, the WT mice treated with BLM and EC-SREBP2(N)-Tg mice treated with saline had a similar reduction and fragmentation of VE-cad (Figure 3.6B). Significantly, the BLM-treated EC-SREBP2(N)-Tg mice have the highest suppression of VE-cad with the greatest expression of αSMA (Figure 3.6B), demonstrating clear induction of EndoMT.

To further investigate the role of ECs in SREBP2-induced pulmonary fibrosis, we examined the whole lung architecture. H&E staining demonstrated increased mononuclear cell infiltration in the EC-SREBP2(N)-Tg mice treated with BLM (Figure 3.7A). Consistently, Masson's trichrome exhibited increased collagen deposition in areas surrounding lung vasculature as well as parenchymal fibrosis (Figures 3.7B and 3.7C).

Using angiography to depict the vascularization throughout the whole lung, we found that WT mice treated with BLM and EC-SREBP2(N)-Tg mice treated with saline had reduced distal vascularization, whereas they EC-SREBP2(N)-Tg mice treated with BLM had the most severe reduction in small to medium vessels (Figure 3.7D). Overall, we demonstrated that treating mice that overexpressed SREBP2(N) specifically in their ECs worsened the severity of BLM-induced pulmonary fibrosis.

Clinically, lung tissue isolated from IPF patients revealed increased SREBP2 immunostaining in the vasculature, which was localized to nuclei, when compared to normal controls (Figure 3.8A). Furthermore, IPF subjects had increased EndoMT as measured through increased αSMA and decreased CD31 staining in their lung vasculature (Figure 3.8B). Thus, providing evidence that SREBP2 may be a potential therapeutic target in the treatment of pulmonary fibrosis.

Discussion

The current study identifies SREBP2 as a novel transcription factor integral to the regulation of EndoMT. RNA-seq provided a global view of SREBP2 overexpression in ECs, leading us to the activation of the TGF, Wnt, and cytoskeleton remodeling pathways. Upon further investigation, many of the genes induced by SREBP2 overexpression were associated with mesenchymal cell differentiation, hence EndoMT. Moreover, we found that SREBP2 can directly bind to the promoter regions and transcriptionally activate snai1, αSMA, N-cad, and vimentin. This genotypic switch was accompanied with a phenotype that resembles a myofibroblast-like cell with increased proliferation, FN deposition, and stress fiber formation such as that of a contractile cell. The *in vivo* data suggests that endothelial-specific overexpression of SREBP2 exacerbates BLM-induced pulmonary fibrosis, potentially through the activation of EndoMT (see summary in Figure 3.9)

Although SREBP2 promoted the expression of mesenchymal markers and suppressed EC-specific markers, immunostaining experiments indicated that ECs are not fully transitioning to a myofibroblast cell nor migrating to the interstitium. This suggests that the ECs may be undergoing partial EndoMT. The gain of mesenchymal markers that we see in SREBP2-induced pulmonary fibrosis may still facilitate paracrine signals to neighboring cells, including the resident fibroblast population, to proliferate and deposit ECM proteins. Similar findings have been demonstrated in EMT contributing to kidney fibrosis. The transdifferentiated mesenchymal cell maintains association with the basement membrane and did not contribute to the myofibroblast population, but was still played a vital role in the progression of fibrosis[33, 34]. These studies also found that partial EMT may

contribute more to dysfunctional cell-cell communication and that fibrosis could be blocked by inhibiting the EMT-dependent secretome[33, 34]. In regards to pulmonary fibrosis, SREBP2-dependent EndoMT may be regulating secretory factors to the interstitium to promote fibrosis. However, the paracrine effects of partial EndoMT in pulmonary fibrosis warrants further investigation.

Clinically, pulmonary fibrosis remains to have no curative treatment options. Therapeutics targeting inflammatory markers have failed, although this was somewhat expected because the fibroblastic foci in the patient at the time of diagnosis does not contain immune cell infiltrate[5]. Furthermore, clinical trials for pulmonary arterial hypertension medications, such as sildenafil and bosentan, have shown limited endpoint efficacy[35]. However, there are currently two therapeutics that have demonstrated success in slowing the progression of the disease, nintedanib and pirfenidone. Nintedanib is a tyrosine kinase inhibitor that antagonizes the receptors for the growth factors PDGF, VEGF, and TGF[36]. Pirfenidone is an anti-fibrotic that inhibits TGFβ-induced collagen production and suppresses fibroblast proliferation[37]. Although both nintedanib and pirfenidone slow the progression of mild to moderate pulmonary fibrosis, there are severe gastrointestinal adverse effects[38]. Because SREBP2 plays a critical role in EC innate immune response[22] as well as fibrosis, shown in the current study, inhibitors of SREBP2 may be a potential therapeutic target. We established that the SREBP inhibitor, betulin, shows promise in suppressing fibrosis *in vitro* (Figures 3.3F and 3.5D). However, betulin treatment results in liver toxicity and cannot be used for human treatment. Therefore, it would be worthwhile to investigate therapies that block SREBP2 activity with direct lung targeting.

The link between dysregulated cholesterol and metabolic diseases, such as cardiovascular disease and diabetes mellitus type II, have been studied for decades. However, the relationship between dyslipidemia and lung disease has only recently emerged. High levels of circulating cholesterol results in increased lung innate immune response via immune cell infiltration as well as activates the NLRP3 inflammasome through toll-like receptor (TLR) signaling[39, 40]. Furthermore, mice that lack enzymes needed for reverse cholesterol transport, such as ATP-binding cassette (ABC)A1 and ABCG1, have increased macrophage recruitment, airway ECM deposition, and reduced airway compliance[41]. Therefore, therapeutics that are aimed to reduce cholesterol biosynthesis and increase cholesterol reverse transport, i.e., pleotropic statins, may provide potential benefit to lung diseases. Although statins have shown some promise in diseases such as COPD and pulmonary hypertension, the effectiveness in pulmonary fibrosis remains obscure[42]. A meta-analysis of the ASCEND and CAPACITY clinical trials that separated patients treated with statins suggested increase welfare with clinical outcomes[43]. However, several groups have reported that statins worsen interstitial lung disease and that interstitial lung disease may even be a side effect of statins[44, 45]. Notably, BLM-induced pulmonary fibrosis was exacerbated in mice pre-treated with statins, which was found to be through the induction of the NLRP3 inflammasome[44]. These somewhat contradictory results may be explained by the induction of SREBP2. Statins inhibit the first rate limiting step of cholesterol biosynthesis through the blockage of HMG-CoA reductase. This in turn reduces the level of intracellular cholesterol and activates SREBP2. Studies by we and others have also identified SREBP as a key mediator of NLRP3 inflammasome activing in

both ECs and macrophages[22, 46]. This further suggests that the blockade of SREBP2, which is involved in both innate immune response and a pro-fibrotic phenotype, would be beneficial in the progression of pulmonary fibrosis.

We provide evidence to suggest that SREBP2 induction was due to increased oxidative stress incurred from BLM treatment. In a study in collaboration with Dr. Zhen Chen, we also identified that SREBP2 was activated by a number of oxidative stress inducers (i.e., H_2O_2, angiotensin II, and oxidized LDL) in ECs (Figure 3.10A)[21]. Furthermore, treating cells with EUK 134, a catalase mimic and anti-oxidant, prevented the cleavage and activation of SREBP2 (Figure 3.10B). In the context of disease, atherosclerosis progression is well-known to be mediated by increased levels of oxidative stress[47]. We have previously shown that the EC-SREBP2(N)-Tg has increased atherosclerosis when fed a high fat diet via the induction of the NLRP3 inflammasome[22], however the mechanism hasn't been fully elucidated. One study in collaboration with Dr. Ting Lin provided evidence that SREBP2 was a transcriptional activator of TRAF-interacting protein with FHA domain-containing protein A (TIFA), a known mediator of the pro-inflammatory NF-*k*B pathway and NLRP3 inflammasome[48, 49]. In another study in collaboration with Dr. Zhen Chen, we further found through bioinformatics prediction that SREBP2 could serve as a transcription factor for microRNA-92a (miR-92a) (Figure 3.10C)[21]. Additionally, miR-92a was demonstrated to target the 3' UTR of KLF4 using luciferase assays (Figure 3.10D). To verify whether miR-92a targeting KLF4 could contribute to disease progression *in vivo*, EC-SREBP2(N)-Tg mice that were crossed with $ApoE^{-/-}$ were administered angiotensin II to accelerate atherosclerosis. Following tail vein

injection of locked nucleic acid (LNA)-modified miR-92a antisense, to increase the stability of the antisense RNA, mice had reduced atherosclerotic lesion development when compared to the control antisense RNA (Figure 3.10E). Subsequent work in collaboration with Dr. Zhen Chen also suggested that circulating miR-92a plays a role in chronic kidney disease[50]. These data provide an additional mechanism into the key role of SREBP2 in EC dysfunction and vascular disease.

By using a genome-wide, systems approach we found that SREBP2 may be a potential therapeutic target for pulmonary fibrosis. The current study focuses on the role of endothelial dysfunction, a cell type that is often overlooked despite composing more than 30% of lung tissue[13], in the context of pulmonary fibrosis. IPF by definition has an unknown etiology, but is thought to have an initial inflammatory response followed by chronic and unlimited fibrosis. Because SREBP2 is a key mediator of the NLRP3 inflammasome and EndoMT, the blockade of SREBP2 may inhibit both the initial innate immune response and the pro-fibrotic stages of IPF.

References

1. Wolters PJ, Collard HR and Jones KD. Pathogenesis of idiopathic pulmonary fibrosis. *Annual review of pathology*. 2014;9:157-79.

2. Blackwell TS, Tager AM, Borok Z, Moore BB, Schwartz DA, Anstrom KJ, Bar-Joseph Z, Bitterman P, Blackburn MR, Bradford W, Brown KK, Chapman HA, Collard HR, Cosgrove GP, Deterding R, Doyle R, Flaherty KR, Garcia CK, Hagood JS, Henke CA, Herzog E, Hogaboam CM, Horowitz JC, King TE, Jr., Loyd JE, Lawson WE, Marsh CB, Noble PW, Noth I, Sheppard D, Olsson J, Ortiz LA, O'Riordan TG, Oury TD, Raghu G, Roman J, Sime PJ, Sisson TH, Tschumperlin D, Violette SM, Weaver TE, Wells RG, White ES, Kaminski N, Martinez FJ, Wynn TA, Thannickal VJ and Eu JP. Future directions in idiopathic pulmonary fibrosis research. An NHLBI workshop report. *American journal of respiratory and critical care medicine*. 2014;189:214-22.

3. Juarez MM, Chan AL, Norris AG, Morrissey BM and Albertson TE. Acute exacerbation of idiopathic pulmonary fibrosis-a review of current and novel pharmacotherapies. *Journal of thoracic disease*. 2015;7:499-519.

4. Bringardner BD, Baran CP, Eubank TD and Marsh CB. The role of inflammation in the pathogenesis of idiopathic pulmonary fibrosis. *Antioxidants & redox signaling*. 2008;10:287-301.

5. Meltzer EB and Noble PW. Idiopathic pulmonary fibrosis. *Orphanet journal of rare diseases*. 2008;3:8.

6. Kottmann RM, Hogan CM, Phipps RP and Sime PJ. Determinants of initiation and progression of idiopathic pulmonary fibrosis. *Respirology (Carlton, Vic)*. 2009;14:917-33.

7. Fernandez IE and Eickelberg O. The impact of TGF-beta on lung fibrosis: from targeting to biomarkers. *Proceedings of the American Thoracic Society*. 2012;9:111-6.

8. Puglisi S, Torrisi SE, Vindigni V, Giuliano R, Palmucci S, Mule M and Vancheri C. New perspectives on management of idiopathic pulmonary fibrosis. *Therapeutic advances in chronic disease*. 2016;7:108-20.

9. Bagnato G and Harari S. Cellular interactions in the pathogenesis of interstitial lung diseases. *European respiratory review : an official journal of the European Respiratory Society*. 2015;24:102-14.

10. Chapman HA. Epithelial-mesenchymal interactions in pulmonary fibrosis. *Annual review of physiology*. 2011;73:413-35.

11. Piera-Velazquez S, Mendoza FA and Jimenez SA. Endothelial to Mesenchymal Transition (EndoMT) in the Pathogenesis of Human Fibrotic Diseases. *Journal of clinical medicine*. 2016;5.

12. Hashimoto N, Phan SH, Imaizumi K, Matsuo M, Nakashima H, Kawabe T, Shimokata K and Hasegawa Y. Endothelial-mesenchymal transition in bleomycin-induced pulmonary fibrosis. *American journal of respiratory cell and molecular biology*. 2010;43:161-72.

13. Crapo JD, Barry BE, Gehr P, Bachofen M and Weibel ER. Cell number and cell characteristics of the normal human lung. *The American review of respiratory disease*. 1982;126:332-7.

14. Jules-Elysee K and White DA. Bleomycin-induced pulmonary toxicity. *Clinics in chest medicine*. 1990;11:1-20.

15. Sleijfer S. Bleomycin-induced pneumonitis. *Chest*. 2001;120:617-24.

16. O'Sullivan JM, Huddart RA, Norman AR, Nicholls J, Dearnaley DP and Horwich A. Predicting the risk of bleomycin lung toxicity in patients with germ-cell tumours. *Annals of oncology : official journal of the European Society for Medical Oncology*. 2003;14:91-6.

17. Lazo JS, Merrill WW, Pham ET, Lynch TJ, McCallister JD and Ingbar DH. Bleomycin hydrolase activity in pulmonary cells. *The Journal of pharmacology and experimental therapeutics*. 1984;231:583-8.

18. B BM, Lawson WE, Oury TD, Sisson TH, Raghavendran K and Hogaboam CM. Animal models of fibrotic lung disease. *American journal of respiratory cell and molecular biology*. 2013;49:167-79.

19. Gilson AJ and Sahn SA. Reactivation of bleomycin lung toxicity following oxygen administration. A second response to corticosteroids. *Chest*. 1985;88:304-6.

20. Ingrassia TS, 3rd, Ryu JH, Trastek VF and Rosenow EC, 3rd. Oxygen-exacerbated bleomycin pulmonary toxicity. *Mayo Clinic proceedings*. 1991;66:173-8.

21. Chen Z, Wen L, Martin M, Hsu CY, Fang L, Lin FM, Lin TY, Geary MJ, Geary GG, Zhao Y, Johnson DA, Chen JW, Lin SJ, Chien S, Huang HD, Miller YI, Huang PH and Shyy JY. Oxidative stress activates endothelial innate immunity via sterol regulatory element binding protein 2 (SREBP2) transactivation of microRNA-92a. *Circulation*. 2015;131:805-14.

22. Xiao H, Lu M, Lin TY, Chen Z, Chen G, Wang WC, Marin T, Shentu TP, Wen L, Gongol B, Sun W, Liang X, Chen J, Huang HD, Pedra JH, Johnson DA and Shyy JY. Sterol regulatory element binding protein 2 activation of NLRP3 inflammasome in endothelium mediates hemodynamic-induced atherosclerosis susceptibility. *Circulation*. 2013;128:632-42.

23. Malhotra P, Aloman C, Ankireddy A, Khadra H, Ooka K, Gill RK, Saksena S, Dudeja PK and Alrefai WA. Overactivation of intestinal sterol response element-binding protein 2 promotes diet-induced nonalcoholic steatohepatitis. *American journal of physiology Gastrointestinal and liver physiology*. 2017;313:G376-g385.

24. Tomita K, Teratani T, Suzuki T, Shimizu M, Sato H, Narimatsu K, Okada Y, Kurihara C, Irie R, Yokoyama H, Shimamura K, Usui S, Ebinuma H, Saito H, Watanabe C, Komoto S, Kawaguchi A, Nagao S, Sugiyama K, Hokari R, Kanai T, Miura S and Hibi T. Free cholesterol accumulation in hepatic stellate cells: mechanism of liver fibrosis aggravation in nonalcoholic steatohepatitis in mice. *Hepatology (Baltimore, Md)*. 2014;59:154-69.

25. Kim D, Pertea G, Trapnell C, Pimentel H, Kelley R and Salzberg SL. TopHat2: accurate alignment of transcriptomes in the presence of insertions, deletions and gene fusions. *Genome biology*. 2013;14:R36.

26. Roberts A, Trapnell C, Donaghey J, Rinn JL and Pachter L. Improving RNA-Seq expression estimates by correcting for fragment bias. *Genome biology*. 2011;12:R22.

27. Trapnell C, Williams BA, Pertea G, Mortazavi A, Kwan G, van Baren MJ, Salzberg SL, Wold BJ and Pachter L. Transcript assembly and quantification by RNA-Seq reveals unannotated transcripts and isoform switching during cell differentiation. *Nature biotechnology*. 2010;28:511-5.

28. Kel AE, Gossling E, Reuter I, Cheremushkin E, Kel-Margoulis OV and Wingender E. MATCH: A tool for searching transcription factor binding sites in DNA sequences. *Nucleic acids research*. 2003;31:3576-9.

29. Mortada I and Mortada R. Epigenetic changes in mesenchymal stem cells differentiation. *European journal of medical genetics*. 2017.

30. Sanders YY, Ambalavanan N, Halloran B, Zhang X, Liu H, Crossman DK, Bray M, Zhang K, Thannickal VJ and Hagood JS. Altered DNA methylation profile in idiopathic pulmonary fibrosis. *American journal of respiratory and critical care medicine*. 2012;186:525-35.

31. Dakhlallah D, Batte K, Wang Y, Cantemir-Stone CZ, Yan P, Nuovo G, Mikhail A, Hitchcock CL, Wright VP, Nana-Sinkam SP, Piper MG and Marsh CB. Epigenetic regulation of miR-17~92 contributes to the pathogenesis of pulmonary fibrosis. *American journal of respiratory and critical care medicine*. 2013;187:397-405.

32. Jimenez SA. Role of endothelial to mesenchymal transition in the pathogenesis of the vascular alterations in systemic sclerosis. *ISRN rheumatology*. 2013;2013:835948.

33. Lovisa S, LeBleu VS, Tampe B, Sugimoto H, Vadnagara K, Carstens JL, Wu CC, Hagos Y, Burckhardt BC, Pentcheva-Hoang T, Nischal H, Allison JP, Zeisberg M and Kalluri R. Epithelial-to-mesenchymal transition induces cell cycle arrest and parenchymal damage in renal fibrosis. *Nature medicine*. 2015;21:998-1009.

34. Grande MT, Sanchez-Laorden B, Lopez-Blau C, De Frutos CA, Boutet A, Arevalo M, Rowe RG, Weiss SJ, Lopez-Novoa JM and Nieto MA. Snail1-induced partial epithelial-to-mesenchymal transition drives renal fibrosis in mice and can be targeted to reverse established disease. *Nature medicine*. 2015;21:989-97.

35. Nathan SD and King CS. Treatment of pulmonary hypertension in idiopathic pulmonary fibrosis: shortfall in efficacy or trial design? *Drug design, development and therapy*. 2014;8:875-85.

36. Richeldi L, du Bois RM, Raghu G, Azuma A, Brown KK, Costabel U, Cottin V, Flaherty KR, Hansell DM, Inoue Y, Kim DS, Kolb M, Nicholson AG, Noble PW, Selman M, Taniguchi H, Brun M, Le Maulf F, Girard M, Stowasser S, Schlenker-Herceg R, Disse B and Collard HR. Efficacy and Safety of Nintedanib in Idiopathic Pulmonary Fibrosis. *New England Journal of Medicine*. 2014;370:2071-2082.

37. King TEJ, Bradford WZ, Castro-Bernardini S, Fagan EA, Glaspole I, Glassberg MK, Gorina E, Hopkins PM, Kardatzke D, Lancaster L, Lederer DJ, Nathan SD, Pereira CA, Sahn SA, Sussman R, Swigris JJ and Noble PW. A Phase 3 Trial of Pirfenidone in Patients with Idiopathic Pulmonary Fibrosis. *New England Journal of Medicine*. 2014;370:2083-2092.

38. Vancheri C, Kreuter M, Richeldi L, Ryerson CJ, Valeyre D, Grutters JC, Wiebe S, Stansen W, Quaresma M, Stowasser S and Wuyts WA. Nintedanib with Add-on Pirfenidone in Idiopathic Pulmonary Fibrosis: Results of the INJOURNEY Trial. *American journal of respiratory and critical care medicine*. 2017.

39. Yvan-Charvet L, Welch C, Pagler TA, Ranalletta M, Lamkanfi M, Han S, Ishibashi M, Li R, Wang N and Tall AR. Increased inflammatory gene expression in ABC transporter-deficient macrophages: free cholesterol accumulation, increased signaling via toll-like receptors, and neutrophil infiltration of atherosclerotic lesions. *Circulation*. 2008;118:1837-47.

40. Duewell P, Kono H, Rayner KJ, Sirois CM, Vladimer G, Bauernfeind FG, Abela GS, Franchi L, Nunez G, Schnurr M, Espevik T, Lien E, Fitzgerald KA, Rock KL, Moore KJ, Wright SD, Hornung V and Latz E. NLRP3 inflammasomes are required for atherogenesis and activated by cholesterol crystals. *Nature*. 2010;464:1357-61.

41. Wang W, Xu H, Shi Y, Nandedkar S, Zhang H, Gao H, Feroah T, Weihrauch D, Schulte ML, Jones DW, Jarzembowski J, Sorci-Thomas M and Pritchard KA, Jr. Genetic deletion of apolipoprotein A-I increases airway hyperresponsiveness, inflammation, and collagen deposition in the lung. *Journal of lipid research*. 2010;51:2560-70.

42. Gowdy KM and Fessler MB. Emerging roles for cholesterol and lipoproteins in lung disease. *Pulmonary pharmacology & therapeutics*. 2013;26:430-7.

43. Kreuter M, Bonella F, Maher TM, Costabel U, Spagnolo P, Weycker D, Kirchgaessler KU and Kolb M. Effect of statins on disease-related outcomes in patients with idiopathic pulmonary fibrosis. *Thorax*. 2017;72:148-153.

44. Xu JF, Washko GR, Nakahira K, Hatabu H, Patel AS, Fernandez IE, Nishino M, Okajima Y, Yamashiro T, Ross JC, Estepar RS, Diaz AA, Li HP, Qu JM, Himes BE, Come CE, D'Aco K, Martinez FJ, Han MK, Lynch DA, Crapo JD, Morse D, Ryter SW, Silverman EK, Rosas IO, Choi AM and Hunninghake GM. Statins and pulmonary fibrosis: the potential role of NLRP3 inflammasome activation. *American journal of respiratory and critical care medicine*. 2012;185:547-56.

45. Fernandez AB, Karas RH, Alsheikh-Ali AA and Thompson PD. Statins and interstitial lung disease: a systematic review of the literature and of food and drug administration adverse event reports. *Chest*. 2008;134:824-30.

46. Im SS, Yousef L, Blaschitz C, Liu JZ, Edwards RA, Young SG, Raffatellu M and Osborne TF. Linking lipid metabolism to the innate immune response in macrophages through sterol regulatory element binding protein-1a. *Cell metabolism*. 2011;13:540-9.

47. Bonomini F, Tengattini S, Fabiano A, Bianchi R and Rezzani R. Atherosclerosis and oxidative stress. *Histology and histopathology*. 2008;23:381-90.

48. Lin TY, Wei TW, Li S, Wang SC, He M, Martin M, Zhang J, Shentu TP, Xiao H, Kang J, Wang KC, Chen Z, Chien S, Tsai MD and Shyy JY. TIFA as a crucial mediator for NLRP3 inflammasome. *Proceedings of the National Academy of Sciences of the United States of America*. 2016;113:15078-15083.

49. Wei TW, Wu PY, Wu TJ, Hou HA, Chou WC, Teng CJ, Lin CR, Chen JM, Lin TY, Su HC, Huang CF, Yu CR, Hsu SL, Tien HF and Tsai MD. Aurora A and NF-kappaB Survival Pathway Drive Chemoresistance in Acute Myeloid Leukemia via the TRAF-Interacting Protein TIFA. *Cancer research*. 2017;77:494-508.

50. Shang F, Wang SC, Hsu CY, Miao Y, Martin M, Yin Y, Wu CC, Wang YT, Wu G, Chien S, Huang HD, Tarng DC, Shiu YT, Cheung AK, Huang PH, Chen Z and Shyy JY. MicroRNA-92a Mediates Endothelial Dysfunction in CKD. *Journal of the American Society of Nephrology : JASN*. 2017.

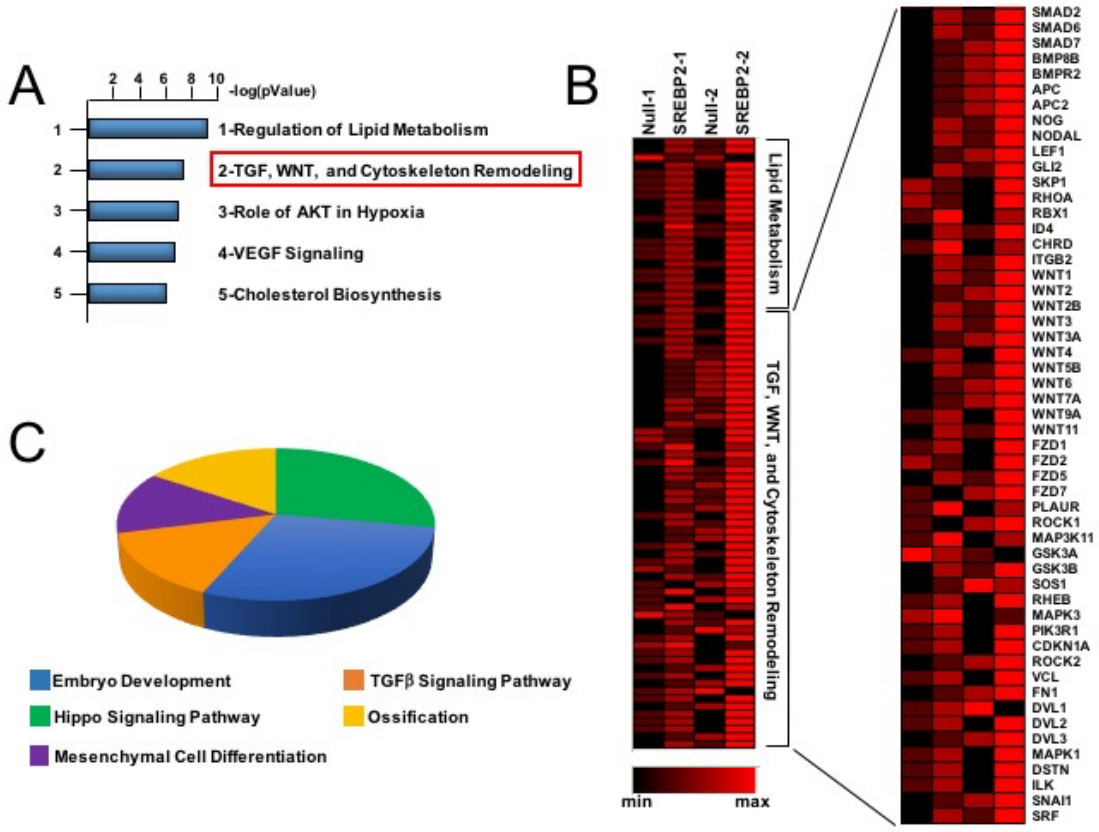

Figure 3.1. SREBP2(N) mediates pro-fibrotic genes in ECs. HUVECs were infected with Ad-SREBP2(N) or Ad-null (empty vector) for 72 hr, followed by RNA-sequencing. (A) Gene ontology (GO) analysis of the top 500 genes induced by SREBP2(N) overexpression. (B) Heat map indicated the genes in the TGF, WNT, Cytoskeleton Remodeling pathway. (C) PANTHER analysis of the genes listed in panel B.

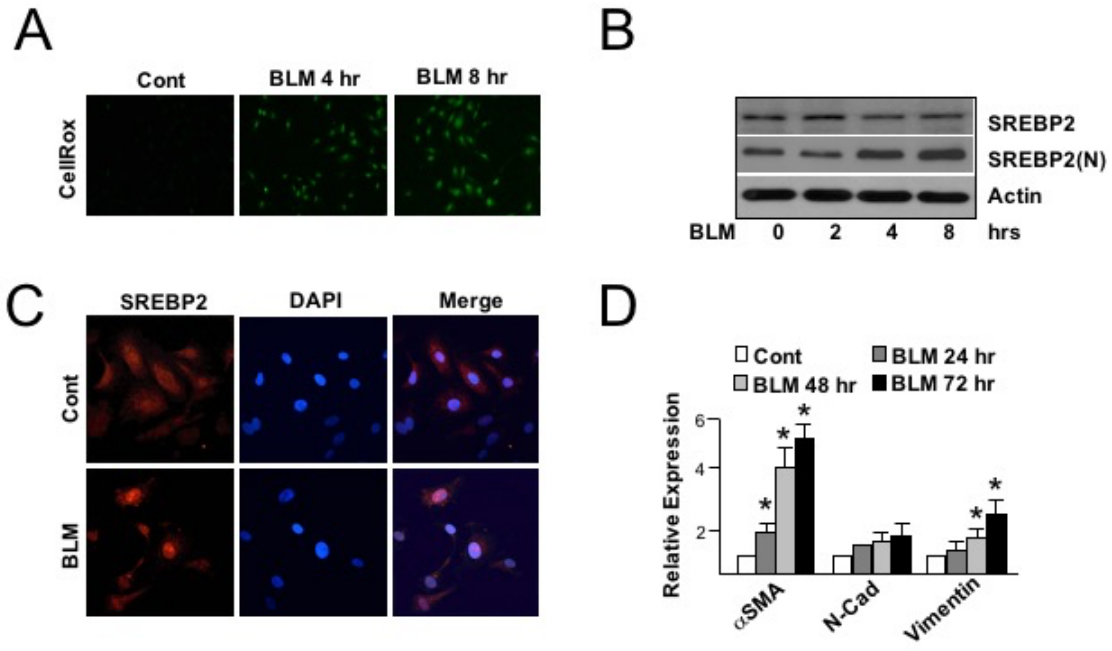

Figure 3.2. BLM induces SREBP2 N-terminal cleavage and EndoMT. HUVECs were stimulated with BLM (1 mU) for increasing time points. (A) Intracellular ROS was staining using CellRox (green). (B) N-terminal cleavage of SREBP2 was measured using Western blot. (C) Immunostaining of SREBP2 to identify cellular localization (SREBP2 is red, nuclei stained blue with DAPI). (D) Mesenchymal markers were measured using qPCR. Data presented are mean± SEM from three independent experiments. *p <0.05 between the indicated groups.

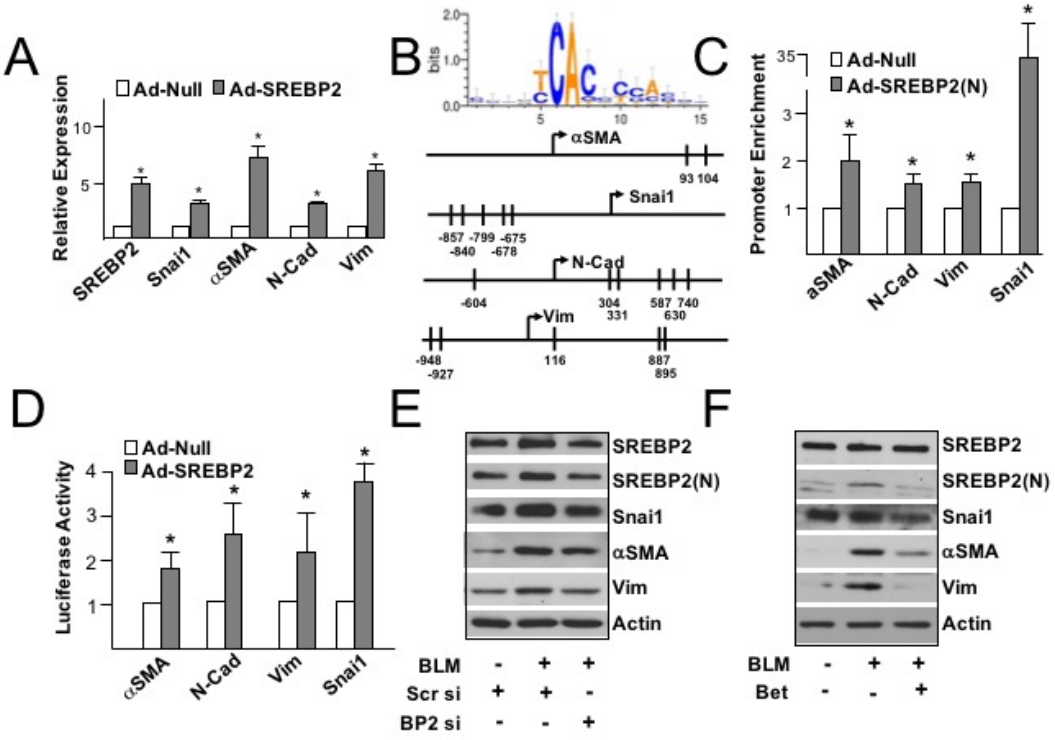

Figure 3.3. SREBP2 transactivates mesenchymal gene expression. (A) HUVECs were infected with Ad-SREBP2 or empty vector for 72 hr. mRNA of the indicated genes were measured by qPCR. (B) Depiction of the predicted sterol regulatory elements (SREs) in the promoter regions of αSMA, snai1, N-Cad, and vimentin. (C-D) HUVECs were infected with Ad-SREBP2 or empty vector for 72 hr. (C) Chromatin immunoprecipitation (ChIP) assays were performed on the promoter regions and (D) luciferase activity was measured and compared to that of Renilla. (E) HUVECs were transfected with SREBP2 or scrambled control siRNA (20 nM) for 16 hr prior to stimulation with BLM for an additional 48 hr. (F) HUVECs were pre-treated with betulin (6 μg/mL) for 2 hr, followed by BLM treatment for an additional 72 hr. Protein expression was measured by Western blot. Error bars represent mean±SEM from three independent experiments. *p<0.05 between the indicated groups.

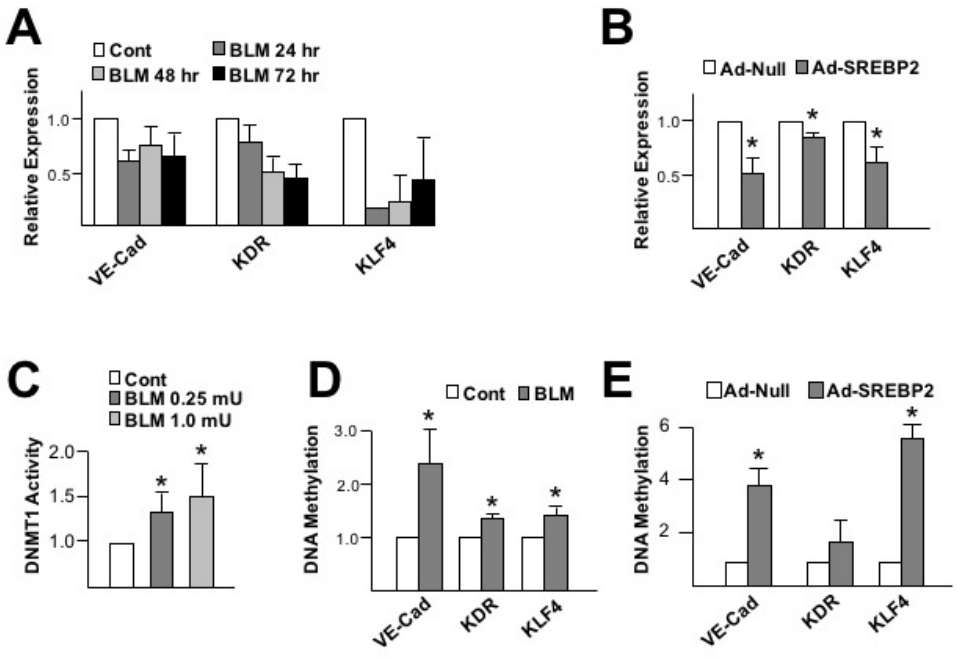

Figure 3.4. BLM-induced SREBP2 suppresses endothelial markers via increased DNA methylation. (A) HUVECs were treated with increasing time points of BLM (1 mU) followed by endothelial specific markers measured using qPCR. (B) HUVECs were infected with Ad-SREBP2 or Ad-Null for 72 hr. mRNA expression of the indicated genes were measured by qPCR. (C) HUVECs were treated with the indicated concentration of BLM for 72 hr. DNMT1 activity was measured quantitatively using ELISA. (D-E) HUVECs treated with BLM or infected with adenovirus for 72 hr. Isolated DNA was bisulfite converted and subjected to methylation specific qPCR. Error bars represent mean±SEM from three independent experiments. *p<0.05 between the indicated groups.

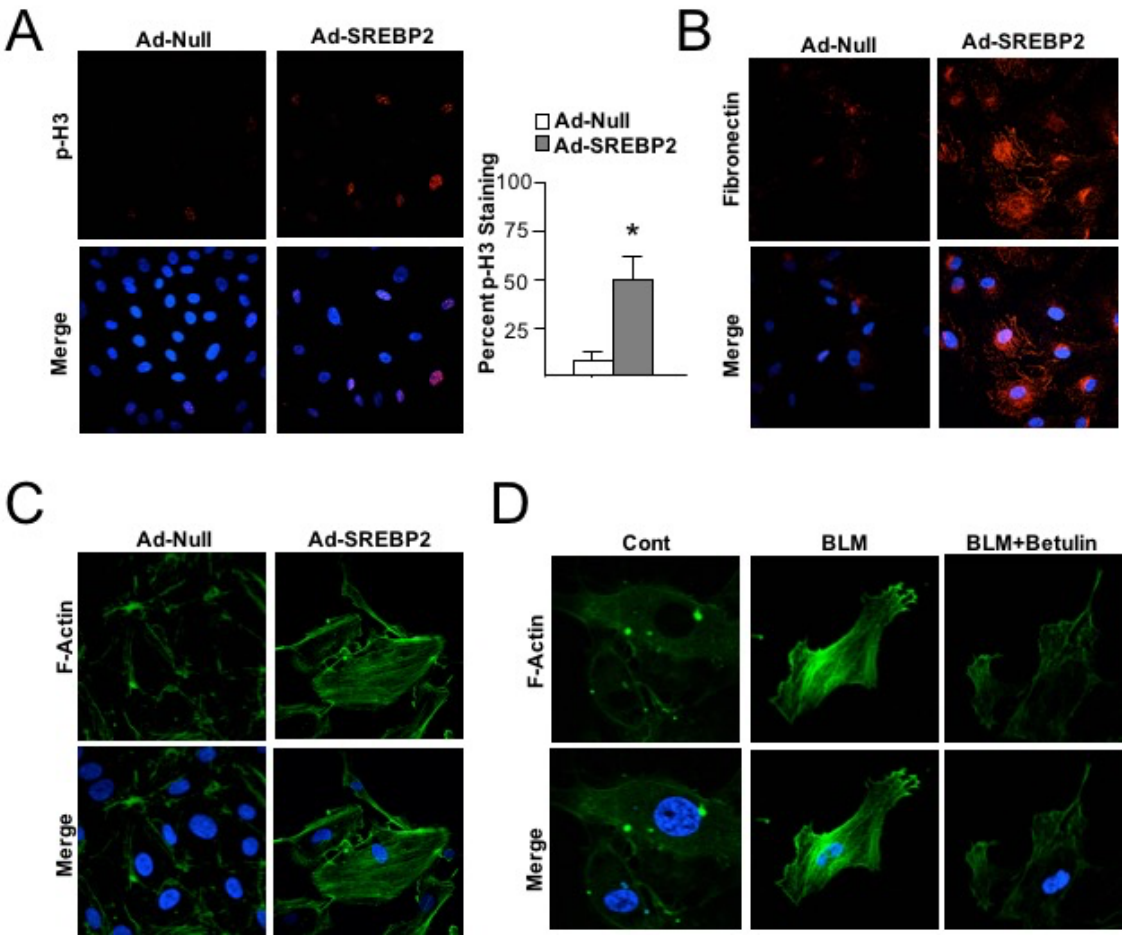

Figure 3.5. SREBP2 promotes a phenotypic switch in ECs undergoing EndoMT. (A-C) HUVECs were infected with Ad-SREBP2 or Ad-Null for 72 hr prior to being fixed with 4% PFA and subjected to immunostaining. (A) Proliferation was measured using phospho-histone 3 (red), (B) ECM deposition was measured using fibronectin (red), and (C) stress fiber formation was measured using F-actin (green). (D) HUVECs were pre-treated with betulin for 2 hr, followed by BLM for 72 hr. Stress fiber formation was measured using F-actin (green). Nuclei were stained using DAPI (blue). Error bars represent mean±SEM from three independent experiments. *p<0.05 between the indicated groups.

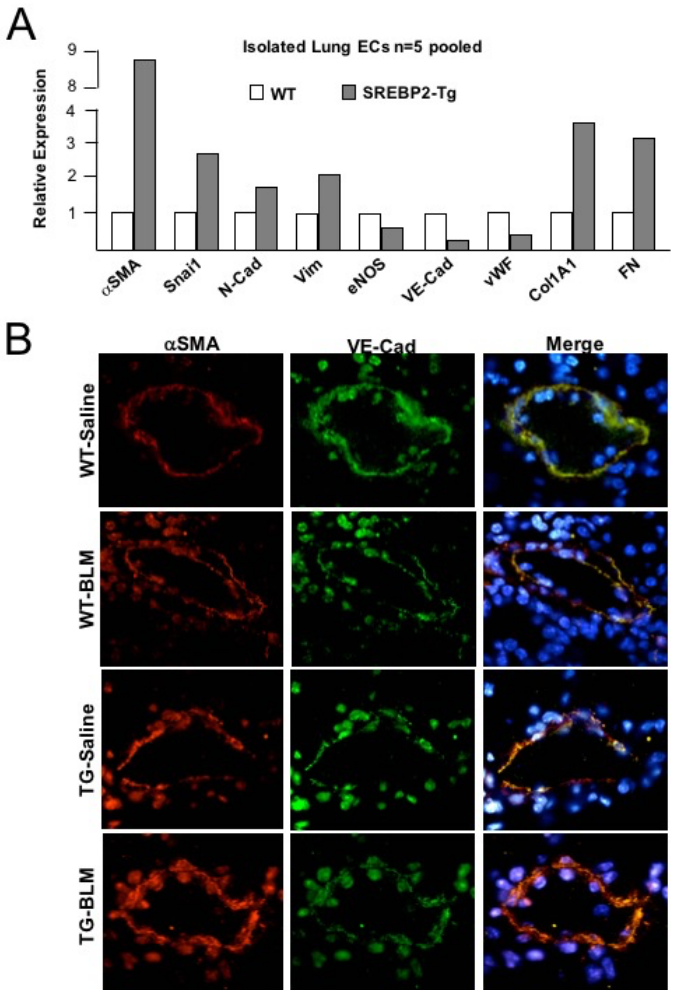

Figure 3.6. SREBP2 promotes EndoMT *in vivo*. (A) Lung microvascular ECs were isolated from age-matched EC-SREBP2(N)-Tg mice and compared to their wildtype littermates (n=5 per group pooled). mRNA of the indicated genes were measured using qPCR. (B) Age-matched EC-SREBP2(N)-Tg or wildtype littermates were administered 5 intraperitoneal (i.p.) injections of BLM (8 units/injection) on Days 0, 4, 7, 10, and 14. Following an additional 14 days, lungs were perfused with PBS, harvested, and fixed in 4% PFA overnight. Frozen lung sections were immunostained for the EC-marker VE-Cad (green) and the mesenchymal marker aSMA (red). Nuclei were stained using DAPI (blue).

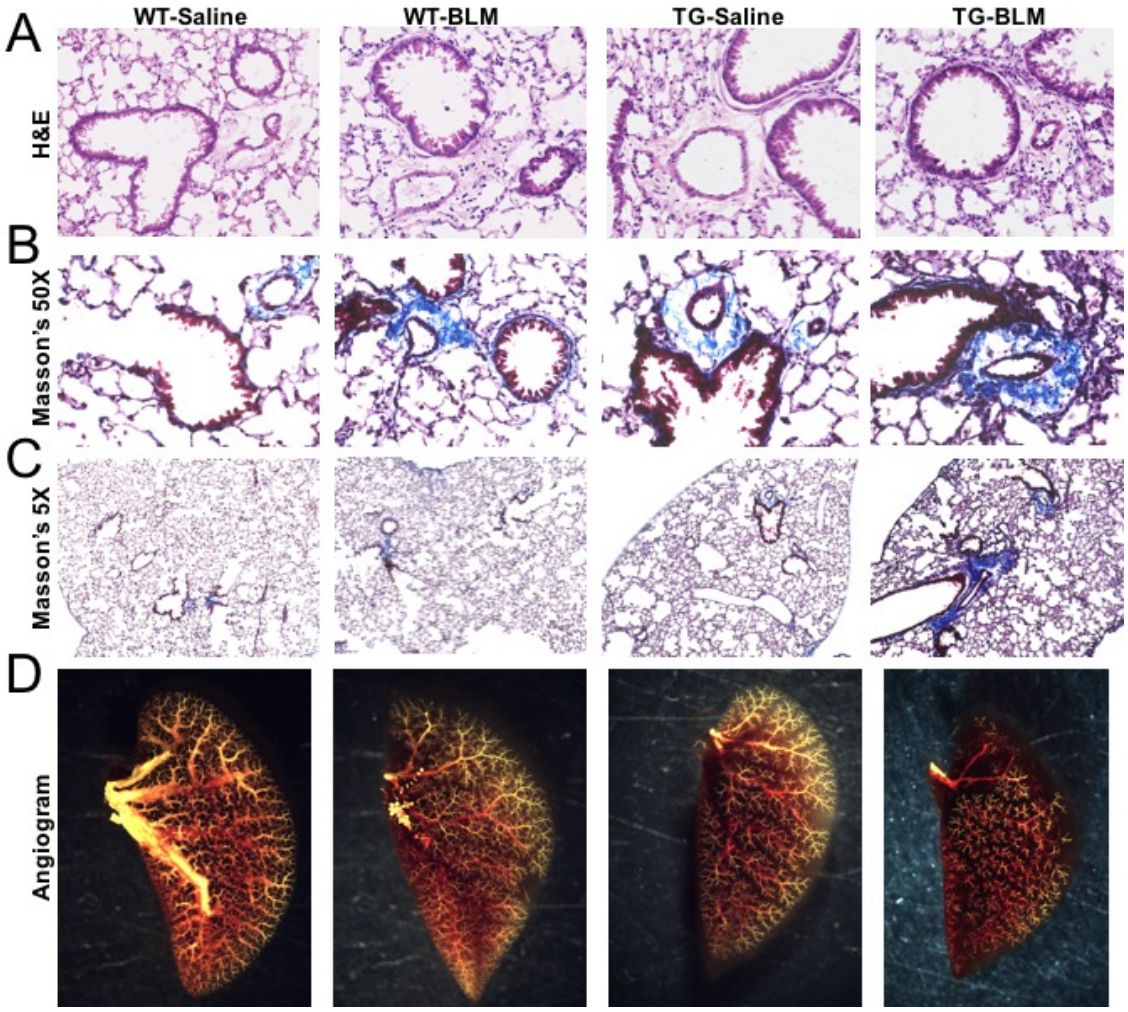

Figure 3.7. BLM-induced pulmonary fibrosis is exacerbated in EC-SREBP2(N)-Tg mice. Age-matched EC-SREBP2(N)-Tg or wildtype littermates were administered 5 i.p. injections of BLM (8 units/injection) on Days 0, 4, 7, 10, and 14. Following an additional 14 days, lungs were harvested. (A-C) Perfused lungs were fixed in 4% PFA overnight, followed by histology of frozen sections. (A) H&E stains cells (red) and nuclei (black), (B-C) Masson's Trichrome stains cells (red) and collagen (blue). (D) Microfil was used to visualize the lung vascularization (yellow). n=4-6 mice per group for all experiments.

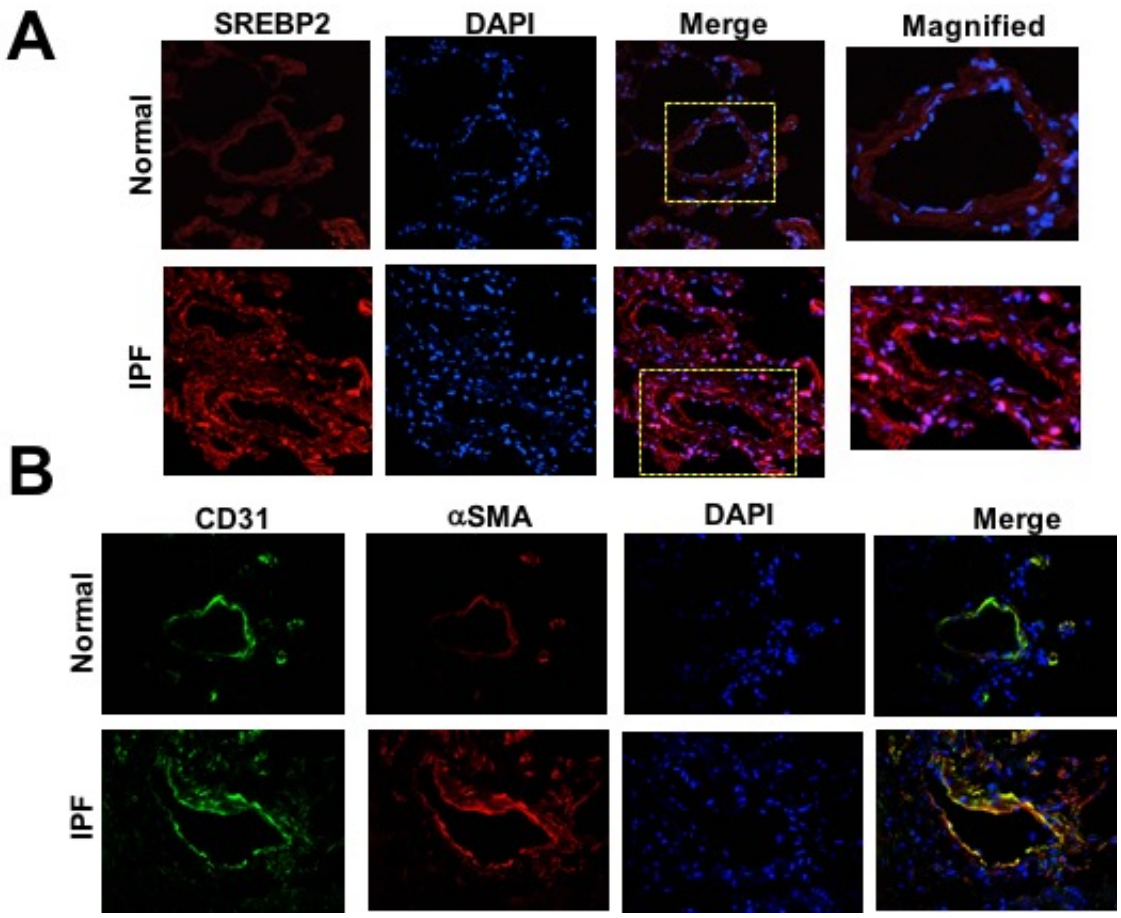

Figure 3.8. SREBP2 and EndoMT is induced in human IPF. Human lung tissue samples from IPF patients were compared to normal lung transplant controls (n=3 per group). Immunostaining was performed for (A) SREBP2 (red), and (B) the EC-marker CD31 (green) and the mesenchymal marker αSMA (red). Nuclei were stained with DAPI (blue). The yellow boxes highlight vessels within the lung.

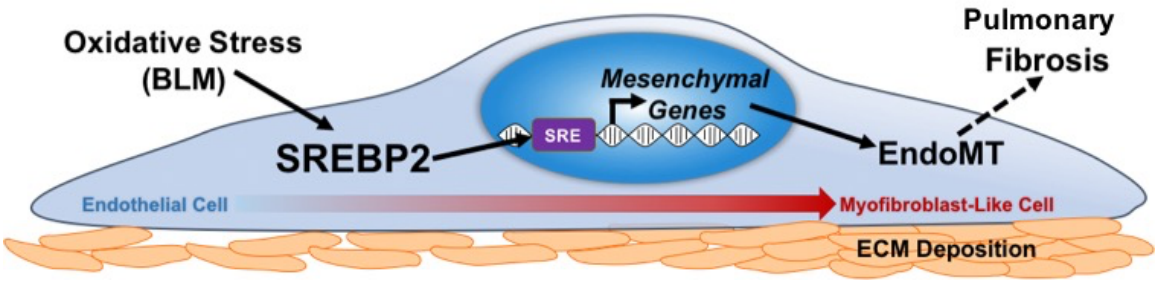

Figure 3.9. SREBP2-induced EndoMT contributes to pulmonary fibrosis. Oxidative stress (e.g., bleomycin [BLM]) can activate SREBP2. SREBP2 can then serve as a transcription factor to induce genes associated with mesenchymal differentiation (i.e., snai1, aSMA, N-cad, and vimentin). This genotypic change promotes a phenotypic switch in the endothelial cell to become more myofibroblast-like, including increased ECM deposition and contractility. Overall, the EC-derived myofibroblast-like cell can exacerbate pulmonary fibrosis.

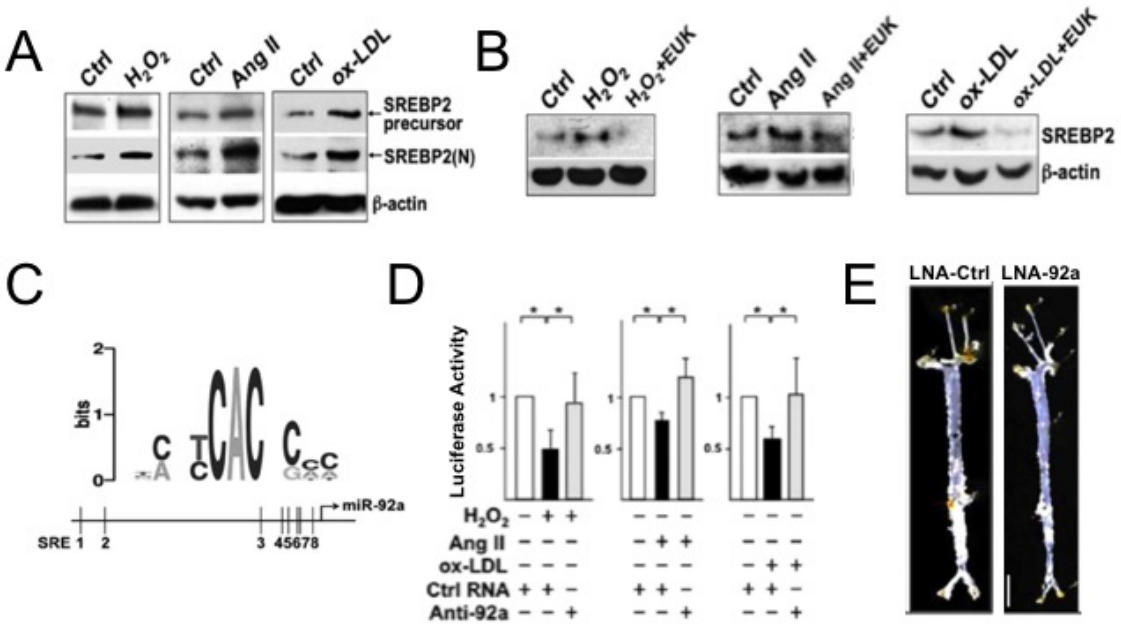

Figure 3.10. SREBP2 transactivates miR-92a contributing to atherosclerosis. This figure is an adaptation from Chen Z, et al. *Circulation* 2015. (A) HUVECs were treated with H_2O_2 (100 μmol/L, Ang II (100 nmol/L), or ox-LDL (100 μg/mL) for 16 hr. SREBP2 N-terminal cleavage was measured by using Western blot. (B) HUVECs were pre-treated with EUK-134 (1 μmol/L) for 2 hr, followed by treatment with H_2O_2, Ang II, or ox-LDL for an additional 16 hr. SREBP2 protein expression was measured by Western blot. (C) Depiction of predicted SREs in the promoter region of miR-92a. (D) ECs were transfected with a luciferase reporter containing 3 tandem miR-92a responsive elements in the KLF4 3'UTR. ECs were then incubated with anti-miR-92a or control RNA for 24 hr, then treated with H2O2, Ang II, or ox-LDL for an additional 16 hr. Luciferase activity was normalized to that of Renilla. (E) EC-SREBP2(N)-Tg mice were crossed with ApoE-null background and infused with Ang II (1 μg/min/kg) via mini osmotic pump for 28 days (n=4 per group). Tail vein injections of locked nucleic acid (LNA)-modified miR-92a antisense or LNA-modified control RNA were administered 1 week prior to Ang II osmotic pump implantation and 10 days after pump implantation. Atherosclerotic lesion area was quantified using *en face* imaging. Bar indicates 0.5 cm. Error bars represent mean±SEM from three independent experiments. *p<0.05 between the indicated groups.

CHAPTER 4

Conclusion and Perspectives

4.1 Introduction

A monolayer of ECs taken from an adult human would be able to span 8 tennis courts[1]. It is therefore foreseeable that endothelial homeostasis is a major contributor to human health or disease. In this dissertation, I found that EC function is tightly associated with cholesterol regulation via two principal transcription factors, i.e., KLF4 and SREBP2. Assessing the opposing role of these two transcription factors, KLF4 being beneficial and SREBP2 being detrimental, provided new insights to the delicate interplay between EC and cholesterol homeostasis. This dual and reciprocal approach identified that KLF4, essential for eNOS-derived NO bioavailability and the anti-inflammatory properties of a functional endothelium[2, 3], is also necessary for the induction of Ch25h and LXR, regulators of cholesterol oxidation and efflux. Conversely, SREBP2, a canonical master regulator of cholesterol uptake and biosynthesis[4], promotes EC dysfunction through the induction of EndoMT. Both studies used global approaches to identify novel signaling pathways regulated by each transcription factor. Therefore, these studies not only provide a nexus between EC function and cholesterol homeostasis, but also an innovative method for identifying seemingly unrelated pathways and functional outcomes in ECs.

4.2 Bioinformatic analyses to investigate EC function

Because both KLF4 and SREBP2 are transcription factors, it was inherent to measure transcriptome data. However, both data sets in Chapter 2 and 3 used exogenous overexpression through adenovirus. Despite comparing to an empty adenovirus vector as

a control, the artificial overexpression may cause a misrepresentation of what could be physiologically attainable at the cellular and tissue levels. We therefore also investigated the loss-of-function using genetic or pharmacological perturbations to confirm our hypotheses. Although systems approaches are useful in identifying pathway enrichment and novel mediators of cell processes, there are limitations caused by over estimations and sequence bias during data analyses. RNA-sequencing data has revolutionized the current vascular biology field for transcriptome data sets, greatly surpassing the data available through microarray. RNA-sequencing has improved in limiting background noise and increasing accuracy between technical replicates when compared to microarray[5]. However, the first step of RNA-sequencing library preparation is to PCR amplify and over amplification can lead to false positives. Even with standard normalization to reads per kilo base exon per million mapped reads (RPKM) to adjust for ambiguities between accumulating reads on genes that are relatively long, sequencing bias can still arise[6]. To overcome these limitations, we performed two biological repeats for each data set. Furthermore, all gene expression was validated using Western blot and qPCR before continuing the study.

From the KLF4 transcriptome data, we identified several gene ontology pathways in which KLF4 was already known to regulate, thereby adding more certainty to our analysis. KLF4 overexpression increased nitric oxide biosynthesis, as well as those involved in vascular development and function (e.g., blood vessel morphogenesis, circulatory system process, and leukocyte migration). We further validated that KLF4 did indeed regulate Ch25h and LXR not only at the cellular level using *in vitro* experiments,

but also at the tissue level using mice in which KLF4 was overexpressed or ablated specifically in the ECs (EC-KLF4-Tg and EC-KLF4-KO mice, respectively). The top gene ontology pathway for SREBP2 overexpression, regulation of lipid metabolism, is also well-documented to be regulated by SREBP2. We pursued the TGF, Wnt, and cytoskeleton remodeling pathway because it was the second most significantly induced pathway. However, SREBP2 overexpression also induced other novel gene ontology pathways (i.e., the role of Akt in hypoxia, and vascular endothelial growth factor [VEGF] signaling). It would be interesting to investigate whether these pathways also play a role in EC dysfunction related to fibrosis. In theory, hypoxia induces Akt to promote cell survival and proliferation, a mechanism that is commonly seen in tumor angiogenesis[7]. Furthermore, VEGF is a potent inducer of connective tissue growth factor (CTGF), a potential marker of EndoMT[8]. Both pathways could play a role in promoting EndoMT and tissue fibrosis. However, the mechanism by which would need to be further investigated.

4.3 KLF4 and epigenetic regulation

KLF4 has been suggested to be a "pioneer transcription factor" along with OCT4, c-MYC, and SOX2[9]. Pioneer transcription factors are able to directly bind to DNA and modify nucleosome complexes allowing the chromatin structure to relax[10]. I found that KLF4 transactivation of *Ch25h*, *LXRα*, and *LXRβ* involves direct *cis*-element binding measured through ChIP assays. Furthermore, KLF4 can function as a transcriptional repressor of SREBP2[11]. Thus, beneficial stimuli which enhance KLF4 expression, such as atheroprotective flow and statins, would increase KLF4 interaction with the cognate DNA binding sequences. Further chromatin relaxation is likely through the *trans*-dependent

modifications of H3K27ac and H3K4me3 as shown in Figure 2.4. Additionally, both athero-protective flow and KLF4 overexpression reduced DNA methylation in the promoter region of *Ch25h*. However, promoter methylation of several athero-protective genes was increased by atheroprone flow, resulting from increased expression of DNA methyltransferase 1 (DNMT1) and DNMT3a[12, 13]. KLF4 is able to directly bind to methylated DNA, of which the function remains elusive but has been eluded to be required for cellular reprogramming and stem cell differentiation[14, 15]. As a pioneering transcription factor, whether KLF4 regulates the epigenetic landscape of an array of genes crucial for EC function at the genome-wide scale warrants further study.

Recent advancement in next generation sequencing analyses have enabled us to investigate not only transcriptional regulation, but also chromatin accessibility and epigenetic regulation at the genome-wide scale. Chromatin structure could be assessed through an assay for transposase-accessible chromatin (ATAC)-seq, which is used to determine areas that are free of nucleosomes and accessible to transcriptional machinery. ATAC-seq is advantageous in that it uses relatively few cells (around 50,000) and will only identify areas of active transcription[16]. Chromatin immunoprecipitation (ChIP)-seq is highly valuable in establishing transcription factor binding loci in the genome, although this comes with limitations[17]. The method for protein to DNA crosslinking can vary, but the specificity of the antibodies used to pull down protein-DNA complexes has the greatest effect in the analysis. Unfortunately, the antibodies for both KLF4 and SREBP2 are less than ideal for ChIP-seq analyses. ChIP-seq has gained traction by using the histone code to identify active, poised, or inactive genes globally[18]. An active or poised enhancer region

is free of nucleosomes and the DNA is loose or "open" for transcription factor or transcription machinery to bind. Active enhancers also contain modified histone tail marks such as Histone 3 Lysine 27 acetylation (H3K27ac), Histone 3 Lysine 4 mono- and tri-methylation (H3K4me and H3K4me3), while poised enhancers contain some active histone marks (e.g., H3K4me3), but also repressive marks including Histone 3 Lysine 27 tri-methylation (H3K27me3)[19]. Inactive genes with only H3K27me3 are tightly compact around nucleosomes and are "closed" for transcription factor binding[20]. The different histone modifications also recruit co-activators/repressors, mediator complex, and RNA polymerase II (Pol II). For example, acetylated histone tails are recognized by the SWI/SNF transcription machinery through their bromodomain[20]. Once recruited, SWI/SNF facilitates nucleosome remodeling and chromatin opening. Conversely, H3K27me3 is recognized by polycomb repressive complex 2 (PRC2), which promotes chromatin compaction[20]. It would be interesting to see whether KLF4 overexpression promotes open chromatin of beneficial genes in EC function, while the opposing role of SREBP2 may facilitate chromatin compaction. Our lab has begun histone-ChIP-seq experiments to address these questions for a later study. However, the age-old question remains as to why KLF4 only activates beneficial genes and why SREBP2 seems to only activate detrimental genes in EC biology. Utilizing the genome loci that are activated by KLF4 or SREBP2 to perform additional motif enrichment analyses may provide answers to which co-activators, co-repressors, or other transcriptional machinery are involved in the dynamic regulation of EC and cholesterol homeostasis. A multi-layered approach,

including ATAC-seq, ChIP-seq, and transcriptome data would be required to further elucidate this complex regulatory network.

4.4 CRISPR/Cas9 genome editing in endothelial cells

An efficient and reliable method to edit genome in living endothelial cells has recently become available. Although small interfering RNA (siRNA) and the various virus gene delivery systems can partially manipulate the specific gene expression, they are limited by low efficiency, immunogenicity, and cytotoxicity[21]. In the recent three years, CRISPR/Cas9 (Clustered Regularly Interspaced Short Palindromic Repeats/CRISPR-associated protein-9), become a powerful tool for genome editing *in vitro* and *in vivo* due to its simplicity and efficiency[22, 23]. This technique was first identified in the bacterial immune system, which uses a short RNA-guide to induce nuclease-mediated precise genome editing. Furthermore, other genome editing tools can only manipulate protein coding regions or regulate gene expression. However, CRISPR/Cas9 can also be engineered to target noncoding regions, such as DNA enhancer elements. For example, the mutation or deletion of sterol responsive elements (SREs) or KLF4 DNA element motifs in the promoter region of target genes will help us to elucidate the regulatory network defined by SREBP2 or KLF4 binding, respectively. Specifically, CRISPR/Cas9 libraries to screen genome-wide DNA elements[24, 25], such as SREs or KLF4 binding sites, will elucidate further associations among transcription factors, DNA binding elements, and target genes that regulate endothelial (dys)function and vascular biology.

4.5 Regulation of SREBP2 in ECs

In most cell types, SREBP2 regulation is tightly controlled by the levels of intracellular cholesterol. In high cholesterol conditions, SREBP2 is sequestered to the endoplasmic reticulum. While in low cholesterol conditions, SREBP2 is transported to the Golgi apparatus where the N-terminal portion is cleaved and serves as a transcription factor. However, the regulation of SREBP2 cleavage in ECs is suggested to be cholesterol independent[26]. Our lab has identified numerous oxidative stress inducers that can stimulate the N-terminal cleavage and activation of SREBP2 in ECs (e.g., disturbed flow, H_2O_2, Ang II, ox-LDL, and BLM)[26, 27]. To date, the upstream mechanism of how SREBP2 is cleaved and activated when cholesterol independent remains to be seen. I postulate that SREBP2 would be retained in the endoplasmic reticulum, being that there would not be a sterol signal for translocation, and that there may be an oxidative stress sensitive protease in which cleaves the N-terminal portion of SREBP2. To explore this concept would require further investigation.

In this study, SREBP2 was found to be sufficient in the direct transactivation of downstream mesenchymal targets identified in this study (i.e., snai1, αSMA, N-cad, and vimentin) and promoting EndoMT both *in vitro* and *in vivo*. One question that remains unanswered is whether SREBP2 is necessary for the induction of EndoMT contributing to pulmonary fibrosis *in vivo*. Loss-of-function experiments in which SREBP2 expression was perturbed using siRNA knockdown or the pharmacological inhibitor betulin, suggested that SREBP2 was indeed necessary to induce EndoMT *in vitro*. However, to verify that this mechanism is also true at the tissue level, genetic or pharmacological

inhibition *in vivo* are needed. Unfortunately, systemic SREBP2 knockout animals are not available because they are embryonic lethal[28]. Our lab has attempted to create SREBP2 floxed mice in order to generate tissue specific SREBP2 knockout in hopes for better viability, but have thus far been unsuccessful. Experiments using betulin to inhibit SREBP2 *in vivo* are ongoing. However, betulin also has its limitations due to it being a pan SREBP inhibitor, which is not specific for mechanisms involving SREBP2. Furthermore, betulin is an orally administered and is not localized to the pulmonary vasculature.

Despite the limitations of our *in vivo* study, we were able to identify SREBP2 as a potential therapeutic target for pulmonary fibrosis. EC-specific overexpression of SREBP2 resulted in increased mesenchymal marker expression (i.e., snai1, aSMA, and vimentin) as well as increased markers of fibrosis (i.e., FN and Col1A1). Conversely, SREBP2 overexpression suppressed the expression of EC-specific markers (i.e., eNOS and VE-cad) in the lung ECs isolated from EC-SREBP2(N)-Tg mice. Furthermore, angiography suggested that the EC-SREBP2(N)-Tg mice treated with saline had a loss of distal pulmonary arteries, similar to that of the WT mice treated with BLM. EC-SREBP2(N)-Tg mice treated with BLM had obliterated lung vascularization and exacerbated pulmonary fibrosis as measured by Masson's trichrome stain. Clinically, patient lung samples further confirmed that SREBP2 expression is greatly increased in IPF patients when compared to normal controls.

4.6 Summary

By using a genome-wide, systems approach, we established that two transcription factors, KLF4 and SREBP2, are key in maintaining the sensitive balance between EC

homeostasis and cholesterol regulation. Serving as a ligand to LXR while inhibiting SREBP2 activation, 25-HC maintains a balance between cholesterol efflux and cholesterol biosynthesis[29]. Cholesterol efflux, regulated by LXR downstream targets such as ABCA1 and ABCG1, is known to be mediated by the innate immune response in macrophages[30]. Furthermore, upregulated SREBP is associated with unresolved innate immunity, leading to inflammasome activation in both ECs and macrophages[26, 31]. Here, we further defined that KLF4 regulates a counterbalance between LXR and SREBP via the regulation of Ch25h-25-HC. Reciprocally, the induction of SREBP2 in ECs leads to unresolved innate immune response via NLRP3 inflammasome activation and promotes EndoMT through the direct transactivation of mesenchymal markers snai1, αSMA, N-cad, and vimentin. SREBP2 overexpression not only mediated the genotypic changes, but also the phenotypic switch associated with a myofibroblast-like cell including increased proliferation, ECM deposition, and stress fiber formation. Using atherosclerosis and pulmonary fibrosis to represent two very different cardiovascular diseases, we were able to provide insight to the complex molecular network of EC function and cholesterol regulation.

References

1. Leopold JA. Chapter 2 - The Endothelium A2 - Creager, Mark A. In: J. A. Beckman and J. Loscalzo, eds. *Vascular Medicine: A Companion to Braunwald's Heart Disease (Second Edition)* Philadelphia: W.B. Saunders; 2013: 14-24.

2. Hamik A, Lin Z, Kumar A, Balcells M, Sinha S, Katz J, Feinberg MW, Gerzsten RE, Edelman ER and Jain MK. Kruppel-like factor 4 regulates endothelial inflammation. *The Journal of biological chemistry*. 2007;282:13769-79.

3. Zhou G, Hamik A, Nayak L, Tian H, Shi H, Lu Y, Sharma N, Liao X, Hale A, Boerboom L, Feaver RE, Gao H, Desai A, Schmaier A, Gerson SL, Wang Y, Atkins GB, Blackman BR, Simon DI and Jain MK. Endothelial Kruppel-like factor 4 protects against atherothrombosis in mice. *The Journal of clinical investigation*. 2012;122:4727-31.

4. Horton JD, Goldstein JL and Brown MS. SREBPs: activators of the complete program of cholesterol and fatty acid synthesis in the liver. *The Journal of clinical investigation*. 2002;109:1125-31.

5. Zhao S, Fung-Leung WP, Bittner A, Ngo K and Liu X. Comparison of RNA-Seq and microarray in transcriptome profiling of activated T cells. *PloS one*. 2014;9:e78644.

6. Conesa A, Madrigal P, Tarazona S, Gomez-Cabrero D, Cervera A, McPherson A, Szczesniak MW, Gaffney DJ, Elo LL, Zhang X and Mortazavi A. A survey of best practices for RNA-seq data analysis. *Genome biology*. 2016;17:13.

7. Muz B, de la Puente P, Azab F and Azab AK. The role of hypoxia in cancer progression, angiogenesis, metastasis, and resistance to therapy. *Hypoxia (Auckland, NZ)*. 2015;3:83-92.

8. Piera-Velazquez S, Mendoza FA and Jimenez SA. Endothelial to Mesenchymal Transition (EndoMT) in the Pathogenesis of Human Fibrotic Diseases. *Journal of clinical medicine*. 2016;5.

9. Soufi A, Garcia MF, Jaroszewicz A, Osman N, Pellegrini M and Zaret KS. Pioneer transcription factors target partial DNA motifs on nucleosomes to initiate reprogramming. *Cell*. 2015;161:555-568.

10. Chen T and Dent SY. Chromatin modifiers and remodellers: regulators of cellular differentiation. *Nature reviews Genetics*. 2014;15:93-106.

11. Rowland BD, Bernards R and Peeper DS. The KLF4 tumour suppressor is a transcriptional repressor of p53 that acts as a context-dependent oncogene. *Nature cell biology*. 2005;7:1074-82.

12. Jiang YZ, Jimenez JM, Ou K, McCormick ME, Zhang LD and Davies PF. Hemodynamic disturbed flow induces differential DNA methylation of endothelial Kruppel-Like Factor 4 promoter in vitro and in vivo. *Circulation research*. 2014;115:32-43.

13. Dunn J, Qiu H, Kim S, Jjingo D, Hoffman R, Kim CW, Jang I, Son DJ, Kim D, Pan C, Fan Y, Jordan IK and Jo H. Flow-dependent epigenetic DNA methylation regulates endothelial gene expression and atherosclerosis. *The Journal of clinical investigation*. 2014;124:3187-99.

14. Spruijt CG, Gnerlich F, Smits AH, Pfaffeneder T, Jansen PW, Bauer C, Munzel M, Wagner M, Muller M, Khan F, Eberl HC, Mensinga A, Brinkman AB, Lephikov K, Muller U, Walter J, Boelens R, van Ingen H, Leonhardt H, Carell T and Vermeulen M. Dynamic readers for 5-(hydroxy)methylcytosine and its oxidized derivatives. *Cell*. 2013;152:1146-59.

15. Hu S, Wan J, Su Y, Song Q, Zeng Y, Nguyen HN, Shin J, Cox E, Rho HS, Woodard C, Xia S, Liu S, Lyu H, Ming GL, Wade H, Song H, Qian J and Zhu H. DNA methylation presents distinct binding sites for human transcription factors. *eLife*. 2013;2:e00726.

16. Buenrostro J, Wu B, Chang H and Greenleaf W. ATAC-seq: A Method for Assaying Chromatin Accessibility Genome-Wide. *Current protocols in molecular biology / edited by Frederick M Ausubel [et al]*. 2015;109:21.29.1-9.

17. Meyer CA and Liu XS. Identifying and mitigating bias in next-generation sequencing methods for chromatin biology. *Nature Reviews Genetics*. 2014;15:709.

18. O'Geen H, Echipare L and Farnham PJ. Using ChIP-seq technology to generate high-resolution profiles of histone modifications. *Methods in molecular biology (Clifton, NJ)*. 2011;791:265-86.

19. Heinz S, Romanoski CE, Benner C and Glass CK. The selection and function of cell type-specific enhancers. *Nature reviews Molecular cell biology*. 2015;16:144-54.

20. Bannister AJ and Kouzarides T. Regulation of chromatin by histone modifications. *Cell Research*. 2011;21:381-395.

21. Sung LY, Chen CL, Lin SY, Li KC, Yeh CL, Chen GY, Lin CY and Hu YC. Efficient gene delivery into cell lines and stem cells using baculovirus. *Nature protocols*. 2014;9:1882-99.

22. Mali P, Yang L, Esvelt KM, Aach J, Guell M, DiCarlo JE, Norville JE and Church GM. RNA-guided human genome engineering via Cas9. *Science (New York, NY)*. 2013;339:823-6.

23. Jinek M, Chylinski K, Fonfara I, Hauer M, Doudna JA and Charpentier E. A programmable dual-RNA-guided DNA endonuclease in adaptive bacterial immunity. *Science (New York, NY)*. 2012;337:816-21.

24. Shalem O, Sanjana NE, Hartenian E, Shi X, Scott DA, Mikkelson T, Heckl D, Ebert BL, Root DE, Doench JG and Zhang F. Genome-scale CRISPR-Cas9 knockout screening in human cells. *Science (New York, NY)*. 2014;343:84-87.

25. Sanjana NE, Shalem O and Zhang F. Improved vectors and genome-wide libraries for CRISPR screening. *Nature methods*. 2014;11:783-784.

26. Xiao H, Lu M, Lin TY, Chen Z, Chen G, Wang WC, Marin T, Shentu TP, Wen L, Gongol B, Sun W, Liang X, Chen J, Huang HD, Pedra JH, Johnson DA and Shyy JY. Sterol regulatory element binding protein 2 activation of NLRP3 inflammasome in endothelium mediates hemodynamic-induced atherosclerosis susceptibility. *Circulation*. 2013;128:632-42.

27. Chen Z, Wen L, Martin M, Hsu CY, Fang L, Lin FM, Lin TY, Geary MJ, Geary GG, Zhao Y, Johnson DA, Chen JW, Lin SJ, Chien S, Huang HD, Miller YI, Huang PH and Shyy JY. Oxidative stress activates endothelial innate immunity via sterol regulatory element binding protein 2 (SREBP2) transactivation of microRNA-92a. *Circulation*. 2015;131:805-14.

28. Shimano H, Shimomura I, Hammer RE, Herz J, Goldstein JL, Brown MS and Horton JD. Elevated levels of SREBP-2 and cholesterol synthesis in livers of mice homozygous for a targeted disruption of the SREBP-1 gene. *The Journal of clinical investigation*. 1997;100:2115-24.

29. Cyster JG, Dang EV, Reboldi A and Yi T. 25-Hydroxycholesterols in innate and adaptive immunity. *Nature reviews Immunology*. 2014;14:731-43.

30. Tall AR and Yvan-Charvet L. Cholesterol, inflammation and innate immunity. *Nature reviews Immunology*. 2015;15:104-16.

31. Im SS, Yousef L, Blaschitz C, Liu JZ, Edwards RA, Young SG, Raffatellu M and Osborne TF. Linking lipid metabolism to the innate immune response in macrophages through sterol regulatory element binding protein-1a. *Cell metabolism*. 2011;13:540-9.